January 2014

SPIN CIRCUIT REPRESENTATION OF ELECTRONIC TRANSPORT IN MATERIALS WITH SPIN ORBIT COUPLING

Seokmin Hong
Purdue University

Graduate School Form 30
(Revised 08/14)

PURDUE UNIVERSITY
GRADUATE SCHOOL
Thesis/Dissertation Acceptance

This is to certify that the thesis/dissertation prepared

By Seokmin Hong

Entitled
Spin Circuit Representation of Electronic Transport in Materials With Spin Orbit Coupling

For the degree of Doctor of Philosophy

Is approved by the final examining committee:

SUPRIYO DATTA

MARK S. LUNDSTROM

MUHAMMAD A. ALAM

YONG P. CHEN

To the best of my knowledge and as understood by the student in the Thesis/Dissertation Agreement, Publication Delay, and Certification/Disclaimer (Graduate School Form 32), this thesis/dissertation adheres to the provisions of Purdue University's "Policy on Integrity in Research" and the use of copyrighted material.

SUPRIYO DATTA

Approved by Major Professor(s): _____

_____

Approved by: V. Balakrishnan 12/02/2014

Head of the Department Graduate Program Date

SPIN CIRCUIT REPRESENTATION OF ELECTRONIC TRANSPORT IN MATERIALS WITH SPIN ORBIT COUPLING

A Dissertation

Submitted to the Faculty

of

Purdue University

by

Seokmin Hong

In Partial Fulfillment of the

Requirements for the Degree

of

Doctor of Philosophy

December 2014

Purdue University

West Lafayette, Indiana

To my family.

ACKNOWLEDGMENTS

It has been a great experience for me to work with Prof. Datta whose unique and original perspectives benefited my whole Ph.D. life. His numerous demonstrations of bringing in clarity, simplicity, and common sense about various complicated subjects while maintaining the essential physics have impressed me deeply and will remain as an essential part of my academic and working knowledge.

I also greatly appreciate Prof. Lundstrom and Prof. Alam for their exemplary academic attitude and guidance with various coursework that broadens my perspective. I specially thank Prof. Chen for introducing me into the field of topological insulators and many feedbacks during my research.

I thank Dr. Abu Naser Zainuddin, Vinh Diep, Shehrin Sayed, Dr. Lutfe Siddiqui, and Dr. Tony Low who helped me through many interactions during my research together with other group members: Samiran, Kerem, Brian, Faria, and Dr. Kuntal. I am also indebted to many of my colleagues and friends, Dr. Changwook Jeong, Dr. Youngki Yoon, Dr. Hoon Ryu, Dr. Sunhee Lee, Dr. Jaeyoung Park, Dr. Mirang Park, Dr. Raseong Kim, Dr. Seung Hyun Park, Dr. Honghyun Park, Dr. Jesse Maassen, Woochan Lee, Yusung Kim, Dr. Jonghyun Go, Dr. SungGeun Kim, Dr. Jaehyuk Jang, Dr. Mathieu Luisier, Sang Hoon Shin, and more.

Finally, this work is dedicated to my family: my parents, and my brother who showed their continued support and encouragement.

TABLE OF CONTENTS

Page

Page

LIST OF FIGURES

Figure Page

Figure Page

ABSTRACT

Hong, Seokmin Ph.D., Purdue University, December 2014. Spin Circuit Representation of Electronic Transport in Materials with Spin Orbit Coupling. Major Professor: Supriyo Datta.

Modern nanomagnetic devices involve materials and phenomena featuring both spin and charge transport. SPICE compatible spin circuits with 4-component voltage and current (1 for charge and 3 for spin) have been developed to represent this emerging class of devices. However there has not been much work on circuit representation for materials with high spin-orbit coupling (SOC) which are becoming increasingly important with the discovery of giant spin Hall effect (GSHE) and topological insulators.

In this work we describe a spin circuit representation for 3D bulk materials like Tantalum or Tungsten exhibiting GSHE, which has received extensive attention recently due to their potential applications to write units in memory. This work shows how this circuit representation leads to many established results in a straightforward way, while providing a versatile tool for the numerical analysis of complex geometries.

Next, we move onto new type of materials called topological insulators where we develop theoretical models for electron transport, benchmark them against available experimental data and make interesting predictions that can be tested experimentally, some aspects of which have recently received experimental support. We believe that this approach is applicable not only to topological insulators but to 2D interfacial channels with SOC in general.

1. INTRODUCTION

Materials with high spin orbit coupling (SOC) exhibit interesting phenomena due to the strong relativistic effect that couples electrons motion to its spin. These include the voltage controlled spin precession effect (so called Datta-Das effect) and spin Hall effect (SHE) etc. Recently, a new type of material called topological insulator (TI) is drawing a lot of attention, which are characterized by insulating bulk and spin polarized conducting surface states. Circuit representation for materials with high SOC is one of the main motivations of this thesis, which can be considered as an extension of similar work in normal metals (NM) and ferromagnetic materials (FM) in the past. Three dimensional (3D) bulk materials with SHE and two dimensional interfacial channels with SOC (Rashba and TI surface states (TISS)) are treated as representative examples due to all the related research and potential applications in spintronics.

1.1 Motivation

One of the main driving forces in semiconductor spintronics [1] has been the voltage controlled spin precession effect, (so called Datta-Das effect). Koo *et al.* reported the experimental demonstration [2] in 2009 of the proposed spin precession by combining spin injection into semiconductor and gate control of Rashba spin orbit interaction. The detailed modeling [3] was also performed subsequently with realistic considerations of experimental structure. Although the basic features are observed experimentally there are great difficulties to overcome regarding the robustness of the signal in order to be considered for practical device applications. Generally, the spin current is not a conserved quantity and it decays quickly as it propagates through the channel or the temperature rises. This problem ordinarily gets worse in materials

with high spin orbit coupling since spin orbit interaction can act as random magnetic fields in the channel. But there are interesting exceptions to this where charge and spin can be tied together due to spin orbit interaction and spin gains more robustness. These are the main topic of this thesis and we consider bulk materials with SHE and two dimensional materials of topological insulator surface states and Rashba channel as representative examples.

1.2 Brief Introduction to Spin Hall Effect (SHE)

Spin Hall effect (SHE) was experimentally observed [4] in 2004, where the accumulation of spin polarization on the edges was shown by optical Kerr rotation microscopy. Recent giant SHE observed in heavy metals like Pt, Ta or W shows one or two orders of magnitude improvement, which is usually quantified by the spin Hall angle ($\theta_{SH} = J^s/J^c$) with J^s being the spin current density and J^c being the charge current density (see for example [5,6] and references therein). The reported value is as large as 0.3 and is enough to switch a conventional magnet at room temperature [7,8]. The simple description of SHE and Inverse SHE (ISHE) in a cubic structure is shown in Fig. 1.1 based on the standard equations that have been used in analyzing various experimental results (chapter 2). In SHE the applied charge current ($\vec{I}^c$) generates two transverse spin currents ($\vec{I}^s$) as shown in Fig. 1.1(a). The magnitude of the generated spin current is given by $\left|\vec{I}^s\right| = \theta_{\mathrm{SH}} \left|\vec{I}^c\right|$ with it spin polarization direction being $\vec{I}^c$ and $\vec{I}^s$. In ISHE, the spin current is applied and the transverse charge current can be generated as a result. If we take one of generated spin current in SHE from Fig. 1.1(a) as an applied spin current in ISHE, the generated charge current is opposite in its direction as shown in Fig. 1.1(b).

1.3 Brief Introduction to Topological Insulator

Due to the similarity between classical Hall effect (HE) and SHE there have been interest to propose quantum version of SHE, just as QHE is a quantum version of

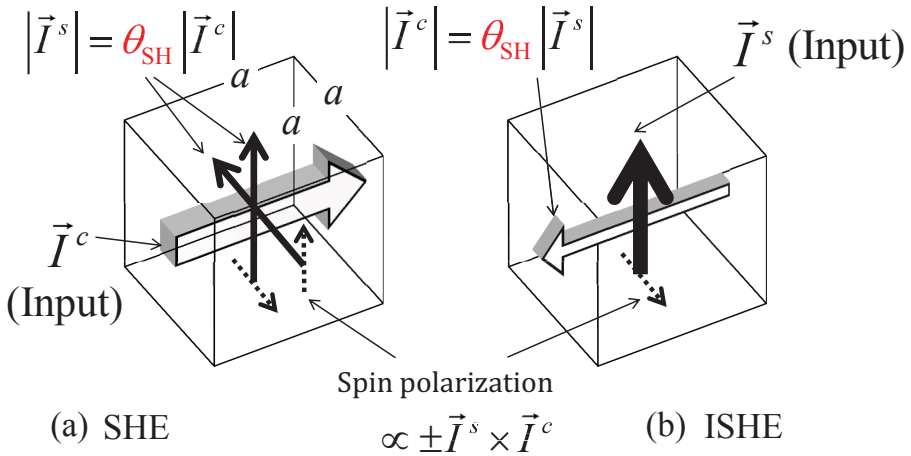

Fig. 1.1. A cubic structure of volume a^3 is shown to represent materials with GSHE. Simple descriptions of spin Hall effect (SHE) and inverse spin Hall effect (ISHE) are shown in (a) and (b) with charge current ($\vec{I}^c = a^2\vec{J}^c$), spin current ($\vec{I}^s = a^2\vec{J}^s$) and spin polarization by 3D, solid and dotted arrows respectively. In SHE, $\vec{I}^c$ induces transverse spin currents $\left|\vec{I}^s\right| = \theta_{\rm SH}\left|\vec{I}^c\right|$ with spin polarizations given by vector product of $\vec{I}^s$ and $\vec{I}^c$. In ISHE, the spin current I^s induces transverse charge current $\left|\vec{I}^c\right| = \theta_{\rm SH}\left|\vec{I}^s\right|$ and with spin polarizations given by vector product of $\vec{I}^c$ and $\vec{I}^s$.

HE (see Fig. 1.2). Although there were several other proposals, the first successful experimental evidence was shown in HgCdTe quantum well structure in 2007 shortly after its theoretical prediction (see for example [9, 10] and references therein). The quantized conductance inside the bandgap was considered as an experimental evidence for the existence of edge states. The material is two dimensional so that the edge states form a one dimensional channel. The generalization to three dimensional material was soon recognized by several groups together with numerous experimental evidences in materials with $Bi_{1-x}Sb_x$ and Bi_2Se_3 with spin and angle resolved photoemission spectroscopy. In this thesis we focus on one surface of TI (Top surface in Fig. 1.2(b)) and explore the unique coupling between charge and spin in this material. But we believe the theoretical approach is general enough to include any 2D channel with Rashba or other SOC.

1.4 Thesis Organization

In chapter 2, we first focus on 3D bulk materials with SOC, namely, materials with spin Hall effect which have drawn a lot of attention due to their ability to write information into a magnet. Circuit representations based on the standard diffusion equation are provided with increasing level of complexity in terms of the boundary conditions. Two new proposals are made based on the circuit representation, namely, spin injection into semiconductor without tunneling barriers and spin ground to enhance spin current in a thin sample.

In chapter 3, we move on 2D materials with SOC like TISS and Rashba where various types of experiment are reported very recently specially in the case of TI. Using the widely accepted Hamiltonian, we present a quantum transport model based on nonequilibrium Greens function (NEGF) formalism to analyze potentiometric measurement where the unique coupling between charge and spin can be captured by voltage change upon reversing magnetization direction of FM contact.

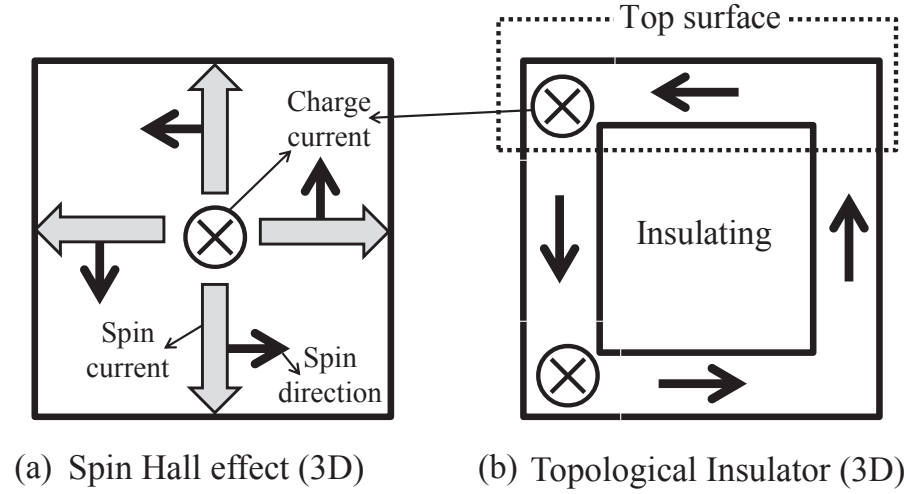

Fig. 1.2. The schematic view of cross section of 3D sample with spin Hall effect (SHE) and topological insulator (TI) are shown under a charge current flowing into the plane. (a) Spin currents are shown in the case of SHE with spin polarization directions given by cross product of charge current direction and spin current direction. (b) In the case of TI we have spin polarized surface states with insulating bulk. The spin polarization direction is same as the one of SHE. The top surface (dotted box) can be treated as 2D channel which is a topic of the thesis.

In chapter 4, we provide a circuit representation for arbitrary 2D channel with SOC that can include TISS and Rashba. Based on this we explore three new results: effective spin Hall angle, maximum spin current, and angular magnetoresistance.

In chapter 5, we summarize the thesis and suggest possible future directions in materials with high SOC.

2. SPIN CIRCUIT REPRESENTATION FOR BULK MATERIALS WITH THE SPIN HALL EFFECT-PHENOMENOLOGICAL MODEL [SUBMITTED TO IEEE TRANS. ON MAGNETICS]

The contents of this chapter have been extracted and revised from the following submitted paper: Seokmin Hong, Shehrin Sayed, and Supriyo Datta, "Spin circuit representation for the spin Hall effect," *IEEE TRANS. ON MAGNETICS* (submitted).

2.1 Introduction

Circuit representation for normal metal (NM) and ferromagnet (FM) interfaces and structures with non-collinear ferromagnets have been developed and studied using both the Keldysh method [11] and the continuous random matrix theory [12]. Based on these works, circuits [13] with four component voltages and currents have been developed to analyze spin logic devices [14] and interconnects and shown to be compatible with conventional circuit simulators like SPICE [15].

To our knowledge, however, there has not been much work on circuit representation for materials with high spin-orbit coupling which are becoming increasingly important with the discovery of giant spin Hall effect (GSHE) (see for example [5] and references therein) together with other types of spin orbit torques [16–19] like Rashba effect in heavy metals. These demonstrate a new functionality that can replace or add to conventional ferromagnets (FM) in various spintronic applications such as switching of a magnets with perpendicular [7, 16, 17, 20–22] or in-plane [19, 23] anisotropy, domain wall motion [24–26] and spin torque oscialltors [27–29]. One can envision novel and innovative device structures where multiple layers of various ma-

terials such as ferromagnets (FM), ferromagnet insulators (FMI) or semiconductors are driven by GSHE material as shown in Fig. 2.1(a).

Our starting point is following semi-classical equations which have been widely used in the past. The linear response relation (Ohm's law) for materials with spin Hall effect (SHE) is described by the following equation [30, 31]

$$\begin{pmatrix} \vec{J}^c \\ \vec{J}^x \\ \vec{J}^y \\ \vec{J}^z \end{pmatrix} = -\sigma \begin{bmatrix} 1 & \theta_{SH}\hat{x}\times & \theta_{SH}\hat{y}\times & \theta_{SH}\hat{z}\times \\ \theta_{SH}\hat{x}\times & 1 & 0 & 0 \\ \theta_{SH}\hat{y}\times & 0 & 1 & 0 \\ \theta_{SH}\hat{z}\times & 0 & 0 & 1 \end{bmatrix} \begin{pmatrix} \vec{\nabla}V^c \\ \vec{\nabla}V^x \\ \vec{\nabla}V^y \\ \vec{\nabla}V^z \end{pmatrix} \tag{2.1}$$

together with charge and spin diffusion equations,

$$\begin{aligned} \vec{\nabla}\cdot\vec{J}^c &= -\sigma\nabla^2 V^c = 0, \\ \vec{\nabla}\cdot\vec{J}^{x,y,z} &= -\sigma\nabla^2 V^{x,y,z} = -\left(\sigma/\lambda^2\right) V^{x,y,z}, \end{aligned} \tag{2.2}$$

where $\overrightarrow{J}^c$, $\overrightarrow{J}^x$, $\overrightarrow{J}^y$, and $\overrightarrow{J}^z$ are current densities for charge and spin polarizations of x, y, and z respectively. V^c, V^x, V^y, and V^z are voltages for charge and spin polarizations of x, y, and z respectively and related to chemical potentials by $V^\eta = \mu^\eta/q$ with $\eta = c, x, y, z$. Each spin voltage is defined as $(V^\uparrow - V^\downarrow)/2$ where $V^\uparrow$ and $V^\downarrow$ are up and down spin voltages for each spin polarization direction. Here σ is the conductivity of GSHE material, the quantity $\theta_{\rm SH}$ is called as the spin Hall angle, and λ is the spin diffusion length.

What we establish in this paper is that the physics of spin Hall effect as described by Eqs. (2.1) and (2.2) with appropriate boundary conditions can be captured using the conductance matrices shown in Fig. 2.1 which can be associated with equivalent circuits. Here we provide three types of conductance matrices for GSHE material with an increasing level of complexity in boundary conditions. The most general boundary condition is captured by the one shown in Fig. 2.1(e), while simpler boundary conditions are captured by the simpler ones in Fig. 2.1(c) and (d). Additional effects not captured by Eq. (2.1) could require appropriate modifications to the conductance matrices presented here. The advantage of the conductance matrix representation is

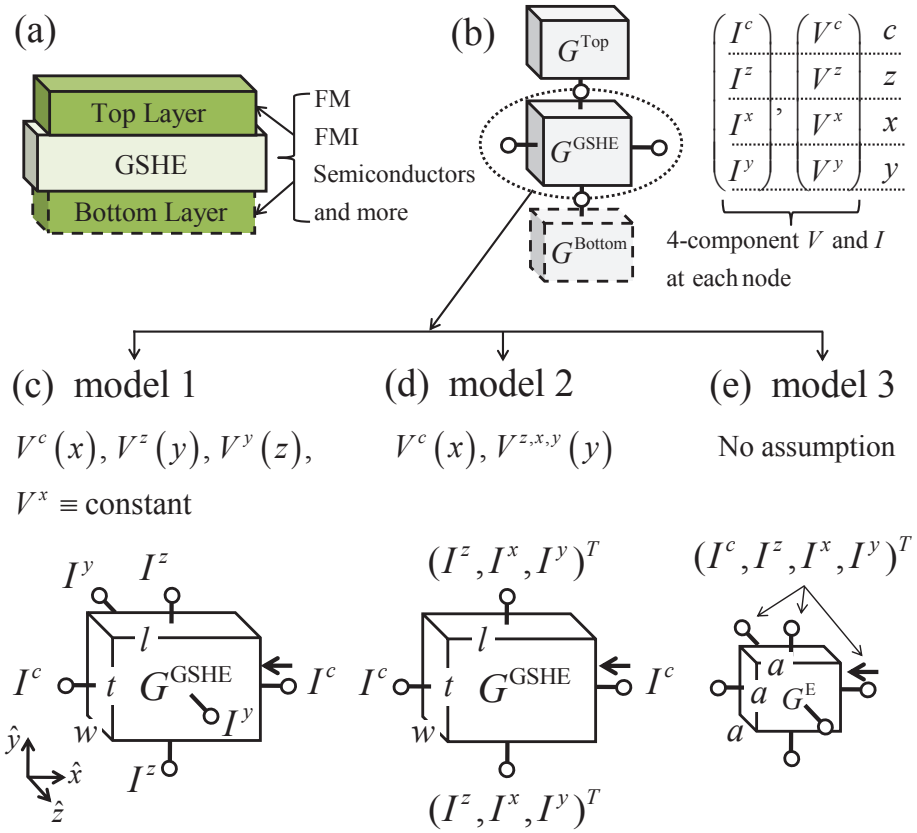

Fig. 2.1. (a) Schematic view of a tri-layer structure consisting of giant spin Hall effect (GSHE) material with various adjacent materials such as ferromagnetic metal (FM), ferromagnetic insulator (FMI), and semiconductors. (b) A conductance matrix representation of the structure (a) is shown. Each layer is represented by its conductance matrix (G^{Top}, G^{GSHE}, G^{Bottom}) and can be connected together to construct the original structure with voltage and current with four components: one for charge and three for z, x, y spin polarization directions. This representation enables a modular approach to analyze various structure of interest. Here we provide three types of conductance matrix for GSHE block. (c) G^{GSHE} with six terminals each of which has either charge and one type of spin polarization (Eq.(2.7)). (d) G^{GSHE} with four terminals : two for charge and two for spin with all three possible polarizations (Eq. (2.19)). In (c) and (d) unspecified charge or spin polarizations ($\eta = c,\ z, x, y$) in each terminal have zero currents or open boundary conditions ($I^\eta = 0$). (e) An elemental conductance matrix (G^{E}) with six terminals for a small cube (Eq.(2.34)). All terminals have voltage and current with four components.

that it enables a modular approach to the analysis and design of GSHE driven devices. For example, the same circuit model for the GSHE material can be used regardless of whether it drives a ferromagnet or a semiconductor, on one or both surfaces (see Fig. 2.1(b)). Each layer has its own associated conductance matrix which combined with that for the GSHE conductance matrix can be used to analyze the device using standard circuit techniques. We start in Section 2 by describing how the conductance matrix of model 1 in Fig. 2.1(c) and its associated equivalent circuits are obtained from the standard semi-classical equations (see Eqs. (2.1) and (2.2)) based on the uniform voltage assumption (see Eq. (2.3)). This conductance matrix is characterized by six terminals with one component of either charge or spin where the rest of three components have open boundary conditions. We then show in Section 3 that this circuit representation straightforwardly leads to the standard results in the literature for both spin Hall effect (SHE) [32, 33] and inverse spin Hall effect (ISHE) [34, 35]. Furthermore it makes predictions about experiments that have not been reported yet such as spin injection into semiconductors without a need of tunneling barrier and provides a simple model to analyze a role of spin ground to enhance the spin injection into the opposite layer in a thin GSHE sample. In Section 4, we derive the conductance matrix of model 2 in Fig. 2.1(d) and its associated equivalent circuits based on a different voltage assumption (see Eq. (2.18)). This conductance matrix has four terminals : two for charge and two for spin where spin terminals now carry all three components. The same open boundary conditions for unspecified components apply here. We then show in Section 5 that this conductance matrix provides the standard result for recently discovered spin Hall magnetoresistance (SMR) [31, 36] where conductance matrices for GSHE material and FMI are connected together using conventional circuit rules for charge and spin. Finally in Section 6, we provide an elemental conductance matrix of model 3 in Fig. 2.1(e) for a small cube with all four charge and spin components at each terminal. These small cubes can be combined together to construct any arbitrarily shaped structure making this approach suitable for numerical modeling of complicated non-uniform geometries.

2.2 Model 1

2.2.1 Conductance Matrix

The standard equations (Eqs. (2.1) and (2.2)) can be converted into a conductance matrix with terminal voltages and currents in Fig. 2.1(c)-(e). Here terminal voltages V_i^η and currents I_i^η for charge and spin are defined on the surfaces of a rectangular box where superscript $\eta = c, z, x, y$ represents charge or spin polarizations and subscript i represents terminal index. Each terminal voltage is assumed to be constant on its surface and a positive terminal current is defined as a total integrated current density flowing perpendicular into the surface. In this section we focus on the model 1 shown in Fig 2.1(c). We apply the voltage assumptions given by

$$V^c \equiv V^c\left(x\right),\ V^z \equiv V^z\left(y\right),\ \text{and } V^x \equiv \text{constant}, \tag{2.3}$$

for a rectangular box of volume $l \times t \times w$ in Fig 2.2(a). Then we can reduce Eq. (2.1) into following ones after collecting all nonzero current components

$$\begin{aligned}
\hat{x} \cdot \overrightarrow{J}^c &= J_x^c = -\sigma\left(\partial_x V^c + \theta_{\mathrm{SH}}\partial_z V^y - \theta_{\mathrm{SH}}\partial_y V^z\right) \\
\hat{y} \cdot \overrightarrow{J}^z &= J_y^z = -\sigma\left(\theta_{\mathrm{SH}}\partial_x V^c + \partial_y V^z\right) \\
\hat{z} \cdot \overrightarrow{J}^y &= J_z^y = -\sigma\left(-\theta_{\mathrm{SH}}\partial_x V^c + \partial_z V^y\right),
\end{aligned} \tag{2.4}$$

where subscript indices indicate transport direction and superscript indices indicate charge or spin polarization. The diffusion equations for V^c, V^y, and V^z can be obtained after plugging Eq. (2.4) into Eq. (2.2) under the assumptions in Eq. (2.3)

$$\begin{aligned}
\partial_x^2 V^c &= 0 \\
\partial_y^2 V^z &= V^z/\lambda^2 \\
\partial_z^2 V^y &= V^y/\lambda^2,
\end{aligned} \tag{2.5}$$

which have following solutions with boundary values provided by terminal voltages of a rectangular box

$$\begin{aligned} V^c(x) &= \frac{V_2^c x + V_1^c(l-x)}{l} \\ V^z(y) &= \frac{V_4^z \sinh\left(\frac{y}{\lambda}\right) + V_3^z \sinh\left(\frac{t-y}{\lambda}\right)}{\sinh\left(t/\lambda\right)} \\ V^y(z) &= \frac{V_6^y \sinh\left(\frac{z}{\lambda}\right) + V_5^y \sinh\left(\frac{w-z}{\lambda}\right)}{\sinh\left(w/\lambda\right)} \end{aligned} \tag{2.6}$$

with V_i^η representing the i^{th} terminal voltage for each surface. After plugging Eq. (2.6) into Eq. (2.4) and integrating current densities over corresponding surfaces, we obtain $I_{1,2}^c$, $I_{3,4}^z$, and $I_{5,6}^y$ (total charge and spin currents through each surface) in terms of and (see APPENDIX A) in a form of a conductance matrix as

$$\begin{aligned} \begin{pmatrix} I_{1,2}^c \\ I_{3.4}^z \\ I_{5,6}^y \end{pmatrix} &= \begin{bmatrix} G^{cc} & G^{cz} & G^{cy} \\ G^{zc} & G^{zz} & 0 \\ G^{yc} & 0 & G^{yy} \end{bmatrix} \begin{pmatrix} V_{1,2}^c \\ V_{3.4}^z \\ V_{5,6}^y \end{pmatrix} \\ &= \begin{bmatrix} tw\frac{\sigma}{l}D & -w\sigma\theta_{\text{SH}}D & t\sigma\theta_{\text{SH}}D \\ w\sigma\theta_{\text{SH}}D & lw\frac{\sigma}{t}S(t) & 0 \\ -t\sigma\theta_{\text{SH}}D & 0 & lt\frac{\sigma}{w}S(w) \end{bmatrix} \begin{pmatrix} V_{1,2}^c \\ V_{3.4}^z \\ V_{5,6}^y \end{pmatrix} \end{aligned} \tag{2.7}$$

where $I_{i,j}^\eta = \begin{pmatrix} I_i^\eta \\ I_j^\eta \end{pmatrix}$, $V_{i,j}^\eta = \begin{pmatrix} V_i^\eta \\ V_j^\eta \end{pmatrix}$, $D = \begin{pmatrix} 1 & -1 \\ -1 & 1 \end{pmatrix}$, and $S(x) = \frac{x}{\lambda}\begin{pmatrix} \coth\frac{x}{\lambda} & -\text{csch}\frac{x}{\lambda} \\ -\text{csch}\frac{x}{\lambda} & \coth\frac{x}{\lambda} \end{pmatrix}$. There are three 2×2 matrices (G^{cc}, G^{zz}, and G^{yy}) on the diagonals representing conventional 1D diffusion of charge and spin along $\hat{x}$,$\hat{y}$, and $\hat{z}$ directions respectively. G^{cc} represent charge current flow between terminals 1 and 2, G^{zz} and G^{yy} represents z and y polarized spin currents between terminals 3 and 4 and between terminals 5 and 6 respectively. In addition, there are four 2×2 matrices (G^{cz}, G^{cy}, G^{zc} and G^{yc}) on the off-diagonals which couple charge and spin diffusion. Two upper off-diagonal blocks G^{cz}, G^{cy} represent ISHE where spin voltages of V^z and

V^y induce a charge current. Their Onsager reciprocity pairs (G^{zc}, G^{yc}) which appear as the two lower off-diagonal blocks, represent SHE where charge voltage V^c induces spin current of z and y polarizations. Note that additional negative signs [37, 38] between Onsager pairs ($G^{cz} = -G^{zc}$ and $G^{cy} = -G^{yc}$) appear, which couple charge and spin in the conductance matrix. Unspecified component of charge or spin at each terminal has open boundary condition ($I^\eta = 0$). For example, at charge terminal 1 all spin currents ($I_1^{z,x,y} = 0$) are zero.

2.2.2 Circuit Representation

We can translate the conductance matrix in Eq. (2.7) into equivalent circuit for each charge and spin in a straightforward way. The first row of Eq. (2.7) gives a circuit for charge as in Fig. 2.2(b) with following identifications

$$\begin{aligned} I_0^c &= \beta_1 G_0 (V_3^z - V_4^z) - \beta_2 G_0 (V_5^y - V_6^y) \\ G_0 &= \sigma t w / l \\ \beta_1 &= \theta_{\rm SH} l / t \\ \beta_2 &= \theta_{\rm SH} l / w. \end{aligned} \tag{2.8}$$

The second row of Eq. (2.7) gives a Π circuit for z polarized spin as in Fig. 2.2(c) with each circuit element given by

$$\begin{aligned} I_0^z &= \beta_1 G_0 (V_1^c - V_2^c) \\ G_1^z &= \frac{\sigma l w}{\lambda} \tanh \frac{\mathrm{t}}{2\lambda} \\ G_2^z &= \frac{\sigma l w}{\lambda} \mathrm{csch} \frac{\mathrm{t}}{\lambda}. \end{aligned} \tag{2.9}$$

Likewise, circuit elements in the Π circuit for y polarized spin in Fig. 2.2(c) are given by

$$\begin{aligned} I_0^y &= \beta_2 G_0 (V_1^c - V_2^c) \\ G_1^y &= \frac{\sigma l t}{\lambda} \tanh \frac{\mathrm{w}}{2\lambda} \\ G_2^y &= \frac{\sigma l t}{\lambda} \mathrm{csch} \frac{\mathrm{w}}{\lambda}. \end{aligned} \tag{2.10}$$

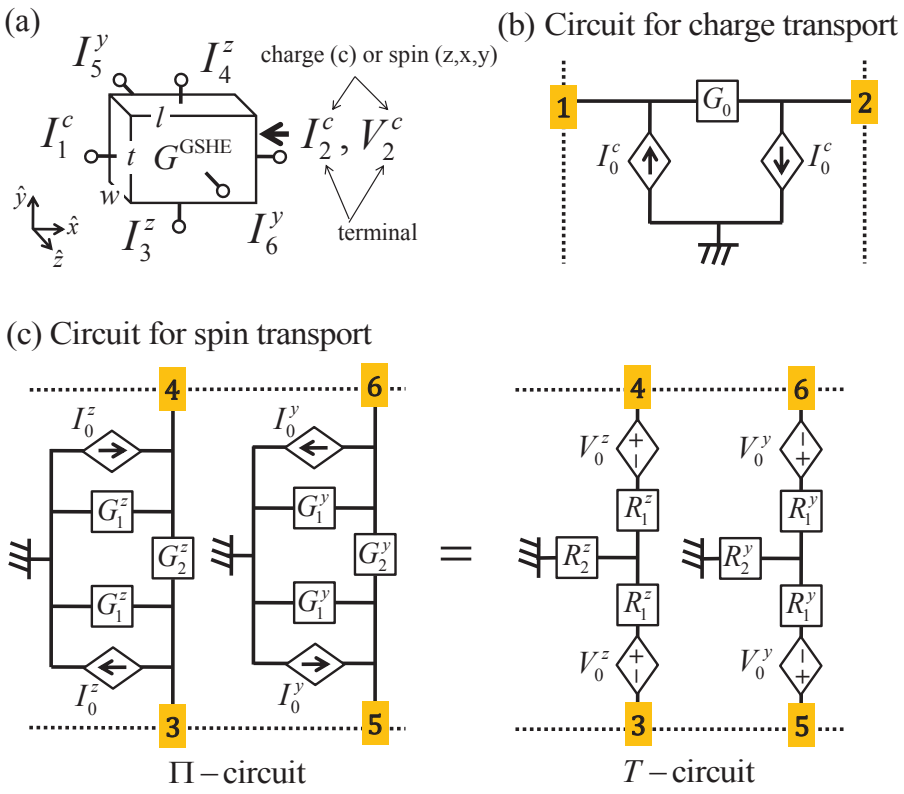

Fig. 2.2. (a) A rectangular structure of volume $l \times t \times w$ defining six terminals at each surface for G^{GSHE} in Fig 2.1(c) is shown. There are charge transport along $\hat{x}$ direction and spin transport along $\hat{y}$ and $\hat{z}$ directions with z and y spin polarizations respectively. These three are coupled together by dependent current or voltage sources due to spin Hall effect (SHE) and inverse spin Hall effect (ISHE). Each 1D transport can be represented by an equivalent circuit for (b) charge transport, and (c) two spin transport (there are two equivalent representations: Π and T). Note that there are six terminals: 1, 2 for charge and 3, 4 and 5, 6 for spin.

The gain factor (β_1 or β_2) depends on a geometrical ratio [23] between the length of the charge transport direction and the length of the corresponding spin transport direction. We can convert Π circuits into T circuits as in Fig. 2.2(c) by identifying each circuit element by

$$\begin{aligned} V_0^z &= \frac{\theta_{\mathrm{SH}}\lambda}{l}(V_1^c - V_2^c)\tanh\frac{t}{2\lambda} \\ R_1^z &= \frac{\lambda}{\sigma w l}\mathrm{tanh}\frac{\mathrm{t}}{2\lambda} \\ R_2^z &= \frac{\lambda}{\sigma w l}\mathrm{csch}\frac{\mathrm{t}}{\lambda}, \end{aligned} \tag{2.11}$$

for z polarized spin and

$$\begin{aligned} V_0^y &= \frac{\theta_{\mathrm{SH}}\lambda}{l}(V_1^c - V_2^c)\tanh\frac{w}{2\lambda} \\ R_1^y &= \frac{\lambda}{\sigma t l}\mathrm{tanh}\frac{\mathrm{w}}{2\lambda} \\ R_2^y &= \frac{\lambda}{\sigma t l}\mathrm{csch}\frac{\mathrm{w}}{\lambda}, \end{aligned} \tag{2.12}$$

for y polarized spin. It is worth noting that SHE or ISHE in this material give rise to dependent current or voltage sources in Π or T circuit representations.

2.3 Application of Model 1

We are often interested in transport where charge and one particular type of spin flow occur. For the present discussion we focus on the spin current along $\hat{y}$ direction i.e., between terminals 3 and 4. For terminals 5 and 6 we can apply, for example, either by applying (a) floating boundary condition ($I_5^y = I_6^y = 0$) or (b) ground boundary condition ($V_5^y = V_6^y = 0$). Although these boundary conditions should be chosen to reflect the status of a given sample we assume the width of the sample (w) is wide enough to satisfy the condition of $w \gg \theta_{\mathrm{SH}}^2\lambda$ where these two boundary conditions give same result. We use boundary condition (b) on terminals 5 and 6 in the following discussion.

2.3.1 Spin Hall Effect (SHE)

In a typical SHE setup, charge current flows through GSHE material (between terminals 1 and 2 in Fig. 2.2(b)) and the spin voltage or current is measured at the top or bottom surface (terminal 3 or 4 in Fig. 2.2(c)). When we have terminals 3 and 4 open circuited ($I_3^z = I_4^z = 0$) in Fig. 2.2(c) the open circuit spin voltage ($V_4^z = -V_3^z$) is given by

$$V_4^z|_{I_3^z=I_4^z=0} = \frac{\theta_{\rm SH}}{2\sigma\theta_{\rm SH}^2 + \sigma\frac{t}{\lambda}\coth\frac{t}{2\lambda}}\frac{I_1^c}{w}, \tag{2.13}$$

in terms of $I_1^c = -I_2^c$ (see APPENDIX B) including $\theta_{\rm SH}^2$ correction term, which can be compared with standard results [32]. When we make terminal 3 open circuited ($I_3^z = 0$) and terminal 4 short circuited ($V_4^z = 0$) in Fig. 2.2(c) the short circuit spin current at terminal 4 (I_4^z) is given by

$$\left.\frac{I_4^z}{l}\right|_{V_4^z=0, I_3^z=0} = -\frac{\theta_{\rm SH}}{1 + \frac{\lambda\theta_{\rm SH}^2}{t}\tanh\frac{t}{\lambda}}\left(1 - \operatorname{sech}\frac{t}{\lambda}\right)\frac{I_1^c}{t}, \tag{2.14}$$

in terms of $I_1^c = -I_2^c$ (see APPENDIX B). The boundary condition $V_4^z = 0$ estimates the maximum spin current that can be collected at terminal 4. The degrading factor $1 - \operatorname{sech}(t/\lambda)$ has been noted previously [33].

2.3.2 Inverse Spin Hall Effect (ISHE)

In a typical ISHE setup, a spin current I_3^z is injected from terminal 3 with terminal 4 open circuited ($I_4^z = 0$) and charge voltage or current is measured across the terminals 1 and 2. Here we make terminals 1 and 2 open circuited ($I_1^c = I_2^c = 0$) in Fig. 2.2(b) to measure the open circuit charge voltage across terminals 1 and 2, which is given by

$$(V_1^c - V_2^c)|_{I_1^c=I_2^c=0} = \frac{\theta_{\rm SH}}{2\sigma\theta_{\rm SH}^2 + \sigma\frac{t}{\lambda}\coth\frac{t}{2\lambda}}\frac{I_3^z}{w}, \tag{2.15}$$

in terms of I_3^z (see APPENDIX B) with $\theta_{\rm SH}^2$ correction term as compared to standard results [34]. Terminals 1 and 2 can be connected together (i.e., $V_1^c = V_2^c$) to measure the short circuit charge current given by [35]

$$\left.\frac{I_1^c}{t}\right|_{V_1^c=V_2^c} = \theta_{\rm SH}\frac{\lambda}{t}\frac{I_3^z}{l}\tanh\frac{t}{2\lambda} \tag{2.16}$$

in terms of I_3^z (see APPENDIX B).

2.3.3 Spin Injection into Semiconductor (High Resistive Load)

Experimental work to date has focused on using GSHE material to inject spins into metallic materials with low resistivity. However, an important application of GSHE material in future could be in injecting spins into high resistivity materials like semiconductors where it is well known that high efficiency spin injection requires the use of tunneling barriers [39]. By contrast, our model predicts that efficient spin injection with GSHE material should be possible without the use of tunneling barriers since the GSHE material creates non-equilibrium spin voltage similar to spin pumping [40]. One can quantitatively analyze the spin injection from GSHE material using the T circuit in Fig. 2.2(c) for a structure shown in Fig. 2.3(a). The corresponding spin circuit in Fig. 2.3(b) assumes an ordinary spin diffusion channel for semiconductor that can be modeled as same circuit as GSHE material but with no spin voltage or current sources, which gives $R_L = \lambda_L \coth(t_L/\lambda_L)/(\sigma_L wl)$ with λ_L, t_L, and σ_L of semiconductor. For a relatively thick sample of GSHE material ($t > \lambda$) and semiconductor ($t_L > \lambda_L$) the source resistance ($R_1^z + R_2^z$) of GSHE material and semiconductor load resistance (R_L) per unit area ($w \times l$) are given by the value of λ/σ for each material. The spin voltage V_0^z is mostly dropped across the semiconductor load resistance since λ_L/σ_L of semiconductor is larger due to its longer spin diffusion length λ_L and lower conductivity σ_L compared to GSHE material. In the case of β-W the estimated spin voltage is $100\,\mu V$ with the parameters [41]: $J^c = \sigma(V_1^c - V_2^c)/l \simeq 10^7 \mathrm{A/cm}^2$ with $\theta_{\rm SH} \simeq 0.3$, $\lambda \simeq 1$ nm and $\sigma \simeq 0.004(\mu\Omega\mathrm{cm})^{-1}$.

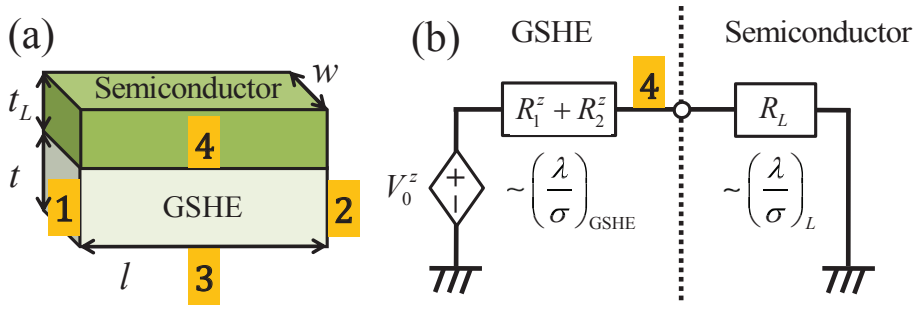

Fig. 2.3. (a) A schematic structure for spin injection into semiconductor from materials with giant spin Hall effect (GSHE) is shown. Note that there is no tunnel barrier at the interface. (b) The corresponding spin circuit representation is given based on the previous circuit model (Fig. 2.2(c)). The nonequilibrium spin voltage (V_o^z) generated from GSHE material is divided between GSHE source resistance ($R_1^z + R_2^z$) and spin resistance of semiconductor ($R_L = \lambda_L \coth(t_L/\lambda_L)/(\sigma_L t_L l)$).

2.3.4 Role of Ferromagnets as a Spin Ground (Low Resistive Load)

The large amount of spin current density generated by GSHE materials is of practical importance due to its ability to manipulate magnetization directions of the adjacent ferromagnetic layer. The maximum spin current density ($J_4^z = I_4^z/(wl)$) can be estimated by the short circuit spin current expression (Eq. (2.14)) given by $J_4^z \simeq -\theta_{\rm SH}\,(1-\mathrm{sech}(t/\lambda))\,J_1^c$ which is proportional to the applied charge current density ($J_1^c = I_1^c/(wt)$) with $\theta_{\rm SH}^2 \ll 1$ in a structure shown in Fig. 2.4(a). Reducing the thickness (t) of a GSHE sample is desirable so that less amount of total charge current I_1^c is required while maintaining same charge and spin current densities for a thick GSHE material ($t >> \lambda$). However as the thickness (t) is comparable to the spin diffusion length (λ) there is a degradation of spin current from a value $\theta_{\rm SH}J_1^c$ by a factor of $1-\mathrm{sech}(t/\lambda)$ [33][25]. Intuitively it is because of the fact that in GSHE material opposite spin polarizations accumulate at opposite surfaces. As the sample gets thinner, two surfaces start to interfere resulting in a cancellation of each spin polarization. This corresponds to the case of increasing G_2^z in Π equivalent spin circuit in Fig. 2.2(c) which connects two opposite surfaces so that two spin current sources start to cancel each other.

In this context the amount of spin current injected into one layer can be enhanced by suppressing the oppositely polarized spin current on the other surface using a low spin resistive load. For the purpose of demonstrating this concept, we have assumed a simple spin conductance for each top and bottom layer (see Fig. 2.4(a)) as G_T and G_B. Based on Π equivalent spin circuit as in Fig. 2.4(b), the spin current density injected into the top layer with the bottom layer is given by

$$J_4^z = G'_T J_0^z \frac{1 - G'_B \sinh\frac{t}{\lambda} - \cosh\frac{t}{\lambda}}{(G'_B + G'_T)\cosh\frac{t}{\lambda} + (1 + G'_B G'_T)\sinh\frac{t}{\lambda}}, \tag{2.17}$$

with $J_4^z = I_4^z/(lw)$, $J_0^z = I_0^z/(lw)$, $G'_T = G_T/(lw\sigma/\lambda)$, and $G'_B = G_B/(lw\sigma/\lambda)$ (see APPENDIX C).

Spin injection into the top layer with or without the bottom layer as a function of a GSHE sample thickness has been shown in Fig. 2.4(a). For a thin GSHE sample,

the spin injection into the top layer enhances significantly with the presence of a bottom layer. This further improves for higher spin conductance loads. The spin sink layer can be introduced by magnetic materials or impurities. In practice low (charge) conductivity or even insulating magnetic materials are desirable to avoid a charge current flow through FM layer. An encouraging experimental observation has been made using FeMn [42] layer whose conductivity is 10 times lower than GSHE material.

2.4 Model 2

2.4.1 Conductance Matrix

Previous conductance matrix (Eq. (2.7)) has terminals with either charge or one type of spin based on the uniform voltage assumptions given by Eq. (2.3). Although a large class of problems can be dealt with this conductance matrix, there are cases where we need to make use of all three components of spin polarizations as in the case of spin Hall magnetoresistance (SMR) which is explained in this section. To have an analytical conductance matrix we are interested in 1D uniform voltage assumptions as before and we modify the assumption in Eq. (2.3) as [36][28]

$$V^c \equiv V^c(x), \text{ and } V^{z,x,y} \equiv V^{z,x,y}(y) \tag{2.18}$$

to include the effect of spin voltage variations with all polarizations along $\hat{y}$ direction. As can be seen in Eq. (2.18) all charge and spin voltages are assumed to be uniform

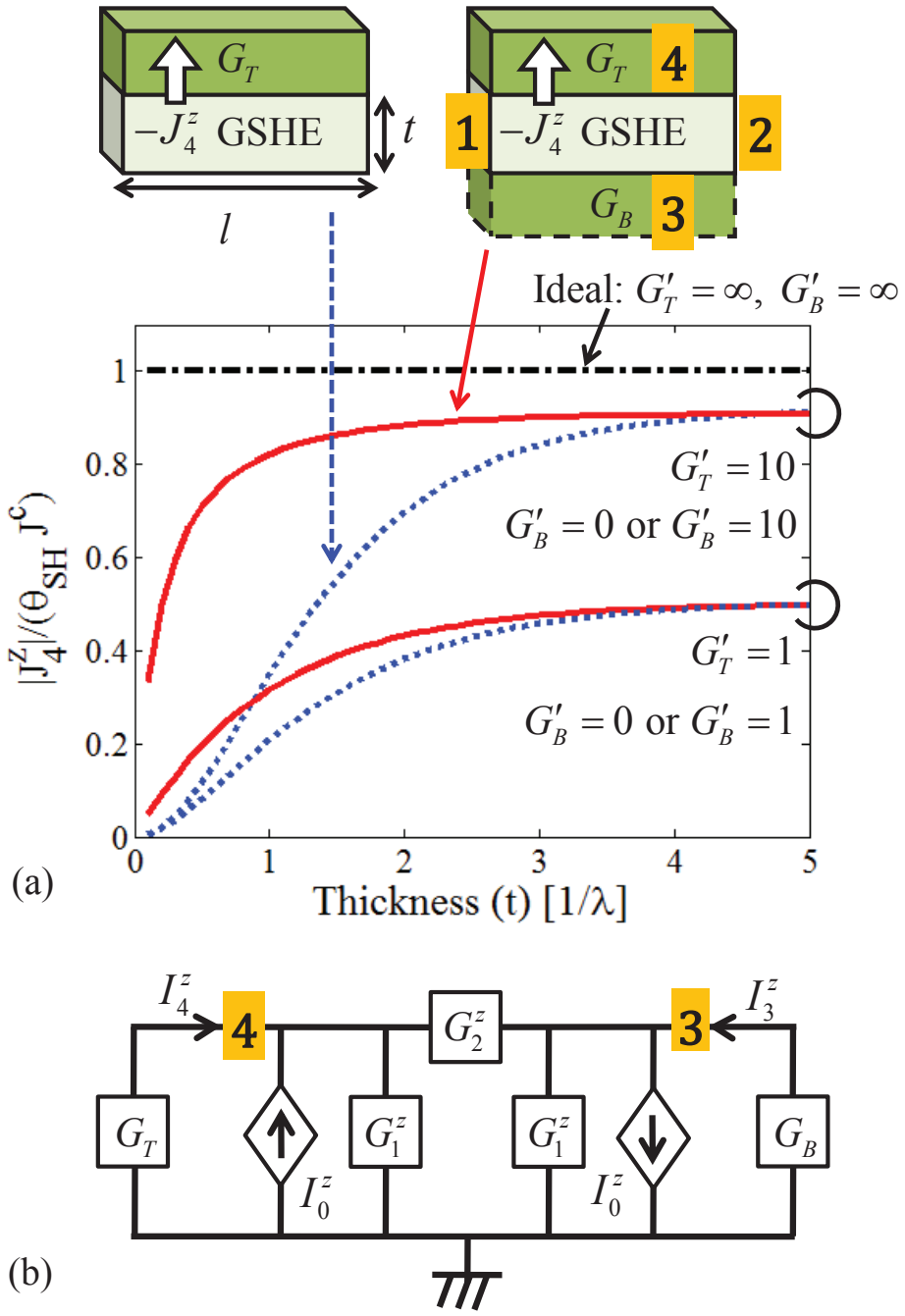

Fig. 2.4. (a) Demonstration of spin injection enhancement at the top layer by introducing spin ground at the bottom layer. Solid and dashed lines indicate spin current densities with and without the bottom layer, respectively. Note that G_T' and G_B' are G_T and G_B normalized by $lw\sigma/\lambda$ of GSHE material. This enhancement is more pronounced for a thin GSHE sample with $J^c = \sigma(V_1^c - V_2^c)/l$. (b) A corresponding spin circuit representation to the structure shown in (a). Top and bottom layers are included as loads at spin terminals 3 and 4 with spin conductances G_T and G_B.

along $\hat{z}$ direction. With this new assumptions (Eq. (2.18)) we obtain following conductance matrix for GSHE material as (see APPENDIX D)

$$\begin{pmatrix} I^c_{1,2} \\ I^z_{3,4} \\ I^x_{3,4} \\ I^y_{3,4} \\ I^c_{5,6} \\ I^y_{5,6} \end{pmatrix} = \begin{bmatrix} tw\frac{\sigma}{l}D & -w\sigma\theta_{\rm SH}D & 0 & 0 \\ w\sigma\theta_{\rm SH}D & lw\frac{\sigma}{t}S(t) & 0 & 0 \\ 0 & 0 & lw\frac{\sigma}{t}S(t) & 0 \\ 0 & 0 & 0 & lw\frac{\sigma}{t}S(t) \\ 0 & 0 & l\sigma\theta_{\rm SH}D & 0 \\ -t\sigma\theta_{\rm SH}D & 0 & 0 & 0 \end{bmatrix} \begin{pmatrix} V^c_{1,2} \\ V^z_{3,4} \\ V^x_{3,4} \\ V^y_{3,4} \end{pmatrix} \tag{2.19}$$

We can identify each 2×2 block matrix element of the above conductance matrix in a following way. The assumptions allow charge and spin diffusion along $\hat{x}$ and $\hat{y}$ directions respectively, which are represented by $tw\sigma D/l$ and three $lw\sigma S(t)/t$ block matrices respectively. Here the charge current along $\hat{x}$ direction and z polarized spin current along $\hat{y}$ direction are coupled by SHE and ISHE, as denoted by $w\sigma\theta_{\rm SH}D$ and $-w\sigma\theta_{\rm SH}D$ respectively. Finally, the charge voltage varying along $\hat{x}$ direction ($V^c_{1,2}$) can induce y polarized spin current along $\hat{z}$ direction given by $-t\sigma\theta_{\rm SH}D$ due to SHE and x polarized spin voltage varying along $\hat{y}$ direction ($V^x_{3,4}$) can generate charge current along $\hat{z}$ direction given by $l\sigma\theta_{\rm SH}D$ due to ISHE.

2.4.2 Circuit Representation

This conductance matrix (Eq. (2.19)) can be represented by equivalent circuits for charge and spin as shown in Fig. 2.5 which is similar to Fig. 2.2 but in this case we have a three component spin circuit where current or voltage sources are vectors with three component and conductances and resistances are 3×3 matrices. For charge transport each circuit element can be identified in a following way based on the conductance matrix (Eq. 2.19)

$$\begin{aligned} I^c_0 &= \beta_1 G_0 (V^z_3 - V^z_4) \\ G_0 &= \sigma tw/l \\ \beta_1 &= \theta_{\rm SH} l/t, \end{aligned} \tag{2.20}$$

from Fig. 2.5(b). Likewise, for spin transport circuit elements in the Π circuit of Fig. 2.5(c) are given by

$$\begin{aligned} \vec{I}_0^s &= \beta_1 G_0 (V_1^c - V_2^c) \begin{pmatrix} 1 \\ 0 \\ 0 \end{pmatrix} \\ [G_1] &= \frac{\sigma l w}{\lambda} \tanh \frac{\mathrm{t}}{2\lambda} [\mathrm{I}_{3\times 3}] \\ [G_2] &= \frac{\sigma l w}{\lambda} \mathrm{csch} \frac{\mathrm{t}}{\lambda} [\mathrm{I}_{3\times 3}], \end{aligned} \tag{2.21}$$

in $z - x - y$ basis with $[I_{3\times 3}]$ a 3×3 identity matrix. We can convert Π circuit for spins into T circuit in Fig. 2.5(c) by identifying each circuit element by

$$\begin{aligned} V_0^s &= \frac{\theta_{\mathrm{SH}} \lambda}{l} (V_1^c - V_2^c) \tanh \frac{t}{2\lambda} \begin{pmatrix} 1 \\ 0 \\ 0 \end{pmatrix} \\ [R_1] &= \frac{\lambda}{\sigma w l} \tanh \frac{\mathrm{t}}{2\lambda} [\mathrm{I}_{3\times 3}] \\ [R_2] &= \frac{\lambda}{\sigma w l} \mathrm{csch} \frac{\mathrm{t}}{\lambda} [\mathrm{I}_{3\times 3}]. \end{aligned} \tag{2.22}$$

Note that there are non-zero charge and spin currents flowing along $\hat{z}$ direction given by $I_z^c = I_5^c = -I_6^c$ and $I_z^y = I_5^y = -I_6^y$ which are not included in the equivalent circuit models in Fig. 2.5(b) and (c) but can be calculated once we know the charge and spin voltages at terminals $1 - 4$. Although we have non-zero currents (I_5, I_6) flowing through the surface 5 and 6 terminals cannot be defined at these surfaces since charge and all spin voltages vary in $x - y$ plane as can be seen from Fig. 2.5(a) with the voltage assumptions of Eq. (2.18).

2.5 Application of Model 2

The new conductance matrix (Eq. (2.19)) can be used to obtain standard results of spin Hall magnetoresistance (SMR) [36, 43, 44] which is characterized by the longitudinal and transverse resistivity (ρ_{xx} and ρ_{xz}) changes depending on the magnetization direction ($\hat{m}$) of ferromagnetic insulator (FMI) layer (yttrium iron garnet

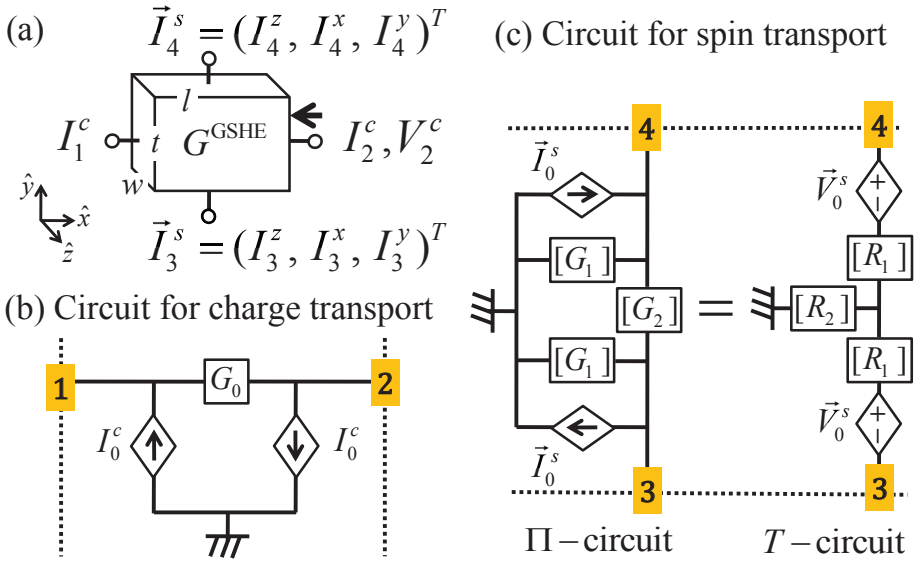

Fig. 2.5. (a) A rectangular structure of volume $l \times t \times w$ defining four terminals for G^{GSHE} in Fig. 2.1(d) is shown. There are two 1D transport : charge transport along $\hat{x}$ direction and all three components of spin transport along $\hat{y}$ direction. The structure is assumed to be uniform along $\hat{z}$ direction and can have charge and spin current along $\hat{z}$ direction. The equivalent circuit representation for 1D (b) charge transport and (c) spin transport are shown. Note that each element of spin circuit becomes a vector for current or voltage sources and a matrix for conductance or resistance as compared to Fig. 2.2(c) to accommodate three components of voltage and current at terminals 3 and 4 for spin.

or YIG) on top of GSHE material (Pt) as shown in Fig. 2.6(a). In this setup, the spin current flowing along $\hat{y}$ direction by SHE due to a charge current along $\hat{x}$ direction, gets absorbed and reflected with mixed spin polarizations at the Pt/YIG interface. The reflected spin current along $\hat{y}$ direction depends on the magnetization direction and gives rise to corrections to charge current along $\hat{x}$ and $\hat{z}$ directions by ISHE, thus affecting ρ_{xx} and ρ_{xz}. No charge current can flow through the ferromagnetic insulator (YIG) layer. Thus one can avoid various unwanted charge current induced effects and focus on pure spin current dependent phenomena in this set-up. We can rewrite the above conductance matrix (Eq. (2.19)) into a terminal basis form for our convenience as

$$\begin{pmatrix} I_1 \\ I_2 \\ I_3 \\ I_4 \\ I_5 \\ I_6 \end{pmatrix} = \begin{bmatrix} G_{11} & G_{12} & G_{13} & G_{14} \\ G_{21} & G_{22} & G_{23} & G_{24} \\ G_{31} & G_{32} & G_{33} & G_{34} \\ G_{41} & G_{42} & G_{43} & G_{44} \\ G_{51} & G_{52} & G_{53} & G_{54} \\ G_{61} & G_{62} & G_{63} & G_{64} \end{bmatrix} \begin{pmatrix} V_1 \\ V_2 \\ V_3 \\ V_4 \end{pmatrix} \tag{2.23}$$

where we use multi-component voltages or currents for V_3, V_4, I_3, I_4, I_5, I_6, and each G_{ij} is in general a matrix. The conductance matrix representation for YIG due to the interface properties between ferromagnetic insulator (YIG) and GSHE material uniform in the $x-z$ plane has been described by [36, 45]

$$\begin{pmatrix} I^z \\ I^x \\ I^y \end{pmatrix} = RG^{YIG}R^{+} \begin{pmatrix} V^z \\ V^x \\ V^y \end{pmatrix} = Rlw \begin{bmatrix} 0 & 0 & 0 \\ 0 & 2G_r & 2G_i \\ 0 & -2G_i & 2G_r \end{bmatrix} R^{+} \begin{pmatrix} V^z \\ V^x \\ V^y \end{pmatrix} \tag{2.24}$$

with its magnetization direction along $\hat{z}$ direction in $z-x-y$ basis and a rotation matrix R for a magnet along an arbitrary direction (see APPENDIX E). $2G_r = 2\mathrm{Re}G^{\uparrow\downarrow}$, and $2G_i = 2\mathrm{Im}G^{\uparrow\downarrow}$ where $G^{\uparrow\downarrow}$ represents spin mixing conductance. Conductance matrix for YIG mixes different polarizations of spin together and induces spin diffusion along y direction, as seen from Eq. (2.24). We can reconstruct the standard results [31, 36] for SMR directly from the conductance matrix. For this purpose we

apply charge voltages $V_1 \equiv V_1^c$ and $V_2 \equiv V_2^c$ at terminals 1 and 2 and then obtain expressions for I_1^c and I_5^c in the structure shown in Fig. 2.6(a) and (b), which can be used to get ρ_{xx} and ρ_{xz}. Our approach is described in Fig. 2.6(b) where two conductance matrices for GSHE and YIG are connected together by ordinary circuit rules for each charge and spin i.e. they share same voltages and satisfy current conservation at a given node. Thus at terminal 4 in Fig. 2.6(b), we have following equation

$$-I_4 = G^{YIG} V_4 \tag{2.25}$$

In this setup, terminal 3 is kept open circuited i.e. $I_3 = 0$. Voltages V_3 and V_4 can be obtained from Eqs. (2.23) and (2.25) as

$$\begin{pmatrix} V_3 \\ V_4 \end{pmatrix} = -\begin{bmatrix} G_{33} & G_{34} \\ G_{43} & G_{44} + G^{YIG} \end{bmatrix}^{-1} \begin{bmatrix} G_{31} & G_{32} \\ G_{41} & G_{42} \end{bmatrix} \begin{pmatrix} V_1 \\ V_2 \end{pmatrix} \tag{2.26}$$

Solving for V_3 and V_4 in Eq. (2.26) and putting them back into Eq. (2.23) gives expressions for charge current at terminals 1 and 5 (I_1^c and I_5^c) in terms of V_1^c and V_2^c, which are given by (see APPENDIX E)

$$\frac{I_1^c}{tw} = \frac{\sigma(V_1^c - V_2^c)}{l}\left[1 + \theta_{\rm SH}^2 \frac{\lambda}{t}\left\{2\tanh\left(\frac{t}{2\lambda}\right) - \left(1 - m_z^2\right)\mathrm{Re}F(t)\right\}\right] \tag{2.27}$$

$$\frac{I_5^c}{lt} = -\theta_{\rm SH}^2 \frac{\sigma\lambda(V_1^c - V_2^c)}{lt}\left(m_x m_z \mathrm{Re} + m_y \mathrm{Im}\right) F(t) \tag{2.28}$$

where

$$F(t) \equiv \frac{\frac{2\lambda(G_r + iG_i)}{\sigma}\tanh^2\left(\frac{t}{2\lambda}\right)}{1 + \frac{2\lambda(G_r + iG_i)}{\sigma}\coth\left(\frac{t}{\lambda}\right)} \tag{2.29}$$

with $\hat{m} = (m_z, m_x, m_y)$, which are same results [31, 36] obtained by directly solving diffusion equations.

2.6 Model 3

Previous discussions have been based on uniform voltage assumptions applied to a rectangular structure. In practice, these assumptions are not always valid due to various non-uniformities [8] in the structures and boundary conditions. One way

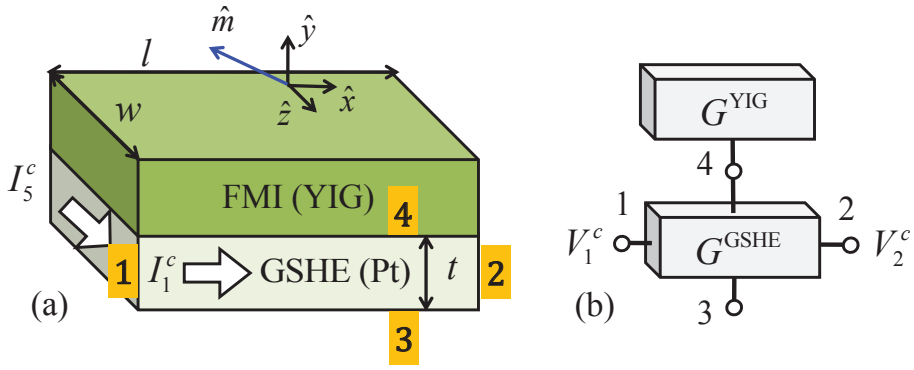

Fig. 2.6. (a) Schematic view of spin Hall magnetoresistance set-up consisting of ferromagnetic insulator (FMI) layer (yttrium iron garnet or YIG) placed on top of GSHE material (Pt) is shown, where longitudinal and transverse currents (I_1^c and I_5^c) are quantities of interest. (b) Conductance matrix representation for GSHE and YIG blocks connected together. Charge voltages V_1^c and V_2^c are applied for terminals 1 and 2 of GSHE block.

to approach this problem is to break an original structure into small and identical cubes of volume a^3 that can be represented by an elemental conductance matrix (see Fig. 2.7(a)). In this sense the elemental conductance matrix presented here can be also viewed as a discretization of Eqs. (2.1) and (2.2) applied to a cube of a^3. The conductance matrix for the original structure can be constructed by combining the elemental conductance matrices together. Here the rules for combining terminals are simple circuit laws for each charge and spin component. To combine i^{th} terminal of one block with j^{th} terminal from another block. we apply

$$V_i^\eta = V_j^\eta \text{ and } I_i^\eta + I_j^\eta = 0, \tag{2.30}$$

with $\eta = c, z, x, y$.

2.6.1 Circuit Representation

There can be multiple representations of the elemental conductance matrix, which is analogous to that we have different ways of discretizing continuum equations (Eqs. (2.1) and (2.2)). Here we first present our particular choice of circuit representation for a structure given in Fig. 2.7(a) which is then used to get the elemental conductance matrix. The resistances r_c, $[r_s]$, and $[r_{\rm sf}]$ are responsible for charge and spin diffusion where $[r_s] = r_s I_{3\times3}$ and $[r_{sf}] = (1/g_{\rm sf})I_{3\times3}$ are 3×3 matrices for three spin polarizations in $z - x - y$ basis. These resistance values are chosen in such a way that the given circuit gives correct analytical expression for ordinary 1D charge and spin diffusion between two confronting terminals when other four terminals are open circuited ($I_i^\eta = 0$), which gives

$$\frac{1}{r_c} = 2a\sigma,\ \frac{1}{r_s} = \frac{a^2\sigma}{\lambda}\coth\frac{a}{2\lambda},\ g_{\rm sf} = \frac{a^2\sigma}{\lambda}\sinh\frac{a}{\lambda}. \tag{2.31}$$

V_m^c and $\vec{V}_m^s = (V_m^z, V_m^x, V_m^y)^T$ represent voltages in the middle node of circuits for charge and spin. The dependent current sources for charge and spin are included to represent the physics of SHE and ISHE and given by

$$\begin{aligned} I_\alpha^c &= a\sigma\theta_{\mathrm{SH}}(V_3^z - V_4^z - (V_5^y - V_6^y)) \\ I_\beta^c &= a\sigma\theta_{\mathrm{SH}}(V_5^x - V_6^x - (V_1^z - V_2^z)) \\ I_\gamma^c &= a\sigma\theta_{\mathrm{SH}}(V_1^y - V_2^y - (V_3^x - V_4^x)), \end{aligned} \tag{2.32}$$

for charge and

$$\begin{aligned} \vec{I}_\alpha^s &= a\sigma\theta_{\mathrm{SH}} \begin{pmatrix} V_3^c - V_4^c \\ 0 \\ -(V_5^c - V_6^c) \end{pmatrix} \\ \vec{I}_\beta^s &= a\sigma\theta_{\mathrm{SH}} \begin{pmatrix} -(V_1^c - V_2^c) \\ V_5^c - V_6^c \\ 0 \end{pmatrix} \\ \vec{I}_\gamma^s &= a\sigma\theta_{\mathrm{SH}} \begin{pmatrix} 0 \\ -(V_3^c - V_3^c) \\ V_1^c - V_2^c \end{pmatrix}, \end{aligned} \tag{2.33}$$

for spin.

2.6.2 Conductance Matrix

The corresponding conductance matrix is given by

$$\begin{pmatrix} I^c \\ I^z \\ I^x \\ I^y \end{pmatrix} = G^E \begin{pmatrix} V^c \\ V^z \\ V^x \\ V^y \end{pmatrix} = \begin{bmatrix} G^{cc} & G^{cz} & G^{cx} & G^{cy} \\ G^{zc} & G^{zz} & 0 & 0 \\ G^{xc} & 0 & G^{xx} & 0 \\ G^{yc} & 0 & 0 & G^{yy} \end{bmatrix} \begin{pmatrix} V^c \\ V^z \\ V^x \\ V^y \end{pmatrix} \tag{2.34}$$

where $I^\eta = (I_1^\eta, I_2^\eta, ..., I_6^\eta)^T$, $V^\eta = (V_1^\eta, V_2^\eta, ..., V_6^\eta)^T$ with $\eta = c, z, x, y$ reflecting six terminals for six surfaces of the cubic element. Charge diffusion block G^{cc} in Eq.

(2.34) is determined from the resistor network with r_c shown in Fig. 2.7(b) and given by

$$[G^{cc}] = A \begin{bmatrix} 5 & -1 & -1 & -1 & -1 & -1 \\ -1 & 5 & -1 & -1 & -1 & -1 \\ -1 & -1 & 5 & -1 & -1 & -1 \\ -1 & -1 & -1 & 5 & -1 & -1 \\ -1 & -1 & -1 & -1 & 5 & -1 \\ -1 & -1 & -1 & -1 & -1 & 5 \end{bmatrix} \tag{2.35}$$

where $A = 1/(6r_c)$. Similarly spin diffusion blocks $G^{zz,xx,yy}$ in Eq. (2.34) are determined from the resistor network with r_s and g_{sf} shown in Fig. 2.7(c) and given by

$$[G^{zz,xx,yy}] = \begin{bmatrix} C & -B & -B & -B & -B & -B \\ -B & C & -B & -B & -B & -B \\ -B & -B & C & -B & -B & -B \\ -B & -B & -B & C & -B & -B \\ -B & -B & -B & -B & C & -B \\ -B & -B & -B & -B & -B & C \end{bmatrix} \tag{2.36}$$

where $B = (2 + r_s g_{\mathrm{sf}})/(r_s(6 + r_s g_{\mathrm{sf}}))$ and $C = B(5 + r_s g_{\mathrm{sf}})$.

The ISHE blocks ($G^{cz},\ G^{cx},\ G^{cy}$) and SHE blocks ($G^{zc},\ G^{xc},\ G^{yc}$) are given by

$$[G^{cz}] = -[G^{zc}]^T = a\sigma\theta_{\rm SH}\begin{bmatrix} 0 & -D & 0 \\ D & 0 & 0 \\ 0 & 0 & 0 \end{bmatrix}$$

$$[G^{cx}] = -[G^{cx}]^T = a\sigma\theta_{\rm SH}\begin{bmatrix} 0 & 0 & 0 \\ 0 & 0 & -D \\ 0 & D & 0 \end{bmatrix} \tag{2.37}$$

$$[G^{cy}] = -[G^{yc}]^T = a\sigma\theta_{\rm SH}\begin{bmatrix} 0 & 0 & D \\ 0 & 0 & 0 \\ -D & 0 & 0 \end{bmatrix},$$

which give rise to source terms at each terminal in the elemental block as in the previous case of Fig. 2.2 and 2.5. The elemental conductance matrix satisfies following important constraints among its components:

1. Time reversal invariance requires the following reciprocity [38]:

$$G^{cc}_{ij} = G^{cc}_{ji},\ G^{ss}_{ij} = G^{ss}_{ji},\ \text{and}\ G^{cs}_{ij} = -G^{sc}_{ji} \tag{2.38}$$

without external magnetic fields with spin index $s = z, x, y$. As noted before there is an additional negative sign [37, 38] in the components of conductance matrix which couples charge and spin.

2. Current conservation requires the following sum rules.

$$\begin{aligned} \sum_i G^{cc}_{ij} &= 0 \text{ for each } j \\ \sum_i G^{cs}_{ij} &= 0 \text{ for each } j. \end{aligned} \tag{2.39}$$

This ensures that the charge current from all terminals add up to zero. Eqs. (2.38) and (2.39) also imply that

$$\sum_i G^{sc}_{ji} = 0 \text{ for each } j. \tag{2.40}$$

This ensures that at equilibrium (V_k^c = constant and $V_k^s = 0$ for all terminals) there is zero spin current at all terminals. Note that there are considerable discussion and debate regarding the equilibrium spin current in materials with high spin orbit coupling (see for example [46, 47]).

2.7 Reduction of Model 3 to Model 1 and Model 2

2.7.1 From Model 3 to Model 1

In principle, the elemental conductance matrix can be combined together to give a conductance matrix for an arbitrary structure of interest. As an illustrative example we reduce it into the previous analytical conductance matrix of Eq. (2.7) using the same voltage assumptions given by Eq. (2.3). First, the assumption $V^c \equiv V^c(x)$ applied to the resistor network in Fig. 2.7(b) gives

$$V_3^c = V_4^c = V_5^c = V_6^c = V_m^c = \frac{V_1^c + V_2^c}{2} \tag{2.41}$$

Likewise with the assumptions $V^z \equiv V^z(y)$ and $V^y \equiv V^y(z)$ applied to the resistor network in Fig. 2.7(c) we obtain

$$V_1^z = V_2^z = V_5^z = V_6^z = \frac{V_3^z + V_4^z}{2 + r_s g_{\rm sf}} \tag{2.42}$$

$$V_1^y = V_2^y = V_3^y = V_4^y = \frac{V_3^y + V_4^y}{2 + r_s g_{\rm sf}} \tag{2.43}$$

Finally, $V^x \equiv$ constant gives

$$V_1^x = V_2^x = V_3^x = V_4^x = V_5^x = V_6^x = V_m^x \tag{2.44}$$

Based on Eqs. (2.41)-(2.44) we can reduce the conductance matrix of Eq. (2.34) into a following one after collecting all non-zero currents

$$\begin{pmatrix} I_{1,2}^c \\ I_{3,4}^z \\ I_{5,6}^y \end{pmatrix} = \begin{bmatrix} a\sigma D & -a\sigma\theta_{\rm SH} D & a\sigma\theta_{\rm SH} D \\ a\sigma\theta_{\rm SH} D & a\sigma S(a) & 0 \\ -a\sigma\theta_{\rm SH} D & 0 & a\sigma S(a) \end{bmatrix} \begin{pmatrix} V_{1,2}^c \\ V_{3,4}^z \\ V_{5,6}^y \end{pmatrix} \tag{2.45}$$

which is the conductance matrix of Model 1 (Eq. (2.7)) with $l = t = w = a$.

2.7.2 From Model 3 to Model 2

Similarly from the voltage assumption of Eq. (2.18) we have

$$\begin{aligned} V_3^c = V_4^c = V_5^c = V_6^c = V_m^c = \frac{V_1^c + V_2^c}{2} \\ V_1^{z,x,y} = V_2^{z,x,y} = V_5^{z,x,y} = V_6^{z,x,y} = \frac{V_3^{z,x,y} + V_4^{z,x,y}}{2 + r_s g_{\rm sf}} \end{aligned} \tag{2.46}$$

Using Eq. (2.46) we can express the conductance matrix of Eq. (2.34) with respect to V_1^c, V_2^c, $V_3^{z,x,y}$, and $V_4^{z,x,y}$, which is given by

$$\begin{pmatrix} I_{1,2}^c \\ I_{3,4}^z \\ I_{3,4}^x \\ I_{3,4}^y \\ I_{5,6}^c \\ I_{5,6}^y \end{pmatrix} = \begin{bmatrix} a\sigma D & -a\sigma\theta_{\rm SH} D & 0 & 0 \\ a\sigma\theta_{\rm SH} D & a\sigma S(t) & 0 & 0 \\ 0 & 0 & a\sigma S(t) & 0 \\ 0 & 0 & 0 & a\sigma S(t) \\ 0 & 0 & a\sigma\theta_{\rm SH} D & 0 \\ -a\sigma\theta_{\rm SH} D & 0 & 0 & 0 \end{bmatrix} \begin{pmatrix} V_{1,2}^c \\ V_{3,4}^z \\ V_{3,4}^x \\ V_{3,4}^y \end{pmatrix} \tag{2.47}$$

which is the conductance matrix of Model 2 (Eq. (2.19)) with $l = t = w = a$.

2.8 Conclusion

We have proposed conductance matrix or equivalent circuit representation for materials with SHE based on the standard semi-classical equations. This not only extends previous four component circuit model to include materials with SHE but also provides a modular approach for various structures involving these materials which are becoming important ingredients in spintronic applications. We provide three types of conductance matrices with an increasing level of complexity in boundary conditions. These conductance matrices can straightforwardly reconstruct the standard results in SHE, ISHE and SMR in the literature. Furthermore we discuss two new examples of spin injection where the circuit representation provides simple models to understand; one for spin injection into semiconductors with GSHE materials and the other one for an enhancement of spin injection by introducing a spin ground on the opposite

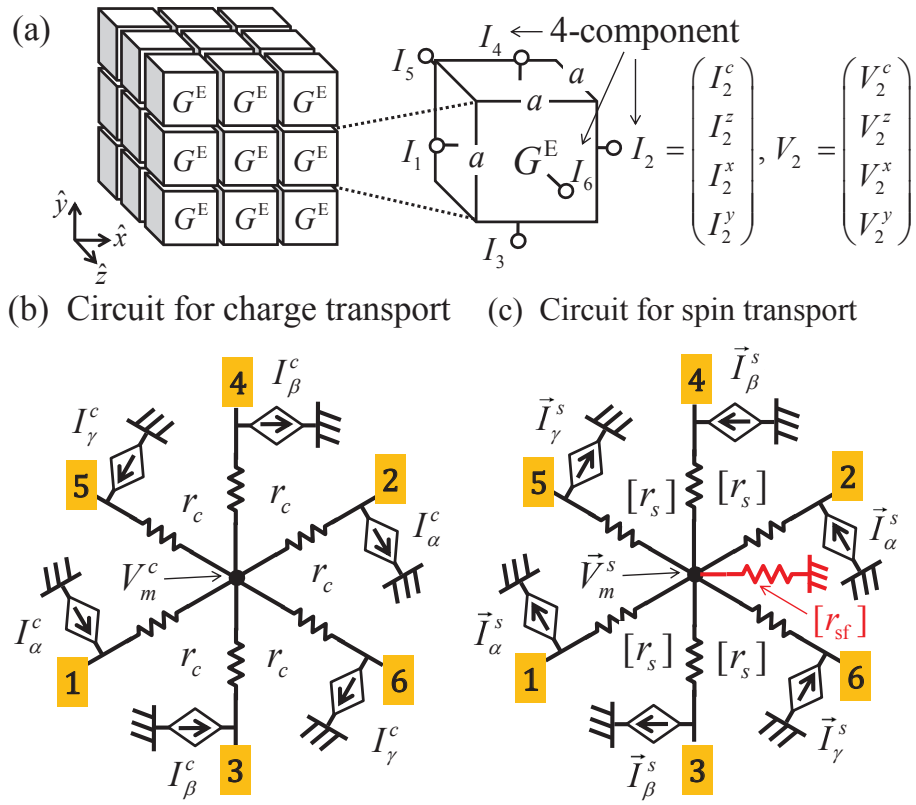

Fig. 2.7. (a) An arbitrary structure can be broken into small and identical cubes of volume a^3 and each of them is represented by an elemental conductance matrix (G^E). This conductance matrix has six terminals, each of which has voltage and current with 4-component (1 charge and 3 spins). (b) Circuit representation for charge transport is shown with six resistances (r_c) and six dependent current sources (I_α^c, I_β^c, I_γ^c). V_m^c denotes a voltage in the middle node of the circuit. (c) Circuit representation for spin transport is shown with six resistances ($[r_s]$) and six dependent current sources ($\vec{I}_\alpha^s$, $\vec{I}_\beta^s$, $\vec{I}_\gamma^s$). Note that each circuit element has three components due to spin polarizations and $[r_{sf}]$ is included for spin relaxation in the channel.

layer of GSHE materials. Finally an elemental conductance matrix is presented for a small cube that can be used to build any arbitrarily shaped structure, making it suitable for numerical modeling.

3. SPIN VOLTAGE GENERATION BY CURRENT FLOW IN 2D CHANNELS [EXCERPTED FROM PHYS. REV. B 86, 085131]

The contents of this chapter have been extracted and revised from the following publication: Seokmin Hong, Vinh Diep, Supriyo Datta, and Yong P. Chen, "Modeling potentiometric measurements in topological insulators including parallel channels," *Phys. Rev. B* 86, 085131 (2012).

3.1 Motivation for 3-terminal Structure in Topological Insulator

Following the discovery of spin-polarized states at the surface of three-dimensional topological insulators (TI) like Bi_2Te_3 and Bi_2Se_3 (see, for example, Refs. [9], [10] and references therein), there is intense interest in possible electrical measurements demonstrating unique signatures of these unusual states [48–50]. A recent interesting proposal [51] suggests that a unique signature of TI material should be a change in the conductance measured between a normal contact and a ferromagnetic (FM) contact when the magnetization of the latter is reversed. We believe that in order to observe this effect it is important to use a multi-terminal measurement in the linear response regime. Any two-terminal resistance measurement using magnetic contacts on a material described by a time reversal invariant (TRI) Hamiltonian should obey a generalized Onsager relation of the form $R(\vec{M}) = R(-\vec{M})$ (see, for example [52–54] and references therein) with $\vec{M}$ being a magnetization in the linear response regime. For multi-terminal measurements, Onsager relation requires that $R_{ab,cd}(\vec{M}) = R_{cd,ab}(-\vec{M})$ where the first and second pair of indices are used to denote contacts to supply current and measure the voltage difference respectively. However, there is no requirement for $R_{ab,cd}(\vec{M})$ to equal $R_{ab,cd}(-\vec{M})$. Indeed in this paper we

will show how the quantity $R_{12,13}(\vec{M}) - R_{12,13}(-\vec{M})$ measured using a specific three-terminal (3T) potentiometric set-up [53] with $R_{12,13}(\vec{M}) = V(\vec{M})/I$ (Fig. 3.1(a)) can be related to the spin orientation of the eigenstates of the channel.

We establish this result starting from a quantitative Non-Equilibrium Green's Function (NEGF) based model that allows us to (1) go seamlessly from the ballistic to the diffusive limits and (2) include multiple conduction paths described by different Hamiltonians that may be in parallel with the TI channel. We will show that the numerical results from the NEGF model can be described well by the following expression, which we will also justify using simple physical arguments.

$$(V(\vec{M}) - V(-\vec{M}))/I = R_B(\vec{p} \cdot \vec{m}), \tag{3.1}$$

with

$$\vec{p} = \frac{\sum_i \sum_{v_x(\vec{k})>0} \hat{s}_i(\vec{k})\delta(E_F - \epsilon_i(\vec{k}))}{\sum_i \sum_{v_x(\vec{k})>0} \delta(E_F - \epsilon_i(\vec{k}))}, \tag{3.2}$$

where $1/R_B$ is a ballistic conductance of the channel which is given by q^2/h time the number of modes or conducting channels $\sim k_F W/\pi$ for each Fermi circle (k_F: Fermi wave number, W: width of channel) and E_F is the Fermi energy. The effective magnet polarization is represented by $P_{FM} = (G_M - G_m)/(G_M + G_m)$ which defines $\vec{m} = P_{FM}\hat{M}$ with $G_{M(m)}$ being the contact conductance for majority (minority) spins and I is the applied current along the x direction. The channel property $\vec{p}$ can be viewed as the degree of the spin polarization per unit current in the x direction and applies to arbitrary dispersion $\epsilon_i(\vec{k})$ and spin orientation $\hat{s}_i(\vec{k})$ including combinations of TI surface states (TI SS) channels and Rashba spin orbit coupling (SOC) materials (Fig. 3.2) each represented by a channel index i. The quantity $\vec{p}$ provides a measure of the average spin polarization of all states with positive group velocity ($v_x(\vec{k}) = \partial\epsilon/\hbar\partial k_x > 0$) which for TRI material is the negative of the average spin polarization of states with negative group velocity. As a result there is no spin polarization at equilibrium, but there is a current induced spin polarization, as discussed in the

literature (see, for example, Refs. [55], [56]). If we reverse the current, I, the measured voltage, $V(\vec{M}) - V(-\vec{M})$ will also reverse.

Two points : (1) The above expression is valid both in the ballistic and diffusive limits, which, we will show, is supported by NEGF results. (Fig. 3.3).

(2) To the best of our knowledge, this type of signal has not been observed in TI yet but it has been experimentally confirmed in Rashba SOC materials [57]. The expression given here applied to Rashba channel is consistent with the one that has been used in the past to describe experimental results quantitatively [58].

In order to ensure that the potentiometric set-up measure a channel property ($\vec{p}$) in a minimally invasive way, it is advisable to use a weakly coupled contact, which also enhances the signal as seen in experimental work on Rashba SOC materials [59, 60].

3.2 Model Description

For the two dimensional (2D) top surface of a three dimensional TI, we adopt the following model Hamiltonian on a discrete lattice:

$$\begin{aligned} H_{TISS} &= \frac{\hbar v_F}{a}[\sigma_x sin(k_y a) - \sigma_y sin(k_x a) \\ &- \sigma_z(cos(k_x a) + cos(k_y a) - 2)], \end{aligned} \tag{3.3}$$

where the $\vec{\sigma}s$ are the Pauli spin matrices, a is the lattice spacing and v_F is the Fermi velocity. The additional σ_z term is added to avoid fermion doubling problem on a discrete lattice (see, Ref. [61] and references therein). Although this term breaks time reversal symmetry it is smaller than the first two terms by a factor (ka) around $k = 0$ and we have checked that all numerical results presented here are not affected if we change a or the sign of the σ_z term.

For 2D Rashba SOC materials we use the standard form for H:

$$H_{Rashba} = \frac{\hbar^2}{2m}(k_x^2 + k_y^2)I_2 + \alpha(\sigma_x k_y - \sigma_y k_x), \tag{3.4}$$

where I_2 is 2 by 2 identity matrix and α is a Rashba SOC strength.

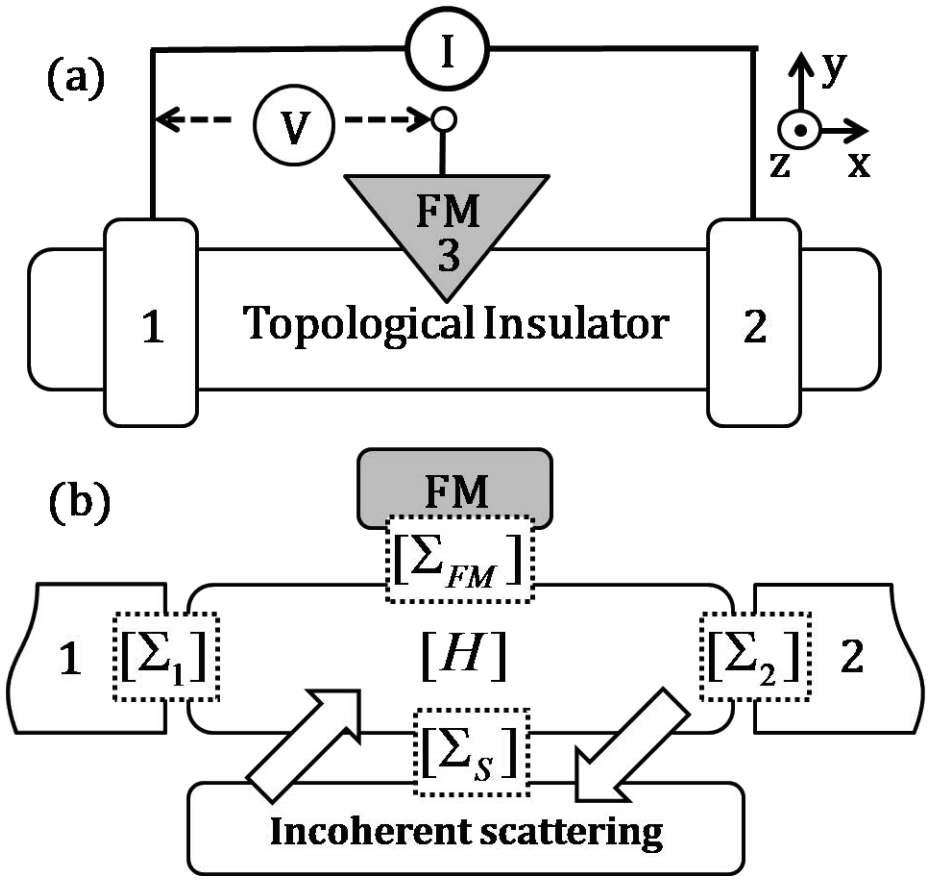

Fig. 3.1. (a) Schematic view of three-terminal potentiometric set-up with two current probes (1 and 2) and one FM voltage probe (3). (b) NEGF model : Hamiltonian (H) with four different self energies. Σ_1 and Σ_2 are used to model contacts 1 and 2. Σ_{FM} is used to model a FM contact. Σ_S is responsible for incoherent processes in the diffusive limit.

The sign of $(\hat{s} \times \vec{k})_z$ for a given Fermi circle depends on whether $\hat{z}$ is chosen as the outward or inward normal to the surface. We have chosen it as the outward normal, which makes α in Eq. (3.4) and $\hbar v_F$ in Eq. (3.3) positive, based on the experimental results [62, 63].

We model the two contacts 1 and 2 as semi infinite left and right contacts (Fig. 3.1(b)) and their self energies are described by $\Sigma_{1(2)} = \tau_{1(2)} g_s \tau^{\dagger}_{1(2)}$ where τ is a coupling matrix between the contact and the channel and g_s is the surface Green's function of each

contact. Contact 3 is modeled with $\Sigma_{FM} = -i\gamma/2(I_2 + \vec{m}\cdot\vec{\sigma}) \otimes I_w$ where we use a value of $\gamma \ll \hbar v_F/a$ to simulate a weakly coupled probe. γ represents the strength of the coupling of the contact and I_w is an identity matrix whose size is same as the width of the channel with $\otimes$ a tensor product.

The incoherent scattering is included through self energies Σ_s in the self consistent Born approximation. We assume isotropic momentum randomizing scattering along with two types of spin scatterings. Following the notations in Ref. [64], the momentum randomizing scattering is described by

$$[\Sigma_s, \Sigma_s^{in}]_{ij} = d_m \delta_{ij}\delta_{ik}\delta_{jl}[G, G^n]_{kl}, \tag{3.5}$$

where i, j, k and l are real space indices. The spin preserving and spin randomizing scattering [64] are described by

$$[\Sigma_s, \Sigma_s^{in}]_{ab} = \delta_{ac}\delta_{bd}[G, G^n]_{cd}, \tag{3.6}$$

and

$$[\Sigma_s, \Sigma_s^{in}]_{ab} = (\vec{\sigma}_{ac}\cdot\vec{\sigma}_{db})[G, G^n]_{cd}, \tag{3.7}$$

respectively where a, b, c and d are used to indicate spin indices.

The charge current I between contact 1 and 2 is calculated assuming $f_1 = 1$ and $f_2 = 0$ where f_j is the occupation factor for contact j. The value of f_3 of a FM contact is a quantity of interest for subsequent discussions. For coherent transport it is common to write $I_i \sim \sum_j \overline{T}_{ij}(f_i - f_j)$, obtaining $\overline{T}_{ij}$ from $Trace[\Gamma_i G \Gamma_j G^\dagger]$ and then solve for $I_1 = -I_2 = I$ and f_3 assuming $f_1 = 1$, $f_2 = 0$ and $I_3 = 0$ [65]. However, with incoherent scattering present there is no simple expression for $\overline{T}_{ij}$ and we evaluate these coefficients numerically using $\overline{T}_{ij} = -\partial I_i/\partial f_j$.

3.3 Results for Ballistic and Diffusive Channels

The NEGF method described in the previous section is quite general but we focus here on a weakly coupled FM contact that does not perturb the channel properties appreciably. By setting $I = 0$ in the NEGF equation [65] for current ($I \sim (Trace[\Gamma A]f -$

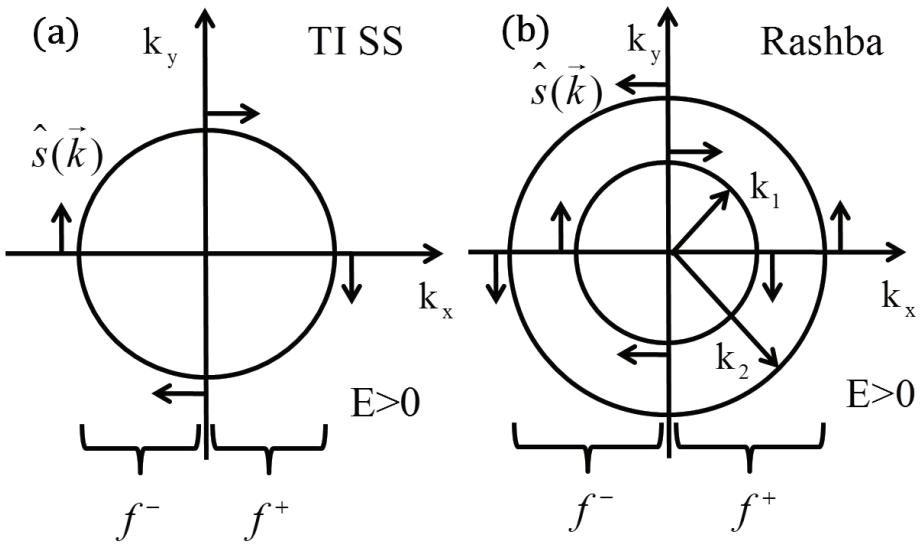

Fig. 3.2. Schematic view of Fermi circles at a given energy for (a) TI SS and (b) Rashba materials from a given dispersion relation $\epsilon_i(\vec{k})$ with positive $\hbar v_F$ and α. The occupation factors for positive and negative propagating states are given by f^+ and f^- respectively. Arrows are unit vectors representing the spin direction $\hat{s}_i(\vec{k})$ of each eigenstate.

$Trace[\Gamma G^n]$)), we can write f for the given probe as $Trace[\Gamma G^n]/Trace[\Gamma A]$ in the limit of $\gamma \to 0$. For a given energy E_F we first plot the occupation factor of contact 3 ($f_3(\vec{m})$) for two cases of $\vec{m}(= \hat{y}, -\hat{y})$ by continuously moving it point by point along the current flow direction. As shown Fig. 3.3 (a) and (b) for TI SS and Rashba channels, with non-zero slopes when spin randomizing scattering processes are included in the channel. The slope of each line is proportional to the magnitude of d_m (see Eq. (3.5)) and can be related to the conventional ohmic drop due to momentum relaxation processes [65]. When we compare f_3 with two opposite magnet directions $\hat{y}$ and $-\hat{y}$ there is a noticeable splitting between them, which is uniform along the channel and this is true for both ballistic and diffusive transport limits with spin preserving/randomizing scattering. In the small bias and low temperature limit NEGF

results at a single energy can be related to the experimentally measurable quantities using the following expression,

$$\frac{V(\vec{m}) - V(-\vec{m})}{I} = \frac{1}{(q^2/h)\overline{T}(E)} \frac{f_3(\vec{m}) - f_3(-\vec{m})}{f_1 - f_2}, \tag{3.8}$$

obtained by combining $f_3(\vec{m}) - f_3(-\vec{m}) = (-\partial f_0/\partial E)(\mu_3(\vec{m}) - \mu_3(-\vec{m}))$ with $I = (q/h)\overline{T}(E)(\mu_1 - \mu_2)$, μ_j being the chemical potential of contact j and f_0, the Fermi function in equilibrium. This resistance value is, in general, energy dependent but is relatively independent of whether we are in the ballistic or diffusive limits. Fig. 3.3(c) shows the values of $\vec{p}$ deduced from the numerically calculated $(V(\vec{m}) - V(-\vec{m}))/I$ using Eq. (3.1), which are labeled 'NEGF'. These agree well with the lines obtained from the analytical expressions in Eq. (3.2) which we will now justify.

3.4 Discussion

The occupation factor for the FM contact which draws no net charge current is given by

$$f_3(\vec{m}) = \frac{\sum_i \sum_{\vec{k}} f(\vec{k})(1 + \vec{m} \cdot \hat{s}_i(\vec{k}))\delta(E - \epsilon_i(\vec{k}))}{\sum_i \sum_{\vec{k}} (1 + \vec{m} \cdot \hat{s}_i(\vec{k}))\delta(E - \epsilon_i(\vec{k}))}, \tag{3.9}$$

assuming that the current due to each state $\vec{k}$ is $(f_3(\vec{m}) - f(\vec{k}))(1 + \vec{m} \cdot \hat{s}_i(\vec{k}))$. This gives

$$f_3(\vec{m}) - f_3(-\vec{m}) = \vec{m} \cdot \frac{\sum_i \sum_{\vec{k}} f(\vec{k})\hat{s}_i(\vec{k})\delta(E - \epsilon_i(\vec{k}))}{\sum_i \sum_{\vec{k}} \delta(E - \epsilon_i(\vec{k}))/2}, \tag{3.10}$$

assuming $\sum_i \sum_{\vec{k}} \hat{s}_i(\vec{k})\delta(E - \epsilon_i(\vec{k})) = 0$, which is true for TRI Hamiltonian since each time reversal pair is composed of two opposite spins and group velocities $(\epsilon_i(\vec{k}, \hat{s}_i(\vec{k})) = \epsilon_i(-\vec{k}, -\hat{s}_i(\vec{k}))$. Assuming that the occupation factor $f(\vec{k})$ equals f^+, f^- for states with positive and negative group velocities respectively, we obtain

$$\frac{f_3(\vec{m}) - f_3(-\vec{m})}{f^+ - f^-} = \vec{p} \cdot \vec{m}, \tag{3.11}$$

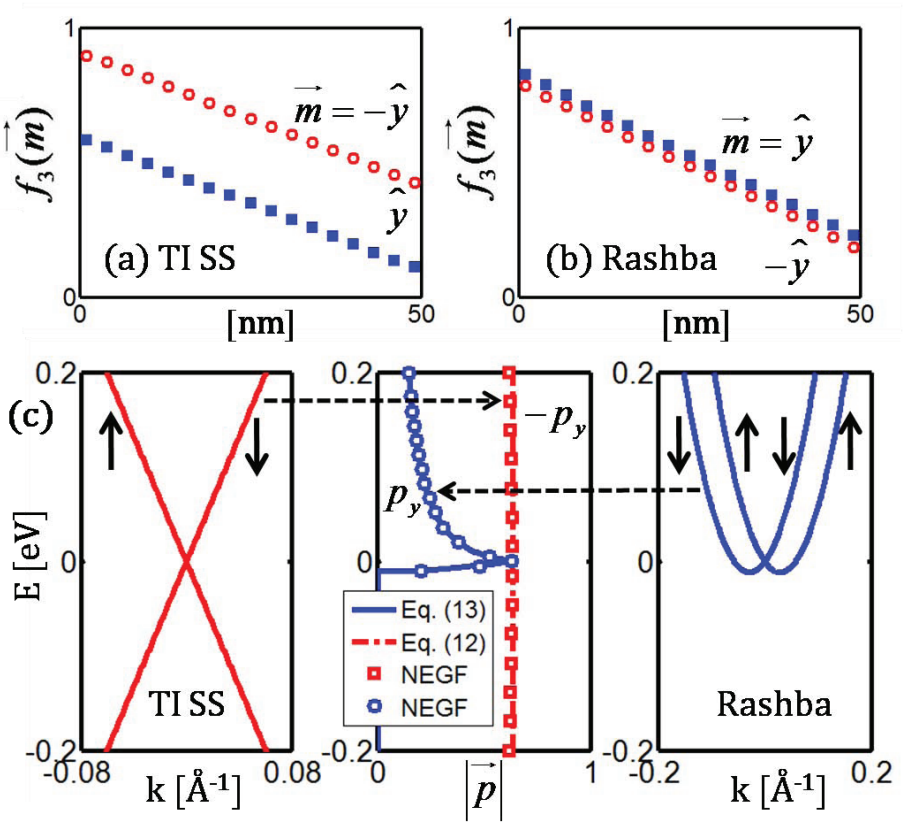

Fig. 3.3. Results of NEGF and simple expressions (3.12) and (3.13). Occupation factor ($f_3(\vec{m})$) along the length the channel when there is a charge current in the diffusive limit (spin randomizing) for the case of (a) TI SS ($E_F = 0.2$ eV, $d_m = 3 \times 10^{-3}$ eV^2) and (b) Rashba channel ($E_F = 0.3$ eV, $d_m = 10^{-3}$ eV^2) with $a = 10$ Å, width= 50 nm. Two cases of $\vec{m}$ ($= \hat{y}$, $-\hat{y}$) are plotted. (c) The magnitude of $\vec{p}$ between TI SS and Rashba channel as a function of energy with their dispersion relations. The NEGF result in (c) assumed a ballistic transport and periodic boundary condition along the width direction. Parameters: $\hbar v_F = 3.3$ eVÅ, $m = 0.28m_e$, $\alpha = 0.79$ eVÅ [66].

where we have made use of the fact that in TRI material the factor $\vec{p}$ defined in Eq. (3.2) for positive group velocity states is the negative of that for for negative group velocity states. We can recover Eq. (3.1) by noting that $I(E)/(f^+ - f^-)$ is same as q/h times the number of conducting channels [65]. It also suggests that the

signal is relatively independent of scattering processes in the channel since the above argument is applicable to both ballistic and diffusive limits.

3.4.1 Topological Insulator Surface States (TISS) Channel

We can evaluate the expression $\vec{p}$ in Eq. (3.2) in the case of TI SS based on, for example, $\epsilon(\vec{k}) = |\hbar v_F k|$ and $\hat{s}(\vec{k}) = \text{sgn}(\hbar v_F)(\hat{x}sin\theta - \hat{y}cos\theta)$ when $\epsilon > 0$ from the TI SS Hamiltonian (3.3) as shown in Fig. 3.2(a) with $tan\theta = k_y/k_x$. Using these, one can get

$$\vec{p}(E) = \text{sgn}(\hbar v_F)(0, -2/\pi, 0). \tag{3.12}$$

As defined, $\vec{p}$ represents the intrinsic spin polarization of the channel of current carrying electrons and $2/\pi$ comes from an angular averaging of 2D electrons. Since $\vec{p}$ is a vector along the y-axis Eq. (3.1) suggests that the signal is maximum when the magnet points along the y direction in the plane of the TI SS.

3.4.2 Rashba Channel

The same procedure can be applied to materials with Rashba SOC using, for example, $\epsilon(\vec{k}) = \hbar^2 k^2/2m \pm \alpha k$ and $\hat{s}(\vec{k}) = \text{sgn}(\alpha)(\pm\hat{x}sin\theta \mp \hat{y}cos\theta)$ when $\epsilon > 0$ with $tan\theta = k_y/k_x$ from the Rashba Hamiltonian (3.4). Upper and lower signs represent inner and outer Fermi circles respectively as shown in Fig. 3.2(b). Following the same procedure, one can get

$$\vec{p}(E) = \text{sgn}(\alpha)(0, \frac{2}{\pi}\frac{k_2 - k_1}{k_2 + k_1}, 0) = \tag{3.13}$$
$$\text{sgn}(\alpha) \begin{cases} (0, (2/\pi)(1 + 2E\hbar^2/m\alpha^2)^{-1/2}, 0), & \text{if } E \geq 0, \\ (0, (2/\pi)(1 + 2E\hbar^2/m\alpha^2)^{1/2}, 0), & \text{if } E \leq 0, \end{cases}$$

where k_1 and k_2 are inner and outer radius of Fermi circles respectively. Note that (1) Even Rashba channels give nonzero $\vec{p}(E)$ as demonstrated earlier (see, for example, [57,58]) (2) Both Eq. (3.13) for Rashba and Eq. (3.12) for TI SS come out of the same general result stated earlier in Eq. (3.2). The polarization for Rashba is reduced with

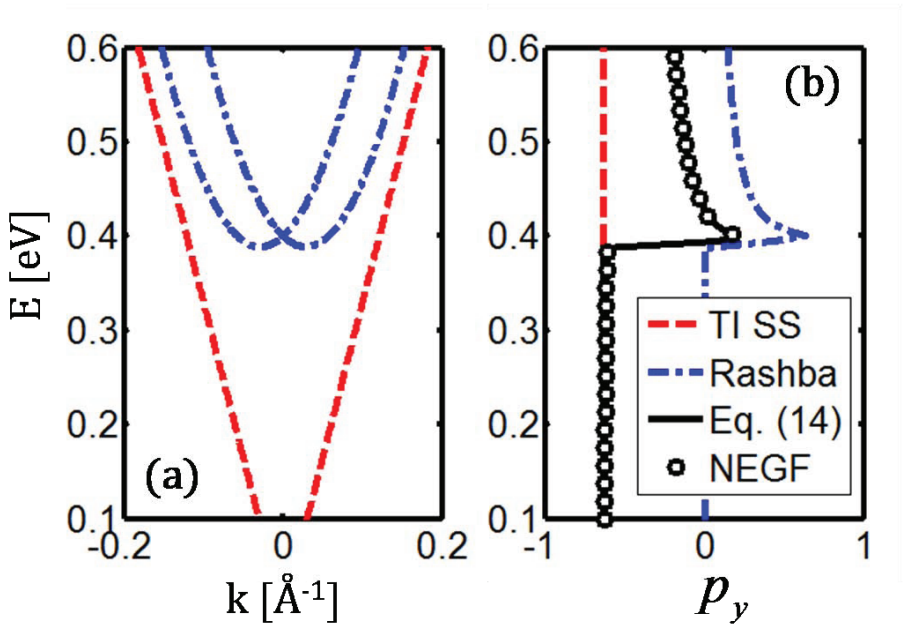

Fig. 3.4. Results of NEGF and simple expression (3.14) for multiple channels. (a) dispersion relation of TI SS (dashed line) together with Rashba bands (dashed-dotted line). (b) y component of $\vec{p}$ for the case of multiple channels (TI SS and Rashba channels) as a function of energy. The NEGF result assumed a ballistic transport and periodic boundary condition along the width direction. Parameters are same as Fig. 3.3(c) except for 0.4 eV shift with Rashba channel.

respect to TI SS due to the imperfect cancellation of two Fermi circles (corresponding to two different 'i' in Eq. (3.2)) with opposite spin orientations. Similar cancellation could also occur for TI SS with multiple bands.

3.4.3 Multiple Channels

The coexistence of bulk states with TI SS is one of the main obstacles to detect and identify surface states in transport measurements. When there are multiple channels

with their own channel polarizations the general expression for $\vec{p}$ is given by a density of states(DOS) average of each $\vec{p}_i$ for a given channel index i,

$$\vec{p}(E) = \frac{\sum_i \vec{p}_i DOS_i}{\sum_i DOS_i}, \tag{3.14}$$

by noting that $DOS_i = 2\sum_{v_x(\vec{k})>0} \delta(E - \epsilon_i(\vec{k}))/A$ with A the area of 2D surface. Recent experimental reports [62,63] suggest the coexistence of Rasbha bands together with TI SS with spin orientations corresponding to positive $\hbar v_F$ and α in Eqs. (3.3) and (3.4). It implies that their contribution to p_y will have opposite signs, which could even cause a change in the sign of p_y around $E = 0.4$ eV, depending on the relative DOS of TI SS and Rashba bands as shown in Fig. 3.4(b). This aspect can be probed experimentally by changing E_F.

3.5 Summary

In summary, we have shown that a 3-terminal potentiometric measurement should show a change in resistance upon reversing the magnetization of a voltage detecting FM contact and this change can be used as a quantitative measure of the channel polarization $\vec{p}$ using Eq. (3.2) which is applicable to TI SS and/or Rashba channels. The key result is summarized in Eqs. (3.1) and (3.2) which have been justified using an NEGF-based quantum transport model as well as simple semiclassical arguments.

3.6 Note added after publication

In the manuscript it is assumed that the interface resistance is low between spin($\vec{p}$) in the channel and the magnet($\vec{M}$) when they are parallel to each other where $\vec{M}$ represent a magnetic moment of the FM contact. As noted in [67] (see, for example [68]) the magnetic moment of an electron is given by $\vec{\mu} = g_e \mu_B \vec{S}/\hbar$ with $g_e \approx -2$ (μ_B: the Bohr magneton) in typical transition metals and is therefore opposite to its spin ($\vec{S}$). But another important point that should be considered is that majority

spins for the magnetization are not necessarily the dominant spins around the Fermi energy which determine the interface resistance as shown in Fig. 3.5. The density of states (DOS) for majority spins around the Fermi energy can be smaller than the one of minority spins as in the case of simplified Stoner mode (see, for example [69]) or typical ferromagnetic materials [70] (Fig. 3.5(b))and this gives a low resistance state between electron's spin ($\vec{p}$) in the channel and magnetic moment of the magnet ($\vec{M}$) as assumed. More correctly, since the DOS of each spin around the energy range of interest is material dependent and can vary with experimental conditions it has to be carefully considered in analyzing experimental data.

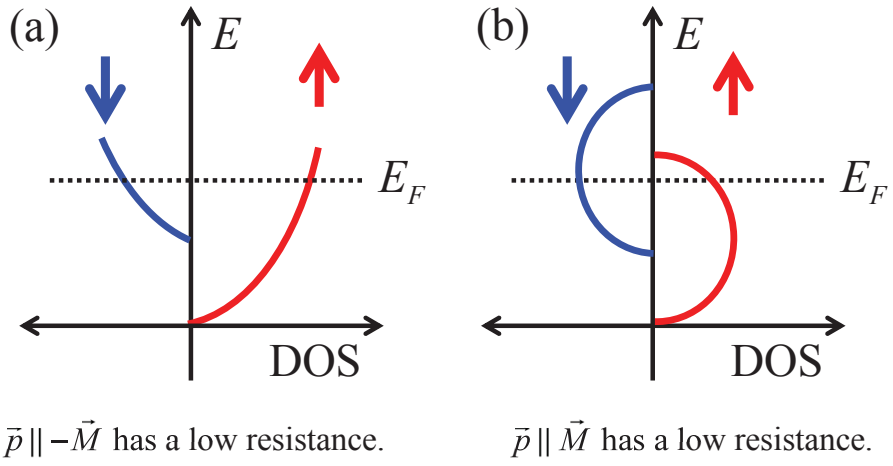

Fig. 3.5. Two possible cases about the density of states (DOS) for each spin direction inside magnets are shown in (a) and (b) respectively. Note that depending on the relative DOS around the Fermi energy (E_F) the low resistance state is determined between spin ($\vec{p}$) in the channel and the magnet ($\vec{M}$).

4. SPIN CIRCUIT REPRESENTATION FOR 2D CHANNELS WITH SPIN ORBIT COUPLING [TO BE SUBMITTED]

The contents of this chapter will be submitted for publication.

4.1 Introduction

Recently there have been various types of electrical measurements showing the unique coupling between charge and spin in new type of materials called topological insulators (TI) where a wide range of ratios between spin and charge current are also reported [71–73]. These include charge current induced spin accumulation [67, 74–76] or spin current measurement [71, 77] and spin current induced charge voltage measurement [73, 78, 79] which are analogous to spin Hall effect (SHE) and inverse spin Hall effect (ISHE) in materials with SHE. This type of coupling between charge and spin is not restricted to TI and indeed it has been observed in two dimensional (2D) channel with Rashba spin orbit coupling (SOC) as well, which is often referred as Rashba Edelstein effect (see for example [53] and references therein). Here we focus on arbitrary 2D channel with SOC that can include TI surface states (TISS) and Rashba SOC and provide a single consistent circuit representation that can be used to provide new insight and guide various experimental results.

The schematic structure of 2D channel with spin orbit coupling (SOC) is shown in Fig. 4.1(a). The phenomena of constant spin accumulation/polarization that can be interpreted as a spin voltage under a longitudinal charge current motivates us to introduce a spin terminal on top of 2D channel as shown in Fig. 1(a). Together with 2 charge terminals (1 and 2) along the longitudinal direction one can think of a three terminal device with a spin terminal on top of 2D channel that can be used to

define terminal characteristics. The purpose of this paper is to provide a conductance matrix or equivalent circuit representations for this three terminal structure in Fig. 4.1(a) that can be independently defined by focusing on terminal quantities of charge and spin and used in various set-ups with general boundary conditions.

The proposed equivalent circuit is based on a simple representation of 2D channel as shown in Fig. 4.1(b). In general, all propagating modes in an arbitrary 2D channel can be categorized into four types depending on their spin (up or down) and propagating directions (positive or negative). Here we assume strong communication and constant equilibration within each of the four types, so that each category can be described by a single quasi-Fermi level. Then the overall system is described by four quasi-Fermi levels: $\mu_+^\uparrow$, $\mu_-^\uparrow$, $\mu_-^\downarrow$, and $\mu_+^\downarrow$. The time reversal invariance of the system dictates that the number of positive propagating modes with up spin M is same as the number of negative propagating modes with down spin. Likewise the same number of modes, N, is given to modes with negative group velocities with up spin and positive group velocities with down spin. In materials with SOC the number M is not in general equal to N, which gives rise to a non-trivial coupling between charge and spin as in the case of Rashba ($M \neq N$) or TISS ($N = 0$) as will be shown. We present two circuit representations for charge and spin which are equivalent to each other in Fig. 4.1(c) and (d). All the circuit elements are defined in terms of only three quantities G_B, G, and p. Here $G_B = (q^2/h)(M+N)$ is the ballistic conductance for the 2D channel with a width W, $G = G_B\lambda_I/L$ is the conductance of intrinsic 2D channel with λ_I is an intrinsic back scattering length (with $\vec{i}^s = 0$).

The quantity p describes a degree of the coupling between charge and spin transport in the channel which is given by

$$p = \frac{2}{\pi}\frac{M-N}{M+N}, \tag{4.1}$$

(a) Structure

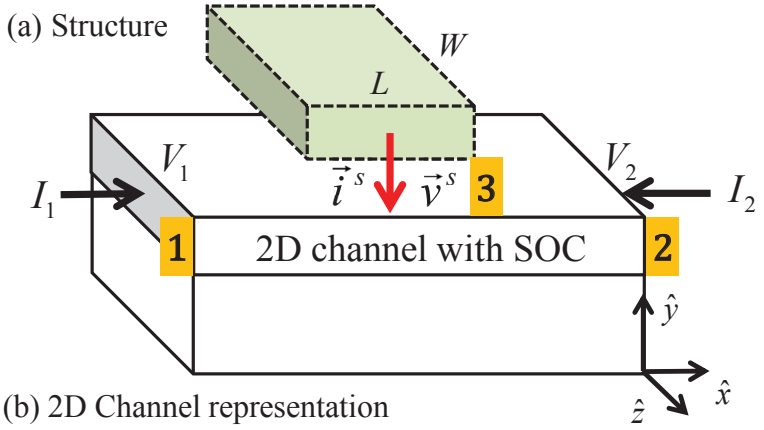

(b) 2D Channel representation

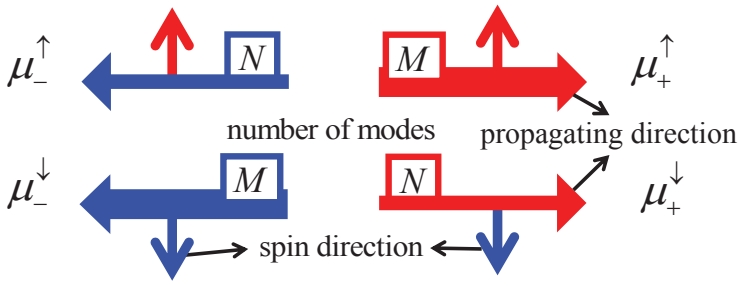

(c) Equivalent circuit (based on conductance matrix)

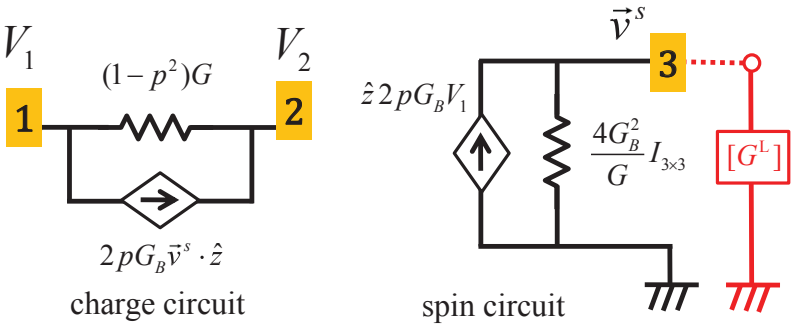

(d) Equivalent circuit (based on resistance matrix)

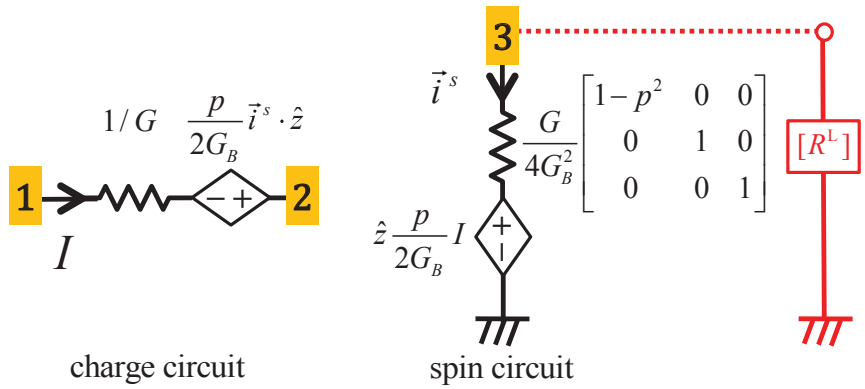

Fig. 4.1. (a) The structure of interest is shown, where two dimensional (2D) channel with spin orbit coupling (SOC) can include topological insulator surface states (TISS) or Rashba SOC. A uniform longitudinal charge current is assumed throughout this paper that can be modeled with two charge terminals 1 and 2 with voltages (V_1, V_2). and currents (I_1, I_2) and one spin terminal 3 with a voltage ($\vec{v}^s = (v^z, v^x, v^y)^T$) and current ($\vec{i}^s = (i^z, i^x, i^y)^T$) on top of 2D channel. (b) All propagating modes in an arbitrary 2D channel can be categorized into four types depending on their spin directions (up or down) and group velocities (positive or negative along $\hat{x}$ direction). M and N denote the number of modes for each type. Note that due to the time reversal invariance of the system the number of channels, M for positive propagating states with up spin is same as the one for negative propagating states with down spin. Two equivalent circuit representations for a structure (a) are shown in (c) and (d) with their dependent current or voltage sources. Here G is a conductance of the intrinsic channel ($\vec{i}^s = 0$), $G_B = q^2/h\,(M+N)$ is the ballistic conductance of the channel, $p = (M-N)/(M+N)$ denotes the degree of spin polarization due to a charge current, and $I_{3\times3}$ is a 3×3 identity matrix. The spin circuits have 3-component voltages and currents with conductance or resistance. Note that the longitudinal charge current is assumed to be coupled with one type of spin (z-spin in our discussion).

where the factor $2/\pi$ is included for the purpose of angular averaging in 2D Fermi circles [80]. For a given Hamiltonian one can estimate p based on the picture in Fig. 4.1(b). For example, in the case of TISS ($N = 0$) it is given by

$$p = \frac{2}{\pi}, \tag{4.2}$$

with a following type of Hamiltonian

$$H = \hbar v_0 (\vec{\sigma} \times \vec{k}) \cdot \hat{n}, \tag{4.3}$$

where $\hat{n}$ an outward normal vector from a surface, $\vec{\sigma}$ is a vector of the Pauli spin matrices, v_0 is the Fermi velocity. For the channel with Rashba SOC ($E \geq 0$), it is given by

$$p = \frac{2}{\pi} \frac{1}{\sqrt{1 + 2E/(mv_0^2)}}, \tag{4.4}$$

with a following type of Hamiltonian

$$H = \frac{\hbar^2 k^2}{2m} I_{2\times 2} - \hbar v_0 (\vec{\sigma} \times \vec{k}) \cdot \hat{n}. \tag{4.5}$$

The polarization direction of spin is determined by $\hat{s} = \text{sign}(\hbar v_0)\, \hat{I} \times \hat{n}$ with $\hat{n}$ a surface normal vector and $\hat{I}$ a charge current direction so that we have $\pm\hat{z} = \pm\hat{x} \times \hat{y}$ polarized spin in the structure of Fig. 4.1(a).

Based on the proposed circuit we present three results in this paper, namely, effective spin Hall angle, maximum spin current, and magnetoresistance. Since the longitudinal charge current couples with z-polarized spin we first assume a diagonal form of the load resistance $[R^{\text{L}}] = [G^{\text{L}}]^{-1} = 1/(G^{\text{L}}) I_{3\times 3}$ where $I_{3\times 3}$ is a 3×3 identity matrix and $G^{\text{L}} = \eta G_B k_F L/4$ with k_F the Fermi wavelength and η being a proportionality constant in Fig. 4.1(d) so that we can work with one component of spin circuit that is coupled with charge (z component or $s \equiv z$).

1. Effective spin Hall angle: The main quantity of interest is the ratio of the generated spin to the applied charge current. Given a charge current I we have

$$\frac{-i^s}{I} = \frac{2p}{(1-p^2)\lambda_I + 8/(\eta k_F)} L, \tag{4.6}$$

from the circuit in Fig. 1(d). We can define the effective spin Hall angle with the limit $\eta \to \infty$ as

$$\frac{\theta_{\rm SH}^{2D}}{t} \simeq \frac{2p}{(1-p^2)\lambda_I} \tag{4.7}$$

by noting that $-i^s/I = \theta_{\rm SH} L/t$ in the case of 3D materials with SHE. Although the effective spin Hall angle $\theta_{\rm SH}^{2D}$ in 2D channel has an unusual dependence of the sample thickness t it is not surprising since the thickness of 2D channel is not a well-defined quantity as compared to 3D bulk materials with giant SHE, suggesting that the conventional definition of the spin Hall angle is inappropriate in 2D channel. It is interesting to note that $\theta_{\rm SH}^{2D}$ inversely depends on the intrinsic back scattering length λ_I.

2. Maximum spin current: The spin current density is given by

$$\frac{i^s}{LW} \approx \frac{2p}{(1-p^2)\lambda_I}\frac{I}{W}, \tag{4.8}$$

from Eq. (4.6) with $\eta \to \infty$. The amount of charge current that can be carried by the channel is often limited by its energy bandwidth of their dispersion relations. In the case of TISS the bandwidth is approximately the band gap E_G suggesting that

$$\left[\frac{I}{W}\right]_{\rm max} = \frac{q}{h} M \, \max(\mu_+ - \mu_-) \sim \frac{q^2}{h}\frac{E_G}{q}\frac{k_F}{\pi} \sim 10 \, \frac{\rm mA}{\mu \rm m}, \tag{4.9}$$

with $\mu_{+/-}$ chemical potentials for positive/negative propagating modes with $E_G \sim$ 0.5eV, $k_F \sim 1.5$/nm. Assuming $p \sim 2/\pi$ and $\lambda_I \sim 0.2\,\mu$m we estimate the maximum spin current density given by $i^s/(LW) \sim 10^7$ A/cm^2 in TISS.

3. Magnetoresistance: Due to the coupling between charge and spin in the 2D channel, the spin current drawn from the spin circuit affects the charge current flow that is described by the dependent voltage source in Fig. 1(d). Specifically, the charge resistance change due to the spin current extracted is given by

$$\Delta R = R(i^s) - R(i^s = 0) = -\frac{2p}{G_B}\frac{i^s}{I}, \tag{4.10}$$

with $R = (V_1 - V_2)/I$, implying that the resistance increases as the spin load absorbs more spin current. For the case of $R^s G^{\rm L} \gg 1$ with $R^s = (1-p^2)G/4G_B^2$, we have

$$\Delta R = \left(\frac{p}{2G_B}\right)^2 \frac{G^{\rm L}}{1 + R^s G^{\rm L}} \approx \frac{p^2}{(1-p^2)G}. \tag{4.11}$$

It suggests a new way of estimating the spin current collected from the 2D channel and is a reminiscent of spin Hall magnetoresistance (SMR) [31,36] in materials with giant SHE where the angular dependence of magnetoresistance (MR) has been observed. In section 5 we make use of full three component spin circuit to include quantum mechanical boundary conditions based on spin mixing conductance and present the corresponding result that can be compared with SMR.

The rest of the paper is organized as followings: A simple justification for the proposed circuit is given in section 2 followed by nonequilibrium Greens function (NEGF) based result for 1D TISS that can be compared with the circuit result in section 3. A formal semi-classical scattering matrix based justification is presented in section 4. In section 5 we show the angular dependence of MR. Finally we describe how our circuit or conductance matrix approach can include various parallel channels in section 6.

4.2 Simple Justification

Here, we provide a simple justification of the proposed circuit (Fig. 4.1(d)) where we have two dependent voltage sources and two source resistances. First of all, let's consider a case where a constant charge current $I = I_1 = -I_2$ is applied in the charge circuit as shown in Fig. 4.2(a). Under this condition it is reasonable to assume that all positive and negative propagating modes have same chemical potentials of μ_+ and μ_- respectively as in Fig. 4.2(b). Then we can define the chemical potentials for up and down spins as weighted average of four types of modes, which are given by

$$\mu^{\uparrow} = \frac{M\mu_+ + N\mu_-}{M+N}, \text{ and } \mu^{\downarrow} = \frac{N\mu_+ + M\mu_-}{M+N}. \tag{4.12}$$

The spin voltage is given by

$$\begin{aligned} v^s|_{i^s=0} &= \frac{\mu^{\uparrow} - \mu^{\downarrow}}{2q} = \frac{M-N}{M+N}\frac{(\mu_+ - \mu_-)}{2q} \\ &= \frac{pI}{2G_B} \end{aligned} \tag{4.13}$$

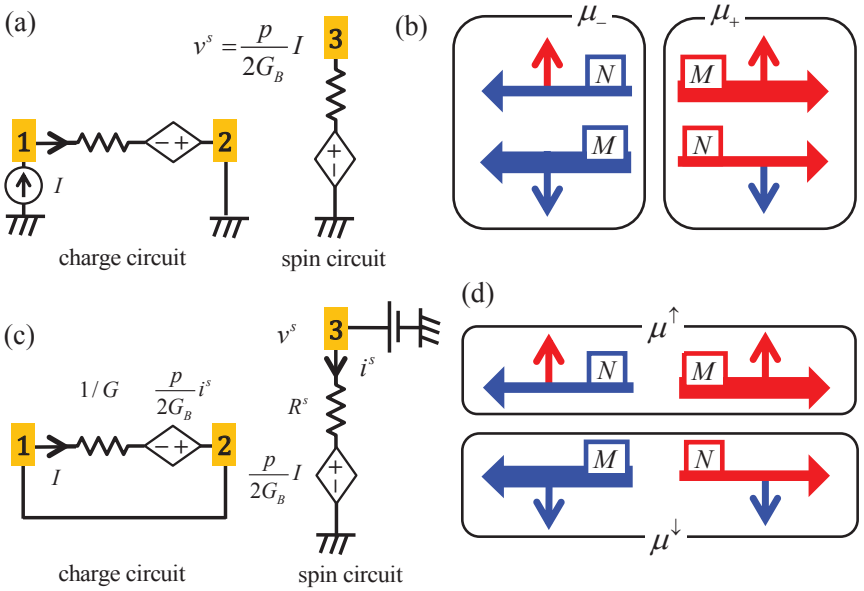

Fig. 4.2. Two configurations for simple justification of the proposed circuit in Fig. 1(d) are presented. (a) A constant charge current $I = I_1 = -I_2$ is applied to the charge circuit with no spin current ($i^s = 0$).The open circuit spin voltage can be obtained by noting that all positive and negative propagating modes share the same chemical potential μ_+ and μ_- respectively as shown in (b). Based on this observation we have $v^s|_{i^s=0} = pI/(2G_B)$. The second figuration is shown in (c) where a constant spin voltage v^s is applied to the spin circuit and the short circuit charge voltage is obtained. Under this condition all propagating modes with up and down spin share the same chemical potential $\mu^\uparrow$ and $\mu^\downarrow$ respectively as shown in (d), which gives $I|_{V=0} = 2pG_B v^s$.

using Eq. (4.12) where we make use of $I = G_B(\mu_+ - \mu_-)/q$ which is valid [81] in both ballistic and diffusive limits and we define spin voltage as $v^s = (\mu^\uparrow - \mu^\downarrow)/(2q)$. Based on Eq. (4.13) we can infer the dependent voltage source in the spin circuit as $pI/(2G_B)$.

Secondly, due to reciprocity we can also get the expression for the dependent voltage source in the charge circuit given by $pi^s/(2G_B)$ with an opposite polarity as shown in Fig. 4.2(a).

Thirdly, we define a source resistance of the charge circuit as an intrinsic resistance $1/G$ under the condition of no terminal spin current ($i^s = 0$) which is an ordinary ohmic resistance.

Finally, a source resistance of the spin circuit can be obtained by the following observation. Let's consider a case where we apply a spin voltage v^s on the terminal 3 and try to get an expression for the short circuit charge current as shown in Fig. 4.2(c). Due to the constant spin voltage v^s applied it is reasonable to assume that all modes with up and down spins have same chemical potentials of $\mu^\uparrow$ and $\mu^\downarrow$ respectively. The chemical potentials for positive and negative propagating modes are given by

$$\mu_+ = \frac{M\mu^\uparrow + N\mu^\downarrow}{M+N}, \text{ and } \mu_- = \frac{N\mu^\uparrow + M\mu^\downarrow_-}{M+N}. \tag{4.14}$$

Then the expression for the short circuit charge current is given by

$$I|_{V=0} = G_B\frac{(\mu_+ - \mu_-)}{q} = G_B\frac{M-N}{M+N}\frac{(\mu^\uparrow - \mu^\downarrow)}{q} = 2pG_Bv^s. \tag{4.15}$$

At the same time we also have

$$0 = \frac{I}{G} - \frac{pi^s}{2G_B}, \tag{4.16}$$

from the charge circuit and

$$v^s = \frac{pI}{2G_B} + i^sR^s, \tag{4.17}$$

from the spin circuit. Using Eqs. (4.15)-(4.17) we can obtain the expression for the source resistance R^s in the spin circuit which is given by $(1-p^2)G/(4G_B^2)$. Since we identified all four elements of the circuit in Fig. 4.1(d) for charge and one type of spin ($s = z$) we have a following form of resistance matrix,

$$\begin{pmatrix} V \\ v^s \end{pmatrix} = \begin{bmatrix} 1/G & -p/(2G_B) \\ p/(2G_B) & (1-p^2)G/(4G_B^2) \end{bmatrix} \begin{pmatrix} I \\ i^s \end{pmatrix}, \tag{4.18}$$

with $I = I_1 = -I_2$ and $V = V_1 - V_2$. This can be inverted to give a conductance matrix form,

$$\begin{pmatrix} I_1 \\ I_2 \\ i^s \end{pmatrix} = [G]\begin{pmatrix} V_1 \\ V_2 \\ v^s \end{pmatrix} = \begin{bmatrix} (1-p^2)G & -(1-p^2)G & 2pG_B \\ -(1-p^2)G & (1-p^2)G & -2pG_B \\ -2pG_B & 2pG_B & 4G_B^2/G \end{bmatrix} \begin{pmatrix} V_1 \\ V_2 \\ v^s \end{pmatrix}, \tag{4.19}$$

while maintaining charge conservation and reciprocity given by

$$[G]_{ij} = (-1)^{n_i n_j}[G]_{ji}, \tag{4.20}$$

with $n_i = 1$ for $i = 1, 2$ (charge terminals) and $n_i = -1$ for $i = 3$ (spin terminal) and

$$\sum_{i=1,2}[G]_{ij} = 0, \tag{4.21}$$

respectively where i and j represent terminal indices. It is straightforward to see that the terminal spin current vanishes at equilibrium ($V_1^c = V_2^c = V$ and $v^{z,x,y} = 0$) [47]. Finally, we obtain a full conductance matrix by adding additional spin polarization directions which is given by

$$\begin{pmatrix} I_1 \\ I_2 \\ i^z \\ i^x \\ i^y \end{pmatrix} = \begin{bmatrix} (1-p^2)G & -(1-p^2)G & 2pG_B & 0 & 0 \\ -(1-p^2)G & (1-p^2)G & -2pG_B & 0 & 0 \\ -2pG_B & 2pG_B & \frac{4G_B^2}{G} & 0 & 0 \\ 0 & 0 & 0 & \frac{4G_B^2}{G} & 0 \\ 0 & 0 & 0 & 0 & \frac{4G_B^2}{G} \end{bmatrix} \begin{pmatrix} V_1 \\ V_2 \\ v^z \\ v^x \\ v^y \end{pmatrix}. \tag{4.22}$$

Note that x and y polarized spins are added with $p = 0$ since they are not coupled with the longitudinal charge current flow as in the case of TISS or Rashba channel. It is straightforward to see that Eq. (4.22) corresponds to the circuit (conductance type) in Fig. 4.1(c) with the identifications of $\vec{i}^s = (i^z, i^x, i^y)^T$ and $\vec{v}^s = (v^z, v^x, v^y)^T$. By inverting Eq. (4.22) after grounding the terminal 2 to avoid the singularity of the matrix one can obtain the second circuit (resistance type) in Fig. 4.1(d).

4.3 NEGF Comparison

In this section we provide a nonequilibrium Greens function (NEGF)-based results that can be compared with the proposed circuit results in the case of ideal 1D TISS ($M = 1$ and $N = 0$). The schematic setup is shown in Fig. 4.3(b) for a structure in Fig. 4.1(a) where we have Hamiltonian H with four different self energies (Σ_L, Σ_R, Σ_S, and Σ_{FM}). The details of NEGF model are provided in the appendix G with the

description of Σ_{FM} in terms of isotropic spin and momentum relaxation scattering process. The correspondences between the circuit model and NEGF are given as

$$\begin{aligned} \Sigma_S &\leftrightarrow G = G_B \frac{\lambda_I}{L} \\ \Sigma_{\mathrm{FM}} &\leftrightarrow G_{\mathrm{FM}} \\ H &\leftrightarrow M, N. \end{aligned} \tag{4.23}$$

Here we vary the magnitude of the Σ_{FM} in NEGF model of Fig. 4.3(a) which corresponds to varying the G^{FM} in the circuit in Fig. 4.3(b). The charge and spin circuits give following relations among charge and spin voltages and currents,

$$\begin{aligned} I &= GV + \frac{G}{2G_B} i^s \\ v^s &= \frac{I}{2G_B}, \end{aligned} \tag{4.24}$$

which can be directly checked with NEGF result. The comparison is shown in Fig. 4.3(c) and (d) for charge and spin circuits in ballistic and diffusive cases showing good agreement. Note that the proposed circuit can capture the ballistic result of NEGF by choosing $G = G_B$.

4.4 Scattering Matrix

In this section we provide a formal justification for the proposed circuit based on a semi-classical scattering matrix. We first define following four quantities

$$\begin{aligned} f &= \frac{M(f_+^{\uparrow} + f_-^{\downarrow}) + N(f_+^{\downarrow} + f_-^{\uparrow})}{2(M+N)} \\ I(E) &= G'_B \frac{M(f_+^{\uparrow} - f_-^{\downarrow}) + N(f_+^{\downarrow} - f_-^{\uparrow})}{M+N} \\ f^s &= \frac{M(f_+^{\uparrow} - f_-^{\downarrow}) - N(f_+^{\downarrow} - f_-^{\uparrow})}{2(M+N)} \\ I^s(E) &= G'_B \frac{M(f_+^{\uparrow} + f_-^{\downarrow}) - N(f_+^{\downarrow} + f_-^{\uparrow})}{M+N}, \end{aligned} \tag{4.25}$$

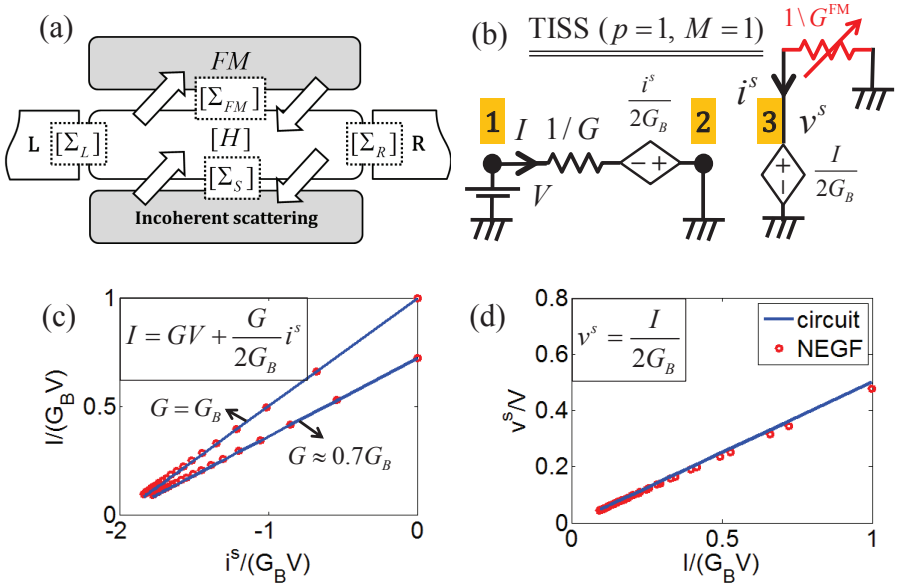

Fig. 4.3. NEGF results compared with the proposed circuit in the case of TISS ($p = 1$) are shown. (a) NEGF model : Hamiltonian (H) with four different self energies are shown. Σ_L and Σ_R are used for left and right contacts. Σ_S represents the incoherent scattering in the intrinsic 2D channel. Σ_{FM} represents the effect of ferromagnet (FM) which is modeled as isotropic spin and momentum relaxation scattering process. (b) The corresponding circuit model is shown. The spin circuit is connected with FM load (G^{FM}) and a charge voltage $V = V_1 - V_2$ is applied in the charge circuit. (c) Comparison of results between the charge circuit (solid lines) and NEGF (circles). (d) Comparison of results between the spin circuit (solid line) and NEGF (circles). Parameters in NEGF : $L = 40$ nm, $a = 1$ nm, $\hbar v_0 = 3.3$ eVÅ, $d_m = 0,\ 5 \times 10^{-2}\mathrm{eV}^2$, $E_{\mathrm{F}} = 0.2$ eV.

in terms of four occupation factors $f_+^\uparrow$, $f_-^\downarrow$, $f_-^\uparrow$, $f_+^\downarrow$ for each type of modes in Fig. 4.1(b) with a charge current $I = \int dE\ I(E)$ and $G'_B = G_B/q$. This can be also written as

$$\begin{pmatrix} f_+^\uparrow \\ f_-^\downarrow \\ f_-^\uparrow \\ f_+^\downarrow \end{pmatrix} = \begin{bmatrix} g_1 & g_1 & g_1/2 & g_1/2 \\ g_1 & -g_1 & g_1/2 & -g_1/2 \\ g_2 & g_2 & -g_2/2 & -g_2/2 \\ g_2 & -g_2 & -g_2/2 & g_2/2 \end{bmatrix} \begin{pmatrix} f \\ f^s \\ \frac{I^s(E)}{2G'_B} \\ \frac{I(E)}{2G'_B} \end{pmatrix}, \tag{4.26}$$

where $g_1 = (1 + N/M)/2$ and $g_2 = (1 + M/N)/2$. We assume a following form of semi-classical scattering matrix among occupation factors $f_+^\uparrow$, $f_-^\downarrow$, $f_-^\uparrow$, $f_+^\downarrow$ that is coupled with a nonequilibrium terminal spin current $i^s(E)$:

$$\frac{d}{dx}\begin{Bmatrix} f_+^\uparrow \\ -f_-^\downarrow \\ -f_-^\uparrow \\ f_+^\downarrow \end{Bmatrix} = \begin{bmatrix} -u & r_s & r & t_s \\ r_s & -u & t_s & r \\ r & t_s & -u & r_s \\ t_s & r & r_s & -u \end{bmatrix} \begin{Bmatrix} f_+^\uparrow \\ f_-^\downarrow \\ f_-^\uparrow \\ f_+^\downarrow \end{Bmatrix} + \frac{i^s(E)}{2gL} \begin{Bmatrix} +1 \\ -1 \\ +1 \\ -1 \end{Bmatrix}, \tag{4.27}$$

with r_s, t_s, r representing various scattering rates per unit length among four types of modes as shown in Fig. 4.4(a). The back scattering length and spin diffusion length can be defined by $\lambda_I = 1/(r + r_s)$, $\lambda_s = 1/(r_s + t_s)$ for a channel with no terminal spin current ($i^s(E) = 0$). There is a sum rule for scattering rates given by $u = r_s + t_s + r$ due to the requirement that Eq. (4.27) is also valid at equilibrium ($f_+^\uparrow = f_-^\uparrow = f_+^\downarrow = f_-^\downarrow = f =$ constant and $i^s(E) = 0$). Note that the terminal spin current $i^s(E)$ is coupled equally to all four occupation factors with a constant factor g. Using Eq. (4.26), we can express $f_+^\uparrow$, $f_-^\downarrow$, $f_-^\uparrow$, $f_+^\downarrow$ in Eq. (4.27) in terms of f, f^s, $I^s(E)$, $I(E)$ which is given by

$$\frac{d}{dx}\begin{pmatrix} f^s \\ \frac{I(E)}{G'_B} \\ f \\ \frac{I^s(E)}{G'_B} \end{pmatrix} = \frac{1}{1-p^2} \times$$
$$\begin{bmatrix} 0 & 0 & 2p\,(r+t_s) & -(r+t_s) \\ 0 & 0 & 4p^2(r+t_s) & -2p(r+t_s) \\ 2p\,(r-t_s) & p^2\,(t_s+r_s)-(r+r_s) & 0 & 0 \\ 4\,(p^2\,(r+r_s)-(t_s+r_s)) & -2p\,(r-t_s) & 0 & 0 \end{bmatrix} \times$$
$$\begin{pmatrix} f^s \\ \frac{I(E)}{G'_B} \\ f \\ \frac{I^s(E)}{G'_B} \end{pmatrix} + \begin{pmatrix} 0 \\ 0 \\ \frac{p\,i^s(E)}{2gL} \\ \frac{i^s(E)}{gL} \end{pmatrix}. \tag{4.28}$$

Due to the assumption of uniform charge flow along the longitudinal direction, we need to have $d(I(E)/G'_B)/dx = 0$, which requires $2pV = I^s(E)/G'_B$ from Eq. (4.28). This gives,

$$\frac{d}{dx}\begin{pmatrix} f^s \\ I(E)/G'_B \end{pmatrix} = \begin{pmatrix} 0 \\ 0 \end{pmatrix}. \tag{4.29}$$

Using the third and fourth row in Eq. (4.28) we have

$$\begin{aligned} 0 &= \frac{d}{dx}\left(2pf - \frac{I^s(E)}{G'_B} \right) \\ &= 2(t_s+r_s)\begin{pmatrix} 2 & -p \end{pmatrix}\begin{pmatrix} f^s \\ I(E)/G'_B \end{pmatrix} - \frac{(1-p^2)i^s(E)}{gL}, \end{aligned} \tag{4.30}$$

which gives

$$f^s = \frac{p\,I(E)}{2\,G'_B} + \frac{(1-p^2)\lambda_s}{4\,gL}\, i^s(E). \tag{4.31}$$

Next, from the third row in Eq. (4.28) together with Eq. (4.31), we have

$$\frac{df}{dx} = \frac{I(E)}{G'_B\,\lambda} - \frac{p}{2gL}\frac{\lambda_s}{\lambda}\, i^s(E). \tag{4.32}$$

After integrating along $\hat{x}$ direction from $x = 0$ (terminal 1) to $x = L$ (terminal 2)

$$f_1 - f_2 = \frac{I(E)\,L}{G'_B\,\lambda} - \frac{p}{2g}\frac{\lambda_s}{\lambda}\,i^s(E). \tag{4.33}$$

Combining Eqs. (4.31) and (4.33) we have

$$\begin{pmatrix} I(E) \\ i^s(E) \end{pmatrix} = \begin{bmatrix} (1-p^2)G/q & 2pG_B/q \\ -2p\lambda g\,/\lambda_s & 4Lg/\,\lambda_s \end{bmatrix} \begin{pmatrix} f_1 - f_2 \\ f^s \end{pmatrix}. \tag{4.34}$$

After integrating over energy E

$$\begin{aligned} \begin{pmatrix} I \\ i^s \end{pmatrix} &= \left\{ \int dE \left(-\frac{\partial f_0}{\partial E} \right) \begin{bmatrix} (1-p^2)G & 2pG_B \\ -2p\lambda qg\,/\lambda_s & 4Lqg/\,\lambda_s \end{bmatrix} \right\} \begin{pmatrix} V \\ v^s \end{pmatrix} \\ &=< \begin{bmatrix} (1-p^2)G & 2pG_B \\ -2p\lambda qg\,/\lambda_s & 4Lqg/\,\lambda_s \end{bmatrix} > \begin{pmatrix} V \\ v^s \end{pmatrix}, \end{aligned} \tag{4.35}$$

with $V = V_1 - V_2$ and $< \cdot >$ representing an average over energy. Finally we recover the desired expression (Eq (4.18)) by requiring that $qg = G_B\lambda_s/\lambda$ due to reciprocity.

4.5 Angular Magnetoresistance

Recently, new type of magnetoresistance was discovered in materials with GSHE, called as spin Hall magnetoresistance (SMR) [31, 36] where simultaneous actions of SHE and ISHE give rise to longitudinal and transverse resistivity changes depending on the magnetization direction of the top FM layer. The same type of measurement can be explored in 2D channels with SOC like TISS and Rashba due to the similarity with materials with SHE regarding the coupling of charge and spin transport. The

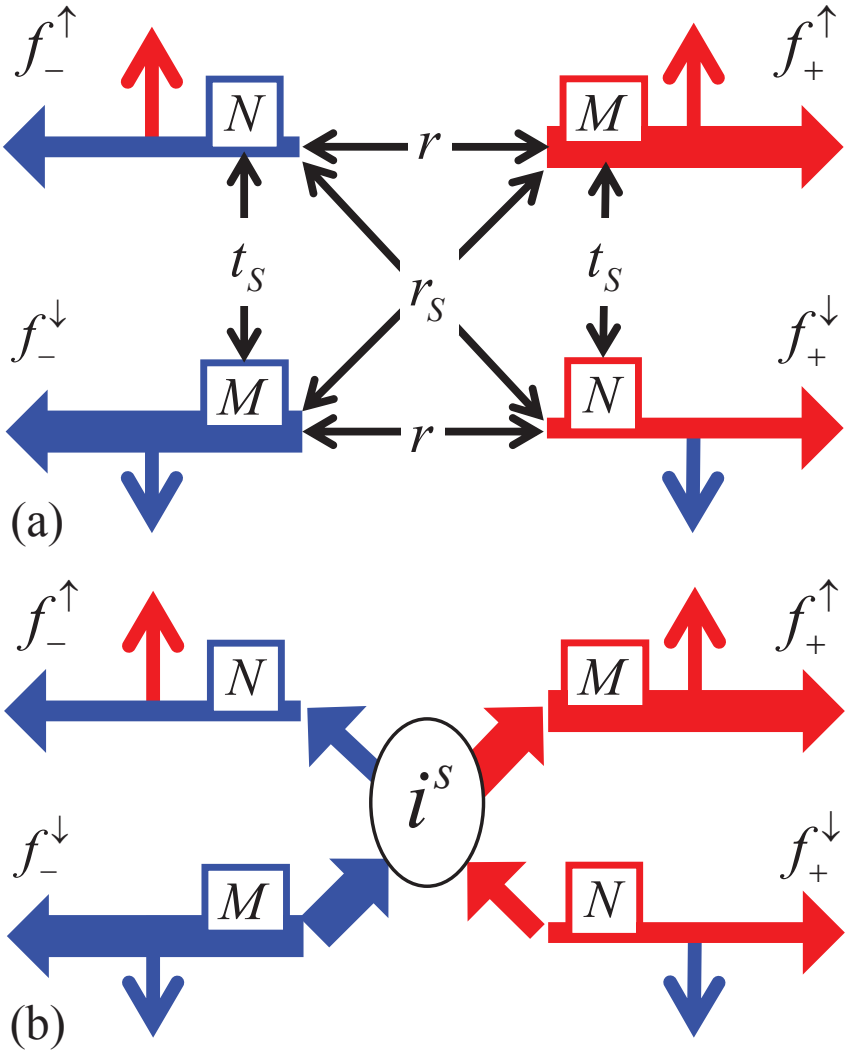

Fig. 4.4. Semi-classical scattering matrix for the justification of the spin circuit proposed based on the Fig. 1(c). $f_+^\uparrow$, $f_-^\uparrow$, $f_+^\downarrow$, and $f_-^\downarrow$ represent occupation factor for each type of mode. (a) There are scattering processes which mix different modes whose rates are denoted as r_s, t_s, and r representing scattering probability per unit length. (b) The effect of positive terminal spin current into the terminal 3 ($-i^s$) to each mode is shown. It is assumed that the spin terminal 3 is connected each mode with equal probability.

charge and spin transport in 2D channels can be described by a following conductance matrix ($[G^{\mathrm{2D}}]$),

$$\begin{pmatrix} I_1 \\ I_2 \\ i^z \\ i^x \\ i^z \\ I_z \\ i_z^y \end{pmatrix} = \begin{bmatrix} (1-p^2)\frac{W\lambda_I}{L}g_B & -(1-p^2)\frac{W\lambda_I}{L}g_B & 2pWg_B & 0 & 0 \\ -(1-p^2)\frac{W\lambda_I}{L}g_B & (1-p^2)\frac{W\lambda_I}{L}g_B & -2pWg_B & 0 & 0 \\ -2pWg_B & 2pWg_B & 4\frac{WL}{\lambda_I}g_B & 0 & 0 \\ 0 & 0 & 0 & 4\frac{WL}{\lambda_I}g_B & 0 \\ 0 & 0 & 0 & 0 & 4\frac{WL}{\lambda_I}g_B \\ 0 & 0 & 0 & -2pLg_B & 0 \\ 2pLg_B & 0 & 0 & 0 & 0 \end{bmatrix} \times \begin{pmatrix} V_1 \\ V_2 \\ v^z \\ v^x \\ v^y \end{pmatrix} \tag{4.36}$$

where $g_B = G_B/W$ is a number of modes per unit width and two currents I_z and i_z^y along $\hat{z}$ direction are added compared to the previous circuit in Fig. 4.1(c) or Eq. (4.22). The charge current $I_z = -2pLg_Bv^x$ is added which is similar to the contribution of spin voltage induced charge current given by $I_1 = 2pWg_Bv^z$ with a spin polarization direction made consistent with properties of TI. Likewise $i_z^y = 2pLg_BV_1$ is added based on the contribution of charge voltage induced spin current which is similar to $i^z = -2pWg_BV_1$.

The interface between nonmagnetic (NM) and FM layers with no charge current flow as in the case of insulating magnet like yttrium iron garnet (YIG) can be described by following form of conductance matrix [36, 45] in $z-x-y$ basis

$$[G^{\mathrm{FM}}] = Rot\, LW \begin{pmatrix} 0 & 0 & 0 \\ 0 & 2G_r & 2G_i \\ 0 & -2G_i & 2G_r \end{pmatrix} Rot^{+} \tag{4.37}$$

with $2G_r = 2\mathrm{Re}G^{\uparrow\downarrow}$ and $2G_i = 2\mathrm{Im}G^{\uparrow\downarrow}$ where $G^{\uparrow\downarrow}$ represents spin mixing conductance. A rotation matrix *Rot* is used for a magnet along arbitrary direction ($\hat{m}$) from the initial $\hat{z}$ direction. Here we assume that the same form of the conductance matrix is valid between 2D channel and FM, which might require further study in the future.

For a bilayer structure in Fig. 4.5(a) the corresponding conductance matrix representation is shown in Fig. 4.5(b) where two independently defined conductance matrices $[G^{\mathrm{2D}}]$ and $[G^{\mathrm{FM}}]$ are combined together following ordinary circuit rules for each spin component. Specifically, we have

$$-\vec{i}^s = G^{\mathrm{FM}}\vec{v}^s \tag{4.38}$$

for the spin terminal 3. From Eqs. (4.36) and (4.38) we can have expression for all currents in terms of charge voltages V_1 and V_2. For the purpose of obtaining longitudinal (σ_{xx}) and transverse (σ_{xz}) conductivities we have

$$I_1 = (1-p^2)g_B\frac{W\lambda_I}{L}(V_1-V_2)\left(1+\frac{p^2}{1-p^2}\left(1-(1-m_z^2)\mathrm{Re}F\right)\right) \tag{4.39}$$

$$I_z = -g_B\lambda_I p^2(V_1-V_2)\left(m_x m_z\mathrm{Re}+m_y\mathrm{Im}\right)F, \tag{4.40}$$

with $F = \frac{\lambda_I(G_r+iG_i)}{2g_B}\Big/1+\frac{\lambda_I(G_r+iG_i)}{2g_B}$ and $\hat{m} = (\cos\alpha\cos\beta,\ \sin\alpha\cos\beta,\ \sin\beta)$. These give the expressions for $\sigma_{xx} = (I_1/W)/((V_1-V_2)/L)$ and $\sigma_{xz} = I_5/(V_1-V_2)$ as shown in Fig. 4.5(c) and (d). There are noticeable similarities regarding the angular dependence of the signals and p^2 dependence in the amplitude (instead of θ_{SH}^2) compared to the results of SMR.

4.6 Parallel Channels

One of the main obstacles in various electrical measurements of TISS is parallel channels that coexist with TISS where these parallel channels can be ordinary spin degenerate channels or Rashba channel on the surface as experimentally observed [62, 63]. As long as the our previous assumption is satisfied (strong communication within four types of channels), we can define an effective conductance matrix for the whole

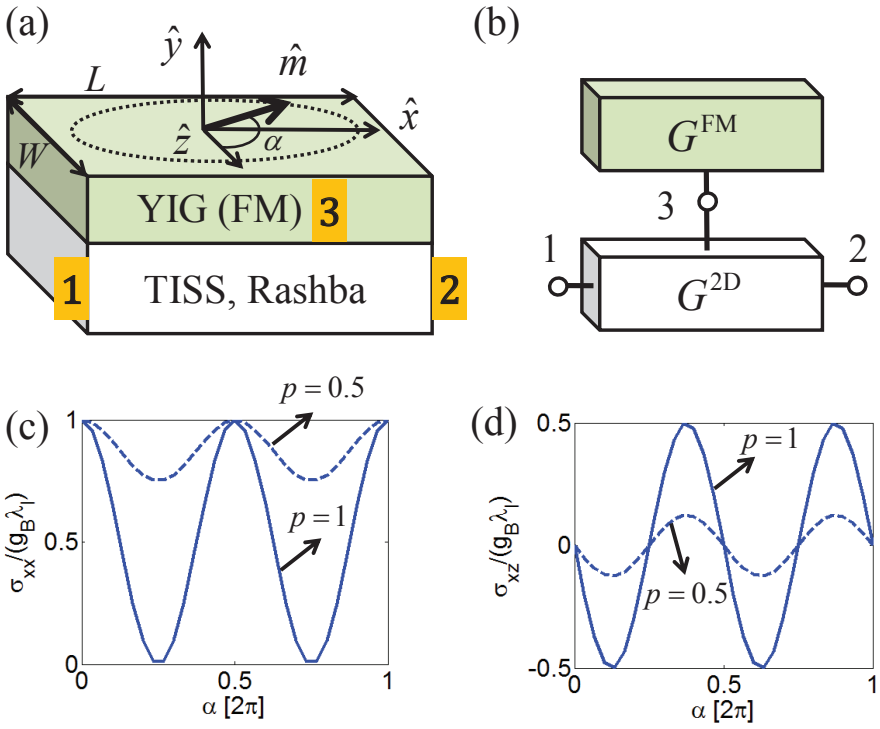

Fig. 4.5. Spin Hall magnetoresistance (SMR) effect in TISS/Rashba channels. (a) The bilayer structure consists of 2D channel (TISS/Rashba) and FM (YIG) with its magnetization direction $\hat{m}$. (b) The corresponding conductance matrix representation of the structure (a). Two independent conductance matrices for each layer (G^{2D} and G^{FM}) are combined together following conventional circuit rules for each charge and spin component. The longitudinal (σ_{xx}) and transverse (σ_{xz}) conductivities are plotted (c) and (d) for two different values of $p = 1, 0.5$ (solid and dotted lines respectively) as the magnet direction ($\hat{m}$) of YIG is rotated in $x-z$ plane by an angle α. The results show the dependence of p^2, which is similar to the case of SMR in bulk materials with GSHE where the result show the dependence of $\theta^2_{\rm SH}$. Parameter values: $G_r\lambda_I^2 = 2.6\times10^4 g_B\lambda_I$, $G_i = 0$.

system since the proposed circuit model is general to include arbitrary 2D channels with three parameters, G_{eff}, $G_{B,\text{eff}}$, and p_{eff} that can be experimentally determined. Note that two parameters $G_{B,\text{eff}}$, and p_{eff} can be determined from the information of the bandstructure for each Hamiltonian without reference to the detailed scattering process in the channel, which are given by

$$G_{B,eff} = \sum_i G_{B,i} \text{ and } p_{\text{eff}} = \sum_i (M_i + N_i)p_i \Big/ \sum_i (M_i + N_i), \tag{4.41}$$

where index i is used for each channel. The conductance G_{eff} in general not the sum of each G_i and depends on the specific scattering processes in the channel. Therefore it is better to be determined experimentally. Although it is straightforward to add conductance matrices of each channel i together to take into account all channels in parallel this approach assumes that there is no internal scattering among different channels (i.e., each channel is physically isolated from other channels and connected by outer charge and spin terminals only) so has to be applied under appropriate conditions.

4.7 Brief connection with experimental results

Our proposed circuit model (Fig. 4.1(d)) has four elements: Two in the charge circuit and two in the spin circuit. In this section we briefly connect each component with available experimental results one by one.

The source resistance of charge circuit in Fig. 4.1(d): This represents a conventional ohmic resistance under the condition of zero spin current, which is satisfied when no spin current is extracted from or injected into 2D channel.

The dependent voltage source of spin circuit in Fig. 4.1(d): This represents a charge current induced spin polarization/accumulation effect which is represented as a spin voltage in the proposed circuit. This effect is often referred as Rashba-Edelstein effect in 2D channel with Rashba SOC. There are extensive theoretical and experimental results in Rashba channel (see for example Ref. [53, 82]). Recently, several experimental results are reported from different groups Ref. [67, 74–76] in

topological insulators where the proposed expression (Eq. (4.13)) is used [74, 75]. Instead of the spin voltage, a spin current can be also measured, which was done in Ref. [77, 83] in topological insulators and there is a great interest in the amount of spin current that is available due to their possible applications in writing information into magnets.

The dependent voltage source of charge circuit in Fig. 4.1(d): This is the inverse process of the previous source term and represents a spin current induced charge voltage. It is often referred as inverse Edelstein effect in the literature. This effect has been observed in the case of Rashba channel [84] and topological insulators [73, 76,78,79]. In particular, Ref. [76] used a same sample to do both types of experiments (charge/spin current induced spin/charge voltage) and reported Onsager reciprocity between them in the magnitude of the observed signal. Ref. [73, 78, 79] used spin pumping to inject spin into topological insulators.

The source resistance of spin circuit in Fig. 4.1(d): This represents a spin source resistance which does not appear in the literature to the best of our knowledge. In the spin voltage measurement this resistance is irrelevant since the spin circuit is supposed to be open circuited. But in the spin current measurement the source resistance can be important. In the theoretical treatment of the experimental result of Ref. [83] this source resistance is assumed to be zero which can be consistent with the proposed circuit model if 2D channel can be approximately treated as ideal 1D topological insulator surface states ($p = 1$) . In realistic conditions, all kinds of parallel channels can coexist and the whole channel should be considered as an effective channel with non-ideal value of p (≤ 1) as discussed and a nonzero source resistance should be included and compared with the spin load resistance in the setup.

4.8 Summary

We have proposed an equivalent circuit representation or conductance matrix for 2D channels with spin orbit coupling (SOC) (including TISS and Rashba) in a

three terminal set-up (2 charge terminals and 1 spin terminal) by focusing on the terminal characteristics of charge and spin. This circuit can be independently defined and combined together with other elements of circuit representing other adjacent materials. Based on the circuit we present three results: effective spin Hall angle, maximum spin current, and angular magnetoresistance for 2D channel with SOC. A simple justification as well as formal justification based on a semi-classical scattering matrix are provided for the proposed circuit and a comparison with NEGF results is made in the case of 1D TISS. Finally the effect of parallel channels that can exist in realistic samples are discussed within our model.

5. SUMMARY

In summary, we have studied transport properties of materials with spin orbit coupling (SOC) with emphasis on spin-charge coupling.

First, we consider bulk materials with spin Hall effect where we provide three different models (conductance matrices or equivalent circuits) starting from standard diffusion equations. The proposed circuits reproduce existing analytical results in the literature by simple application of circuit rules for charge and spin but also provide valuable insights such as spin injection into semiconductors without tunneling barriers and the concept of spin ground for a thin sample to increase the spin current. We complete the story by showing an elemental conductance matrix that can be used to arbitrary shaped structure.

Secondly, we study 2D materials with SOC including Rashba channel or topological insulator surface states (TISS). We model the spin voltage generation by current flow in both quantum transport based on nonequilibrium Green's function model as well as semi-classical transport, which is receiving experimental support. Then we provide a conductance matrix or equivalent circuit for charge and spin, which can capture various kinds of experimental setups in a single picture based on simple view of propagating modes in these materials. This circuit allows us to answer questions such as the effective spin Hall angle in 2D materials, maximum spin current in TISS, and magnetoresistance effect.

The extension of a simple view of propagating modes in 2D materials into 3D bulk materials can be explored as a future work. Bulk SHE with Rashba channel or TISS with Rashba channel are active field of current research that can be explored using the proposed circuits. Broadly, we believe the spin circuit approach can provide a natural framework to incorporate diverse physics of spintronics with new insights.

LIST OF REFERENCES

LIST OF REFERENCES

[1] I. Žutić and S. Das Sarma, "Spintronics: Fundamentals and applications," *Reviews of Modern Physics*, vol. 76, pp. 323–410, Apr. 2004.

[2] H. C. Koo, J. H. Kwon, J. Eom, J. Chang, S. H. Han, and M. Johnson, "Control of spin precession in a spin-injected field effect transistor.," *Science (New York, N.Y.)*, vol. 325, pp. 1515–8, Sept. 2009.

[3] A. N. M. Zainuddin, S. Hong, L. Siddiqui, S. Srinivasan, and S. Datta, "Voltage-controlled spin precession," *Physical Review B*, vol. 84, p. 165306, Oct. 2011.

[4] Y. K. Kato, R. C. Myers, A. C. Gossard, and D. D. Awschalom, "Observation of the spin Hall effect in semiconductors.," *Science (New York, N.Y.)*, vol. 306, pp. 1910–3, Dec. 2004.

[5] A. Hoffmann, "Spin Hall Effects in Metals," *IEEE Transactions on Magnetics*, vol. 49, pp. 5172–5193, Oct. 2013.

[6] J. Sinova, S. O. Valenzuela, J. Wunderlich, C. H. Back, and T. Jungwirth, "Spin Hall effect," *arxiv.org/abs/1411.3249*, Nov. 2014.

[7] I. M. Miron, K. Garello, G. Gaudin, P.-J. Zermatten, M. V. Costache, S. Auffret, S. Bandiera, B. Rodmacq, A. Schuhl, and P. Gambardella, "Perpendicular switching of a single ferromagnetic layer induced by in-plane current injection.," *Nature*, vol. 476, pp. 189–93, Aug. 2011.

[8] L. Liu, R. A. Buhrman, and D. C. Ralph, "Review and Analysis of Measurements of the Spin Hall Effect in Platinum," p. 32, Nov. 2011.

[9] M. Z. Hasan and C. L. Kane, "Colloquium: Topological insulators," *Reviews of Modern Physics*, vol. 82, pp. 3045–3067, Nov. 2010.

[10] X.-L. Qi and S.-C. Zhang, "Topological insulators and superconductors," *Reviews of Modern Physics*, vol. 83, pp. 1057–1110, Oct. 2011.

[11] S. Borlenghi, V. Rychkov, C. Petitjean, and X. Waintal, "Multiscale approach to spin transport in magnetic multilayers," *Physical Review B*, vol. 84, p. 035412, July 2011.

[12] A. Brataas, G. Bauer, and P. Kelly, "Non-collinear magnetoelectronics," *Physics Reports*, vol. 427, pp. 157–255, Apr. 2006.

[13] B. Behin-Aein, A. Sarkar, S. Srinivasan, and S. Datta, "Switching energy-delay of all spin logic devices," *Applied Physics Letters*, vol. 98, p. 123510, Mar. 2011.

[14] S. Srinivasan, A. Sarkar, B. Behin-Aein, and S. Datta, "All-Spin Logic Device With Inbuilt Nonreciprocity," *IEEE Transactions on Magnetics*, vol. 47, pp. 4026–4032, Oct. 2011.

[15] S. Manipatruni, D. E. Nikonov, and I. A. Young, "Modeling and Design of Spintronic Integrated Circuits," *IEEE Transactions on Circuits and Systems I: Regular Papers*, vol. 59, pp. 2801–2814, Dec. 2012.

[16] J. Kim, J. Sinha, M. Hayashi, M. Yamanouchi, S. Fukami, T. Suzuki, S. Mitani, and H. Ohno, "Layer thickness dependence of the current-induced effective field vector in Ta—CoFeB—MgO.," *Nature materials*, vol. 12, pp. 240–5, Mar. 2013.

[17] K. Garello, I. M. Miron, C. O. Avci, F. Freimuth, Y. Mokrousov, S. Blügel, S. Auffret, O. Boulle, G. Gaudin, and P. Gambardella, "Symmetry and magnitude of spin-orbit torques in ferromagnetic heterostructures.," *Nature nanotechnology*, vol. 8, pp. 587–93, Aug. 2013.

[18] C.-F. Pai, M.-H. Nguyen, C. Belvin, L. H. Vilela-Leão, D. C. Ralph, and R. A. Buhrman, "Enhancement of Perpendicular Magnetic Anisotropy and Transmission of Spin-Hall-Effect-Induced Spin Currents by a Hf Spacer Layer in W/Hf/-CoFeB/MgO Layer," Jan. 2014.

[19] X. Fan, H. Celik, J. Wu, C. Ni, K.-J. Lee, V. O. Lorenz, and J. Q. Xiao, "Quantifying interface and bulk contributions to spin-orbit torque in magnetic bilayers.," *Nature communications*, vol. 5, p. 3042, Jan. 2014.

[20] L. Liu, O. J. Lee, T. J. Gudmundsen, D. C. Ralph, and R. A. Buhrman, "Current-Induced Switching of Perpendicularly Magnetized Magnetic Layers Using Spin Torque from the Spin Hall Effect," *Physical Review Letters*, vol. 109, p. 096602, Aug. 2012.

[21] U. H. Pi, K. Won Kim, J. Y. Bae, S. C. Lee, Y. J. Cho, K. S. Kim, and S. Seo, "Tilting of the spin orientation induced by Rashba effect in ferromagnetic metal layer," *Applied Physics Letters*, vol. 97, p. 162507, Oct. 2010.

[22] T. Suzuki, S. Fukami, N. Ishiwata, M. Yamanouchi, S. Ikeda, N. Kasai, and H. Ohno, "Current-induced effective field in perpendicularly magnetized Ta/-CoFeB/MgO wire," *Applied Physics Letters*, vol. 98, p. 142505, Apr. 2011.

[23] L. Liu, C.-F. Pai, Y. Li, H. W. Tseng, D. C. Ralph, and R. A. Buhrman, "Spin-torque switching with the giant spin Hall effect of tantalum.," *Science (New York, N.Y.)*, vol. 336, pp. 555–8, May 2012.

[24] P. P. J. Haazen, E. Murè, J. H. Franken, R. Lavrijsen, H. J. M. Swagten, and B. Koopmans, "Domain wall depinning governed by the spin Hall effect.," *Nature materials*, vol. 12, pp. 299–303, Apr. 2013.

[25] S. Emori, U. Bauer, S.-M. Ahn, E. Martinez, and G. S. D. Beach, "Current-driven dynamics of chiral ferromagnetic domain walls.," *Nature materials*, vol. 12, pp. 611–6, July 2013.

[26] K.-S. Ryu, L. Thomas, S.-H. Yang, and S. Parkin, "Chiral spin torque at magnetic domain walls.," *Nature nanotechnology*, vol. 8, pp. 527–33, July 2013.

[27] V. E. Demidov, S. Urazhdin, H. Ulrichs, V. Tiberkevich, A. Slavin, D. Baither, G. Schmitz, and S. O. Demokritov, "Magnetic nano-oscillator driven by pure spincurrent.," *Nature materials*, vol. 11, pp. 1028–31, Dec. 2012.

[28] L. Liu, C.-F. Pai, D. C. Ralph, and R. A. Buhrman, "Magnetic Oscillations Driven by the Spin Hall Effect in 3-Terminal Magnetic Tunnel Junction Devices," *Physical Review Letters*, vol. 109, p. 186602, Oct. 2012.

[29] R. Liu, W. Lim, and S. Urazhdin, "Spectral Characteristics of the Microwave Emission by the Spin Hall Nano-Oscillator," *Physical Review Letters*, vol. 110, p. 147601, Apr. 2013.

[30] S. Takahashi, H. Imamura, and S. Maekawa, "Concepts in Spin Electronics," in *Concepts in Spin Electronics*, pp. 343–370, Oxford University Press, UK, 2006.

[31] Y.-T. Chen, S. Takahashi, H. Nakayama, M. Althammer, S. T. B. Goennenwein, E. Saitoh, and G. E. W. Bauer, "Theory of spin Hall magnetoresistance," *Physical Review B*, vol. 87, p. 144411, Apr. 2013.

[32] S. Zhang, "Spin hall effect in the presence of spin diffusion," *Physical review letters*, vol. 85, pp. 393–6, July 2000.

[33] L. Liu, T. Moriyama, D. C. Ralph, and R. A. Buhrman, "Spin-Torque Ferromagnetic Resonance Induced by the Spin Hall Effect," *Physical Review Letters*, vol. 106, p. 036601, Jan. 2011.

[34] A. Azevedo, L. H. Vilela-Leão, R. L. Rodríguez-Suárez, A. F. Lacerda Santos, and S. M. Rezende, "Spin pumping and anisotropic magnetoresistance voltages in magnetic bilayers: Theory and experiment," *Physical Review B*, vol. 83, p. 144402, Apr. 2011.

[35] Y. Omori, F. Auvray, T. Wakamura, Y. Niimi, A. Fert, and Y. Otani, "Inverse spin Hall effect in a closed loop circuit," p. 5, May 2014.

[36] H. Nakayama, M. Althammer, Y.-T. Chen, K. Uchida, Y. Kajiwara, D. Kikuchi, T. Ohtani, S. Geprägs, M. Opel, S. Takahashi, R. Gross, G. E. W. Bauer, S. T. B. Goennenwein, and E. Saitoh, "Spin Hall Magnetoresistance Induced by a Nonequilibrium Proximity Effect," *Physical Review Letters*, vol. 110, p. 206601, May 2013.

[37] J. Shi, P. Zhang, D. Xiao, and Q. Niu, "Proper Definition of Spin Current in Spin-Orbit Coupled Systems," *Physical Review Letters*, vol. 96, p. 076604, Feb. 2006.

[38] P. Jacquod, R. S. Whitney, J. Meair, and M. Büttiker, "Onsager relations in coupled electric, thermoelectric, and spin transport: The tenfold way," *Physical Review B*, vol. 86, p. 155118, Oct. 2012.

[39] G. Schmidt and L. W. Molenkamp, "Spin injection into semiconductors, physics and experiments," *Semiconductor Science and Technology*, vol. 17, pp. 310–321, Apr. 2002.

[40] K. Ando, S. Takahashi, J. Ieda, H. Kurebayashi, T. Trypiniotis, C. H. W. Barnes, S. Maekawa, and E. Saitoh, "Electrically tunable spin injector free from the impedance mismatch problem.," *Nature Materials*, vol. 10, pp. 655–659, 2011.

[41] C.-F. Pai, L. Liu, Y. Li, H. W. Tseng, D. C. Ralph, and R. A. Buhrman, "Spin transfer torque devices utilizing the giant spin Hall effect of tungsten," *Applied Physics Letters*, vol. 101, p. 122404, Sept. 2012.

[42] H. Ulrichs, V. E. Demidov, S. O. Demokritov, W. L. Lim, J. Melander, N. Ebrahim-Zadeh, and S. Urazhdin, "Optimization of Pt-based spin-Hall-effect spintronic devices," *Applied Physics Letters*, vol. 102, p. 132402, Apr. 2013.

[43] M. Weiler, M. Althammer, F. D. Czeschka, H. Huebl, M. S. Wagner, M. Opel, I.-M. Imort, G. Reiss, A. Thomas, R. Gross, and S. T. B. Goennenwein, "Local Charge and Spin Currents in Magnetothermal Landscapes," *Physical Review Letters*, vol. 108, p. 106602, Mar. 2012.

[44] S. Y. Huang, X. Fan, D. Qu, Y. P. Chen, W. G. Wang, J. Wu, T. Y. Chen, J. Q. Xiao, and C. L. Chien, "Transport Magnetic Proximity Effects in Platinum," *Physical Review Letters*, vol. 109, p. 107204, Sept. 2012.

[45] X. Jia, K. Liu, K. Xia, and G. E. W. Bauer, "Spin transfer torque on magnetic insulators," *Europhysics Letters*, vol. 96, p. 17005, Oct. 2011.

[46] E. Rashba, "Spin currents in thermodynamic equilibrium: The challenge of discerning transport currents," *Physical Review B*, vol. 68, p. 241315, Dec. 2003.

[47] A. Kiselev and K. Kim, "Prohibition of equilibrium spin currents in multiterminal ballistic devices," *Physical Review B*, vol. 71, p. 153315, Apr. 2005.

[48] F. Xiu, L. He, Y. Wang, L. Cheng, L.-T. Chang, M. Lang, G. Huang, X. Kou, Y. Zhou, X. Jiang, Z. Chen, J. Zou, A. Shailos, and K. L. Wang, "Manipulating surface states in topological insulator nanoribbons.," *Nature nanotechnology*, vol. 6, pp. 216–21, Apr. 2011.

[49] C. Brüne, A. Roth, H. Buhmann, E. M. Hankiewicz, L. W. Molenkamp, J. Maciejko, X.-L. Qi, and S.-C. Zhang, "Spin polarization of the quantum spin Hall edge states," *Nature Physics*, vol. 8, pp. 486–491, May 2012.

[50] J. W. McIver, D. Hsieh, H. Steinberg, P. Jarillo-Herrero, and N. Gedik, "Control over topological insulator photocurrents with light polarization.," *Nature nanotechnology*, vol. 7, pp. 96–100, Feb. 2012.

[51] A. A. Burkov and D. G. Hawthorn, "Spin and Charge Transport on the Surface of a Topological Insulator," *Physical Review Letters*, vol. 105, p. 066802, Aug. 2010.

[52] M. Buttiker, "Symmetry of electrical conduction," *IBM Journal of Research and Development*, vol. 32, pp. 317–334, May 1988.

[53] R. H. Silsbee, "Spinorbit induced coupling of charge current and spin polarization," *Journal of Physics: Condensed Matter*, vol. 16, pp. R179–R207, Feb. 2004.

[54] I. Adagideli, G. Bauer, and B. Halperin, "Detection of Current-Induced Spins by Ferromagnetic Contacts," *Physical Review Letters*, vol. 97, p. 256601, Dec. 2006.

[55] D. Culcer, E. H. Hwang, T. D. Stanescu, and S. Das Sarma, "Two-dimensional surface charge transport in topological insulators," *Physical Review B*, vol. 82, p. 155457, Oct. 2010.

[56] O. V. Yazyev, J. E. Moore, and S. G. Louie, "Spin Polarization and Transport of Surface States in the Topological Insulators Bi_{2}Se_{3} and Bi_{2}Te_{3} from First Principles," *Physical Review Letters*, vol. 105, p. 266806, Dec. 2010.

[57] P. Hammar and M. Johnson, "Potentiometric measurements of the spin-split subbands in a two-dimensional electron gas," *Physical Review B*, vol. 61, pp. 7207–7210, Mar. 2000.

[58] R. Silsbee, "Theory of the detection of current-induced spin polarization in a two-dimensional electron gas," *Physical Review B*, vol. 63, p. 155305, Mar. 2001.

[59] P. R. Hammar and M. Johnson, "Spin-dependent current transmission across a ferromagnetinsulator two-dimensional electron gas junction," *Applied Physics Letters*, vol. 79, p. 2591, Oct. 2001.

[60] Y. H. Park, H. Cheol Jang, H. C. Koo, H.-j. Kim, J. Chang, S. H. Han, and H.-J. Choi, "Observation of gate-controlled spin[horizontal bar]orbit interaction using a ferromagnetic detector," *Journal of Applied Physics*, vol. 111, p. 07C317, Mar. 2012.

[61] R. Stacey, "Eliminating lattice fermion doubling," *Physical Review D*, vol. 26, pp. 468–472, July 1982.

[62] M. Bianchi, D. Guan, S. Bao, J. Mi, B. B. Iversen, P. D. C. King, and P. Hofmann, "Coexistence of the topological state and a two-dimensional electron gas on the surface of Bi(2)Se(3).," *Nature communications*, vol. 1, p. 128, Jan. 2010.

[63] P. D. C. King, R. C. Hatch, M. Bianchi, R. Ovsyannikov, C. Lupulescu, G. Landolt, B. Slomski, J. H. Dil, D. Guan, J. L. Mi, E. D. L. Rienks, J. Fink, A. Lindblad, S. Svensson, S. Bao, G. Balakrishnan, B. B. Iversen, J. Osterwalder, W. Eberhardt, F. Baumberger, and P. Hofmann, "Large Tunable Rashba Spin Splitting of a Two-Dimensional Electron Gas in Bi_{2}Se_{3}," *Physical Review Letters*, vol. 107, p. 096802, Aug. 2011.

[64] S. Datta, "Nanoelectronic Devices: A Unified View," in *Oxford Handbook of Nanoscience and Technology: Volume 1: Basic Aspects* (A. Narlikar and Y. Fu, eds.), p. 920, OUP Oxford, 2010.

[65] S. Datta, *Electronic Transport in Mesoscopic Systems*. Cambridge University Press, 1997.

[66] Z.-H. Zhu, G. Levy, B. Ludbrook, C. N. Veenstra, J. A. Rosen, R. Comin, D. Wong, P. Dosanjh, A. Ubaldini, P. Syers, N. P. Butch, J. Paglione, I. S. Elfimov, and A. Damascelli, "Rashba Spin-Splitting Control at the Surface of the Topological Insulator Bi_{2}Se_{3}," *Physical Review Letters*, vol. 107, p. 186405, Oct. 2011.

[67] J. Tang, L.-T. Chang, X. Kou, K. Murata, E. S. Choi, M. Lang, Y. Fan, Y. Jiang, M. Montazeri, W. Jiang, Y. Wang, L. He, and K. L. Wang, "Electrical detection of spin-polarized surface states conduction in (Bi(0.53)Sb(0.47))2Te3 topological insulator.," *Nano letters*, vol. 14, pp. 5423–9, Sept. 2014.

[68] D. Ralph and M. Stiles, "Spin transfer torques," *Journal of Magnetism and Magnetic Materials*, vol. 320, pp. 1190–1216, Apr. 2008.

[69] M. Johnson and R. Silsbee, "Coupling of electronic charge and spin at a ferromagnetic-paramagnetic metal interface," *Physical Review B*, vol. 37, pp. 5312–5325, Apr. 1988.

[70] K. E. Buschow, *Concise Encyclopedia of Magnetic and Superconducting Materials, 2nd Edition*. Elsevier Science, 2005.

[71] A. R. Mellnik, J. S. Lee, A. Richardella, J. L. Grab, P. J. Mintun, M. H. Fischer, A. Vaezi, A. Manchon, E. A. Kim, N. Samarth, and D. C. Ralph, "Spin Transfer Torque Generated by the Topological Insulator Bi_2Se_3," p. 34, Feb. 2014.

[72] G. Yu, P. Upadhyaya, Y. Fan, J. G. Alzate, W. Jiang, K. L. Wong, S. Takei, S. A. Bender, L.-T. Chang, Y. Jiang, M. Lang, J. Tang, Y. Wang, Y. Tserkovnyak, P. K. Amiri, and K. L. Wang, "Switching of perpendicular magnetization by spin-orbit torques in the absence of external magnetic fields.," *Nature nanotechnology*, vol. advance on, May 2014.

[73] P. Deorani, J. Son, K. Banerjee, N. Koirala, M. Brahlek, S. Oh, and H. Yang, "Observation of inverse spin Hall effect in bismuth selenide," *Physical Review B*, vol. 90, p. 094403, Sept. 2014.

[74] C. H. Li, O. M. J. van 't Erve, J. T. Robinson, Y. Liu, L. Li, and B. T. Jonker, "Electrical detection of charge-current-induced spin polarization due to spin-momentum locking in Bi2Se3.," *Nature nanotechnology*, vol. 9, pp. 218–24, Mar. 2014.

[75] A. Dankert, J. Geurs, M. V. Kamalakar, and S. P. Dash, "Room Temperature Electrical Detection of Spin Polarized Currents in Topological Insulators," *arxiv.org/abs/1410.8038*, Oct. 2014.

[76] L. Liu, A. Richardella, I. Garate, Y. Zhu, N. Samarth, and C.-T. Chen, "Spin-Polarized Tunneling Study on Spin-Momentum Locking in the Topological Insulator Bismuth Selenide," *arxiv.org/abs/1410.7494*, Oct. 2014.

[77] Y. Fan, P. Upadhyaya, X. Kou, M. Lang, S. Takei, Z. Wang, J. Tang, L. He, L.-T. Chang, M. Montazeri, G. Yu, W. Jiang, T. Nie, R. N. Schwartz, Y. Tserkovnyak, and K. L. Wang, "Magnetization switching through giant spin-orbit torque in a magnetically doped topological insulator heterostructure.," *Nature materials*, Apr. 2014.

[78] Y. Shiomi, K. Nomura, Y. Kajiwara, K. Eto, M. Novak, K. Segawa, Y. Ando, and E. Saitoh, "Spin-Electricity Conversion Induced by Spin Injection into Topological Insulators," *Physical Review Letters*, vol. 113, p. 196601, Nov. 2014.

[79] M. Jamali, J. S. Lee, Y. Lv, Z. Zhao, N. Samarth, and J.-P. Wang, "Room Temperature Spin Pumping in Topological Insulator Bi2Se3," *arxiv.org/abs/1407.7940*, July 2014.

[80] S. Hong, V. Diep, S. Datta, and Y. P. Chen, "Modeling potentiometric measurements in topological insulators including parallel channels," *Physical Review B*, vol. 86, p. 085131, Aug. 2012.

[81] S. Datta, *Lessons from Nanoelectronics: A New Perspective on Transport*. World Scientific Publishing Company, 2012.

[82] P. Gambardella and I. M. Miron, "Current-induced spin-orbit torques.," *Philosophical transactions. Series A, Mathematical, physical, and engineering sciences*, vol. 369, pp. 3175–97, Aug. 2011.

[83] A. R. Mellnik, J. S. Lee, A. Richardella, J. L. Grab, P. J. Mintun, M. H. Fischer, A. Vaezi, A. Manchon, E.-A. Kim, N. Samarth, and D. C. Ralph, "Spin-transfer torque generated by a topological insulator," *Nature*, vol. 511, pp. 449–451, July 2014.

[84] J. C. R. Sánchez, L. Vila, G. Desfonds, S. Gambarelli, J. P. Attané, J. M. De Teresa, C. Magén, and A. Fert, "Spin-to-charge conversion using Rashba coupling at the interface between non-magnetic materials.," *Nature communications*, vol. 4, p. 2944, Jan. 2013.

[85] D. Nikonov, "Recursive algorithm for NEGF in Matlab. [Online]," *http://nanohub.org/resources/1983*, 2006.

APPENDICES

A. DERIVATION OF EQ. (2.7)

Each terminal current is defined as follows

$$\begin{aligned} I_1 &= \int_0^t dy \int_0^w dz\, J_x|_{x=0}, \quad I_2 = -\int_0^t dy \int_0^w dz\, J_x|_{x=L} \\ I_3 &= \int_0^l dx \int_0^w dz\, J_y\big|_{y=0}, \quad I_4 = -\int_0^l dx \int_0^w dz\, J_y\big|_{y=d} \\ I_5 &= \int_0^l dx \int_0^t dy\, J_z|_{z=0}, \quad I_6 = -\int_0^l dx \int_0^t dy\, J_z|_{z=t}, \end{aligned} \tag{A.1}$$

with J_x, J_y, J_z representing current densities along $\hat{x}$, $\hat{y}$, $\hat{z}$ directions respectively. Using Eq. (2.6) the terminal currents are given by

$$\begin{aligned} I_1^c &= \int_0^t dy \int_0^w dz\, J_x^c|_{x=0} \\ &= -\sigma \int_0^t dy \int_0^w dz\, (\partial_x V^c + \theta_{\rm SH}\partial_z V^y - \theta_{\rm SH}\partial_y V^z)|_{x=0} \\ &= -\sigma \tfrac{wt}{l}\,(V_2^c - V_1^c) - \sigma\theta_{\rm SH} \int_0^t dy\, (V^y|_{z=t} - V^y|_{z=0}) + \sigma\theta_{\rm SH} \int_0^w dz \left(V^z|_{y=d} - V^z|_{y=0} \right) \\ &= -\sigma \tfrac{wt}{l}\,(V_2^c - V_1^c) - \sigma t\theta_{\rm SH}\,(V_6^y - V_5^y) + \sigma w\theta_{\rm SH}\,(V_4^z - V_3^z) \end{aligned} \tag{A.2}$$

$$\begin{aligned} I_3^z &= \int_0^l dx \int_0^w dz\, J_y^z\big|_{y=0} \\ &= -\sigma \int_0^l dx \int_0^w dz\, (\theta_{\rm SH}\partial_x V^c + \partial_y V^z)|_{y=0} \\ &= -\sigma\theta_{\rm SH} \int_0^w dz\, (V^c|_{x=l} - V^c|_{x=0}) - \sigma \tfrac{lw}{\lambda} \left(-V_3^z \coth \tfrac{t}{\lambda} + V_4^z \mathrm{csch}\, \tfrac{t}{\lambda} \right) \\ &= -\sigma w\theta_{\rm SH}\,(V_2^c - V_1^c) + \sigma \tfrac{lw}{\lambda} V_3^z \coth \tfrac{t}{\lambda} - \sigma \tfrac{lw}{\lambda} V_4^z \mathrm{csch}\, \tfrac{t}{\lambda} \end{aligned} \tag{A.3}$$

$$
\begin{aligned}
I_5^y &= \int_0^l dx \int_0^t dy\, J_z^y|_{z=0} \\
&= -\sigma \int_0^l dx \int_0^t dy\, (-\theta_{\rm SH}\partial_x V^c + \partial_z V^y)|_{z=0} \\
&= \sigma\theta_{\rm SH} \int_0^t dy\, (V^c|_{x=l} - V^c|_{x=0}) - \sigma\tfrac{lt}{\lambda}\left(-V_5^y \coth\tfrac{w}{\lambda} + V_6^y {\rm csch}\tfrac{w}{\lambda}\right) \\
&= \sigma t\theta_{\rm SH}\,(V_2^c - V_1^c) + \sigma\tfrac{lt}{\lambda}V_5^y \coth\tfrac{w}{\lambda} - \sigma\tfrac{lt}{\lambda}V_6^y {\rm csch}\tfrac{w}{\lambda}.
\end{aligned}
\tag{A.4}
$$

Other elements in the conductance matrix (Eq. (2.7)) can be worked out following same procedures.

B. DERIVATION OF EQS. (2.13)-(2.16)

We first derive Eq. (2.13) from GSHE equivalent circuit in Fig. 2.2. The open circuit spin voltages at terminals 3 and 4 ($I_3^z = I_4^z = 0$) in Fig. 2.2(c) are given by

$$V_4^z = -V_3^z = V_0^z = \frac{\theta_{\rm SH}\lambda}{l}(V_1^c - V_2^c)\tanh\frac{t}{2\lambda} \tag{B.1}$$

We have expression for charge current from circuit in Fig. 2.2(b)

$$I_1^c = G_0(V_1^c - V_2^c) - I_0^c = G_0\left[(V_1^c - V_2^c) + 2\beta_1 V_4^z\right] \tag{B.2}$$

Combining Eq. (B.1) and (B.2) we have the expression V_4^z in terms of I_1^c as in Eq. (2.13).

Secondly, the short circuit spin current at terminal 4 in Eq. (2.14) is given by

$$I_4^z = I_0^z + G_2^z V_3^z = \left(1 - \sec\mathrm{h}\frac{t}{\lambda}\right)\beta_1 G_0(V_1^c - V_2^c) \tag{B.3}$$

with $V_4^z = 0$ and $I_4^z = 0$ from Fig. 2.2(c). The open circuit spin voltage at terminal 3 are determined by

$$V_3^z = -\frac{I_0^z}{G_1^z + G_2^z} \tag{B.4}$$

From Fig. 2.2(b) we can write

$$I_1^c = G_0\left(V_1^c - V_2^c\right) - I_0^c = G_0\left(V_1^c - V_2^c\right) - \beta_1 G_0 V_3^z \tag{B.5}$$

From Eqs. (B.4) and B.5 we have

$$I_1^c = \left(1 + \frac{\beta_1^2 G_0}{G_1^z + G_2^z}\right) G_0(V_1^c - V_2^c) \tag{B.6}$$

Combining Eq. (B.4) with Eq. (B.6) yields Eq. (2.14).

Thirdly, to derive Eq. (2.15) for ISHE, we make both terminals 1 and 2 open circuited ($I_1^c = 0,\ I_2^c = 0$) then we have from Fig. 2.2(b)

$$V_1^c - V_2^c = \frac{I_0^c}{G_0} = \beta_1\left(V_3^z - V_4^z\right). \tag{B.7}$$

With terminal 4 open circuited ($I_4^z = 0$), we have

$$I_4^z = 0 = G_1^z V_4^z - G_2^z \left(V_3^z - V_4^z\right) - I_0^z \tag{B.8}$$

$$I_3^z = G_1^z V_3^z + G_2^z \left(V_3^z - V_4^z\right) + I_0^z \tag{B.9}$$

Subtracting Eq. (B.8) from Eq. (B.9) we have

$$I_3^z = G_1^z \left(V_3^z - V_4^z\right) + 2G_2^z \left(V_3^z - V_4^z\right) + 2I_0^z \tag{B.10}$$

Solving Eqs. (B.7) and (B.10) we have

$$I_3^z = \left\{ \frac{G_1^z + 2G_2^z + 2\beta_1^2 G_0}{\beta_1} \right\} \left(V_1^c - V_2^c\right) \tag{B.11}$$

which is Eq. (2.15). Lastly, to derive Eq. (2.16) we connect terminals 1 and 2 ($V_1^c = V_2^c$) together and keep terminal 4 open ($I_4^z = 0$) then we have from Fig. 2.2(b) and (c)

$$I_1^c = -I_0^c = -\beta_1 G_0 (V_3^z - V_4^z) \tag{B.12}$$

$$I_3^z = G_1^z V_3^z + G_2^z \left(V_3^z - V_4^z\right) \tag{B.13}$$

$$I_4^z = 0 = G_1^z V_4^z + G_2^z \left(V_4^z - V_3^z\right) \tag{B.14}$$

Subtracting Eq. (B.14) from Eq. (B.13) yields

$$I_3^z = \left(G_1^z + 2G_2^z\right) \left(V_3^z - V_4^z\right) \tag{B.15}$$

Finally, from Eqs. (B.12) and (B.15) we have Eq. (2.16).

C. DERIVATION OF EQ. (2.17) FROM SPIN CIRCUIT

From nodal analysis in the circuit in Fig. 2.4, we have

$$-G_2^z V_4^z + (G_B + G_1^z + G_2^z)\, V_3^z = -I_0^z \tag{C.1}$$

$$(G_T + G_1^z + G_2^z)\, V_4^z - G_2^z V_3^z = I_0^z. \tag{C.2}$$

Solving Eqs. (C.1) and (C.2) we can derive the expression for spin voltage at terminal 4 as

$$V_4^z = \frac{G_B + G_1^z}{G_B G_T + (G_B + G_T)(G_1^z + G_2^z) + G_1^z(G_1^z + 2G_2^z)} I_0^z. \tag{C.3}$$

Then the spin current at terminal 4 through top load is given by

$$\begin{aligned} I_4^z &= -G_B V_4^z \\ &= -{G'}_T I_0^z \frac{{G'}_B \sinh\frac{t}{\lambda} + \cosh\frac{t}{\lambda} - 1}{({G'}_B + {G'}_T)\cosh\frac{t}{\lambda} + (1 + {G'}_B {G'}_T)\sinh\frac{t}{\lambda}}, \end{aligned} \tag{C.4}$$

with $G'_T = G_T/(lw\sigma/\lambda)$ and $G'_B = G_B/(lw\sigma/\lambda)$. We obtain Eq. (2.17) by noting that $J_4^z = I_4^z/(lw)$ and $J_0^z = I_0^z/(lw)$.

D. DERIVATION OF EQ. (2.19)

We provide a conductance matrix for GSHE under the assumption [36] in Eq (2.18). Under this assumption, the diffusion equations for V^c, V^y, and V^z are from Eq. (2.2)

$$\begin{aligned} \partial_x^2 V^c &= 0 \\ \partial_y^2 V^{x,y,z} &= V^{x,y,z}/\lambda^2, \end{aligned} \tag{D.1}$$

which have following solutions with boundary values provided by terminal voltages of a box

$$\begin{aligned} V^c(x) &= \frac{V_2^c x + V_1^c(l-x)}{l} \\ V^{x,y,z}(y) &= \frac{V_4^{x,y,z}\sinh\left(\frac{y}{\lambda}\right) + V_3^{x,y,z}\sinh\left(\frac{t-y}{\lambda}\right)}{\sinh\left(t/\lambda\right)}. \end{aligned} \tag{D.2}$$

We can also reduce Eq. (2.1) into following sets of equations

$$\begin{aligned} \hat{x}\cdot\overrightarrow{J}^c &= J_x^c = -\sigma\left(\partial_x V^c - \theta_{\rm SH}\partial_y V^z\right) \\ \hat{y}\cdot\overrightarrow{J}^x &= J_y^x = -\sigma\partial_y V^x \\ \hat{y}\cdot\overrightarrow{J}^y &= J_y^y = -\sigma\partial_y V^y \\ \hat{y}\cdot\overrightarrow{J}^z &= J_y^z = -\sigma\left(\theta_{\rm SH}\partial_x V^c + \partial_y V^z\right) \\ \hat{z}\cdot\overrightarrow{J}^c &= J_z^c = -\sigma\theta_{\rm SH}\partial_y V^x \\ \hat{z}\cdot\overrightarrow{J}^y &= J_z^y = \sigma\theta_{\rm SH}\partial_x V^c. \end{aligned}$$

The terminal currents are given by

$$\begin{aligned} I_1^c &= \int_0^t dy \int_0^w dz\, J_x^c\big|_{x=0} \\ &= -\sigma\tfrac{wt}{l}\left(V_2^c - V_1^c\right) + \sigma w\theta_{\rm SH}\left(V_4^z - V_3^z\right) \end{aligned} \tag{D.3}$$

$$\begin{aligned} I_3^x &= \int_0^l dx \int_0^w dz\, J_y^x\big|_{y=0} \\ &= -\sigma\tfrac{lw}{\lambda}\left(-V_3^x\coth\tfrac{t}{\lambda} + V_4^x\,\mathrm{csch}\tfrac{t}{\lambda}\right) \end{aligned} \tag{D.4}$$

$$\begin{aligned} I_3^y &= \int_0^l dx \int_0^w dz\, J_y^y\big|_{y=0} \\ &= -\sigma \tfrac{lw}{\lambda} \left(-V_3^y \coth \tfrac{t}{\lambda} + V_4^y \mathrm{csch} \tfrac{t}{\lambda}\right) \end{aligned} \tag{D.5}$$

$$\begin{aligned} I_3^z &= \int_0^l dx \int_0^w dz\, J_y^z\big|_{y=0} \\ &= -\sigma w \theta_{\mathrm{SH}} \left(V_2^c - V_1^c\right) + \sigma \tfrac{lw}{\lambda} V_3^z \coth \tfrac{t}{\lambda} - \sigma \tfrac{lw}{\lambda} V_4^z \mathrm{csch} \tfrac{t}{\lambda} \end{aligned} \tag{D.6}$$

$$\begin{aligned} I_5^c &= \int_0^l dx \int_0^t dy\, J_z^c|_{z=0} \\ &= -\sigma l \theta_{\mathrm{SH}} \left(V_4^x - V_3^x\right) \end{aligned} \tag{D.7}$$

$$\begin{aligned} I_5^y &= \int_0^l dx \int_0^t dy\, J_z^y|_{z=0} \\ &= \sigma t \theta_{\mathrm{SH}} \left(V_2^c - V_1^c\right). \end{aligned} \tag{D.8}$$

Other elements in the conductance matrix (Eq. (2.19)) can be worked out following same procedures.

E. DERIVATION OF EQS. (2.27)-(2.29)

The conductance matrix for YIG with magnetization direction along $(m_z, m_x, m_y) = (\cos\alpha\cos\beta,\ \sin\alpha\cos\beta,\ \sin\beta)$ direction is given by

$$G_{\rm YIG}\left(\vec{m}\right) = R(\hat{y},\alpha)R(\hat{x},-\beta)G_{\rm YIG}R(\hat{x},-\beta)^{+}R(\hat{y},\alpha)^{+}, \tag{E.1}$$

with $R(\hat{y},\alpha)$ and $R(\hat{x},-\beta)$ rotation matrices along $\hat{y}$ and $\hat{x}$ with angles α and β respectively. The charge currents along $\hat{x}$ and $\hat{y}$ directions are given by

$$I_1^c = tw\frac{\sigma}{l}(V_1^c - V_2^c) + w\sigma\theta_{\rm SH}(V_3^z - V_3^z) \tag{E.2}$$

and

$$I_5^c = l\sigma\theta_{\rm SH}(V_3^x - V_4^x) \tag{E.3}$$

from Eq. (2.19) where $V_3^z - V_4^z$ and $V_3^x - V_4^x$ can be expressed in terms of $V_1^c - V_2^c$ from Eq. (2.26) and given by

$$V_3^x - V_4^x = -\frac{\lambda\theta_{\rm SH}}{l}(V_1^c - V_2^c)\tanh^2\left(\frac{t}{2\lambda}\right)(m_x m_z{\rm Re} + m_y{\rm Im})\frac{\frac{2\lambda(G_r+iG_i)}{\sigma}}{1+\frac{2\lambda(G_r+iG_i)}{\sigma}\coth\left(\frac{t}{\lambda}\right)} \tag{E.4}$$

$$\begin{aligned} V_3^z - V_4^z = &-\frac{\theta_{\rm SH}\lambda(V_1^c - V_2^c)}{l}2\tanh\left(\frac{t}{2\lambda}\right) \\ &+\frac{\theta_{\rm SH}\lambda(V_1^c - V_2^c)}{l}\tanh^2\left(\frac{t}{2\lambda}\right)\left(1-m_z^2\right){\rm Re}\frac{\frac{2\lambda(G_r+iG_i)}{\sigma}}{1+\frac{2\lambda(G_r+iG_i)}{\sigma}\coth\left(\frac{t}{\lambda}\right)}. \end{aligned} \tag{E.5}$$

F. DERIVATION OF EQS. (3.12) AND (3.13)

Here we assume positive $\hbar v_F$, α and ϵ. In the case of TI SS, there is single band given by $\epsilon(\vec{k}) = \hbar v_F k$ and $\hat{s}(\vec{k}) = \hat{x}sin\theta - \hat{y}cos\theta$. We start the derivation from Eq. (3.2).

$$\begin{aligned}
\vec{p} &= \frac{\sum\limits_{v_x(\vec{k})>0} \hat{s}_i(\vec{k})\delta(E_F - \epsilon(\vec{k}))}{\sum\limits_{v_x(\vec{k})>0} \delta(E_F - \epsilon(\vec{k}))} \\
&= \frac{\int_{-\pi/2}^{+\pi/2} d\theta(\hat{x}sin\theta - \hat{y}cos\theta) \int_0^{+\infty} kdk\delta(E_F - \epsilon_i(\vec{k}))}{\int_{-\pi/2}^{+\pi/2} d\theta \int_0^{+\infty} kdk\delta(E_F - \epsilon_i(\vec{k}))} \\
&= -\frac{2}{\pi}\hat{y},
\end{aligned}$$

which is Eq. (3.12).

In the case of Rashba channel, first note that we have two Fermi circles with inner and outer radius k_1 and k_2 respectively ($\epsilon_{inner}(\vec{k}) = \hbar^2k^2/2m + \alpha k$, $\hat{s}_{inner}(\vec{k}) = \hat{x}sin\theta - \hat{y}cos\theta$ and $\epsilon_{outer}(\vec{k}) = \hbar^2k^2/2m - \alpha k$, $\hat{s}_{outer}(\vec{k}) = -\hat{x}sin\theta + \hat{y}cos\theta$). For the denominator we have

$$\begin{aligned}
&\sum_i \sum_{v_x(\vec{k})>0} \delta(E_F - \epsilon_i(\vec{k})) \\
&= \sum_{v_x(\vec{k})>0} \{\delta(E_F - \epsilon_{inner}(\vec{k})) + \delta(E_F - \epsilon_{outer}(\vec{k}))\} \\
&= \frac{A}{(2\pi)^2} \int_{-\pi/2}^{+\pi/2} d\theta \int_0^{+\infty} kdk\{\delta(\frac{\hbar^2}{2m}(k - k_1)(k + k_2)) \\
&\quad +\delta(\frac{\hbar^2}{2m}(k + k_1)(k - k_2))\} \\
&= \frac{A}{(2\pi)^2}\frac{2m\pi}{\hbar^2}.
\end{aligned}$$

Based on these,

$$\begin{aligned}\vec{p} &= \frac{k_1}{\pi(k_1+k_2)}\int_{-\pi/2}^{+\pi/2} d\theta(\hat{x}sin\theta - \hat{y}cos\theta) \\ &\quad + \frac{k_2}{\pi(k_1+k_2)}\int_{-\pi/2}^{+\pi/2} d\theta(-\hat{x}sin\theta + \hat{y}cos\theta) \\ &= \frac{2}{\pi}\frac{k_2-k_1}{k_2+k_1}\hat{y},\end{aligned}$$

which is Eq. (3.13). The cases for negative values of $\hbar v_F$, α or $\epsilon < 0$ can be shown similarly.

G. NEGF DETAILS OF CHAPTER 4

In this appendix we describe the details of NEGF model used in section 3 of chapter 4. We generally follow the discussion and notations in Ref. [80] with an efficient algorithm in Ref. [85] here.

Hamiltonian: The model Hamiltonian for TISS is given by

$$H_{\mathrm{TISS}} = \frac{\hbar v_F}{a}[\sigma_x \sin(k_y a) - \sigma_y \sin(k_x a) - \sigma_z(\cos(k_x a) + \cos(k_y a) - 2)], \tag{G.1}$$

with σ_x, σ_y, σ_z the Pauli spin matrices and a, v_0 the lattice spacing and the Fermi velocity respectively.

Self energy for contact: Two self energies Σ_L and Σ_R are used for left and right contacts representing semi-infinite contacts of extended channel.

Self energy for incoherent scattering: The incoherent scattering in the channel is included by the self energy Σ_S with isotropic momentum and spin relaxations in the self-consistent Born approximation. The momentum randomizing scattering is described by [64]

$$\begin{aligned} [\Sigma_s]_{ij} &= d_m \delta_{ij}\delta_{ik}\delta_{jl}[G]_{kl} \\ [\Sigma^{in}{}_s]_{ij} &= d_m \delta_{ij}\delta_{ik}\delta_{jl}[G^n]_{kl}, \end{aligned} \tag{G.2}$$

with i, j, k, and l representing indices in real space. The spin randomizing scattering is described by [64]

$$\begin{aligned} [\Sigma_s]_{ab} &= (\vec{\sigma}_{ac} \cdot \vec{\sigma}_{db})[G]_{cd} \\ [\Sigma^{in}{}_s]_{ab} &= (\vec{\sigma}_{ac} \cdot \vec{\sigma}_{db})[G^n]_{cd}, \end{aligned} \tag{G.3}$$

with a, b, c, and d representing indices in spin space.

Self energy for FM: The self energy for FM (Σ_{FM}) is modeled as an additional scattering process in the channel represented by isotropic momentum and spin relaxations in the self-consistent Born approximation.

Currents and Voltages: The current operator at terminal 'i' is defined as [65],

$$I_i^{op}(E) = \frac{q}{ih}(\left[\Sigma_i^{in}G^A - G^R\Sigma_i^{in}\right] + \left[\Sigma_i G^n - G^n\Sigma_i^+\right]), \tag{G.4}$$

for a given energy. The charge and spin currents are calculated from

$$I(E) = \mathrm{Tr}(I^{op}), \text{ and } \vec{i}^s(E) = \mathrm{Tr}(\vec{\sigma}I^{op}). \tag{G.5}$$

The charge and spin occupation factors are calculated from

$$f = \mathrm{Tr}(G^n)/\mathrm{Tr}(A), \text{ and } \vec{f}^s = \mathrm{Tr}(\vec{\sigma}G^n)/\mathrm{Tr}(A). \tag{G.6}$$

To compare NEGF result with the proposed circuit model the following identifications are made, which can be justified within a linear response regime [81],

$$\begin{aligned} \frac{v^s}{V} &= \frac{f^s}{f_1 - f_2} \\ \frac{I}{G_B V} &= T(E) \\ \frac{i^s}{G_B V} &= \frac{i^s(E)}{(G_B/q)(f_1 - f_2)}, \end{aligned} \tag{G.7}$$

with $I = \int dE\, I(E)$, $i^s = \int dE\ i^s(E)$, and $G/G_B = \lambda_I/(\lambda_I + L)$ to take into account the contact resistance in NEGF result.

H. MATLAB CODES

Codes for Fig. 3.3(a)

```
clear all

% Inputs
hbar=1.06e-34;q=1.6e-19;m=0.04*9.1e-31;
sx=[0 1;1 0];sy=[0 -i;i 0];sz=[1 0;0 -1];

a=10e-10; % 1/kF~1nm
% t0=(hbar^2)/(2*m*(a^2)*q);
qh=q/hbar;BB=0;
% eta=4.1;%[eV A]
eta=3.3;%[eV A]
t0=eta*1e-10/a;
NW=100;
% Np=10;
SX=kron(eye(NW),sx);SY=kron(eye(NW),sy);SZ=kron(eye(NW),sz);
spineye=kron(eye(NW,NW),ones(2,2));
vF=eta/hbar*1e-10*q;
% L=zeros(Np);R=L;L(1,1)=1;R(Np,Np)=1;
zplus=1i*1e-6;
Y=a*([0:1:NW-1]-0.5*NW);
D=3*1e-3; % coupling constant
    %%%%%%%%%%%%%%%%%%%%%%%%%%%%%%%%%%%%%%%%%%%%%%%%%%%%%%%%%%%%
ctr=0.5;
kk=1;
Elo=t0*1;
```

```
dE=1*1e-3; Ehi=Elo;
EE=Elo;
EE=0.2;
% t0=t0*10;
tic
leng_low=50;
leng_high=50;
if D==0
    leng_high=leng_low;
end
%%
HW=eye(NW);

% Ordinary spin degenerate
al=4*t0*eye(2);by=-t0*eye(2);bx=-t0*eye(2);

% Topological insulator
    al=-2*t0*sz;by=t0/2*(sz-1i*sx);bx=t0/2*(sz+1i*sy); % to=eta/a
if NW==1
    al=al/2;
end
% for EE=Elo:dE:Ehi


alpha=kron(HW,al);
alpha=alpha+kron(diag(ones(1,NW-1),+1),by)+kron(diag(ones(1,NW-1),-1),by
    ');

%         alpha=alpha+kron(diag(ones(1,1),1-NW),by')+kron(diag(ones(1,1)
    ,NW-1),by); %PBC
beta=kron(spdiags(exp(i*qh*BB*a*a*[1:1:NW]'),0,NW,NW),bx);


%% self energy of contact %%
galpha=(EE+zplus)*eye(2*NW)-alpha;
```

```
g1=sancho_gs(galpha,beta');
g2=sancho_gs(galpha,beta);
sigL=1*beta'*g1*beta;
sigR=1*beta*g2*beta';
gamL=1i*(sigL-sigL');
gamR=1i*(sigR-sigR');


for length=leng_low:5:leng_high
    leng(kk)=length;
    Np=length
    %% initialization for RGF
    % Al = zeros(2*NW,2*NW,Np-1);
    Ad = zeros(2*NW,2*NW,Np);
    Au = zeros(2*NW,2*NW,Np-1);
    Sigin=zeros(2*NW,2*NW,Np);
    % Sigout=zeros(2*NW,2*NW,Np);
    SigB=zeros(2*NW,2*NW,Np);SiginB=zeros(2*NW,2*NW,Np);

    TMRL(kk)=0;


    %%        BLOCK SET-UP
    fchange1=1;fchange2=1;iter=1;

    while (fchange1+fchange2)>1e-5
        for ii=1:Np-1
            Ad(:,:,ii)=EE*eye(2*NW)-alpha-SigB(:,:,ii);
            Au(:,:,ii)=-beta;
            %         Al(:,:,ii)=-beta';
        end
        Ad(:,:,Np)=EE*eye(2*NW)-alpha-SigB(:,:,Np);

        Ad(:,:,1)=Ad(:,:,1)-sigL;
        Ad(:,:,Np)=Ad(:,:,Np)-sigR;
```

```
        Sigin=SiginB;
        Sigin(:,:,1)=Sigin(:,:,1)+gamL;     %

        [Grd,Gnd,Gpd] = recursealgblock3d_new2(2*NW,Np,Ad,Au,Sigin);
        if iter==1
            TMB=real(trace(gamR*(Gnd(:,:,Np))));
        end
        for ii=1:Np

            SigBnew(:,:,ii)=D*(SX*(spineye.*Grd(:,:,ii))*SX+SY*(spineye.
                *Grd(:,:,ii))*SY+SZ*(spineye.*Grd(:,:,ii))*SZ); % spin
                random
            SiginBnew(:,:,ii)=D*(SX*(spineye.*Gnd(:,:,ii))*SX+SY*(
                spineye.*Gnd(:,:,ii))*SY+SZ*(spineye.*Gnd(:,:,ii))*SZ);

%             SigBnew(:,:,ii)=D*eye(2*NW,2*NW).*Grd(:,:,ii);
%             SiginBnew(:,:,ii)=D*eye(2*NW,2*NW).*Gnd(:,:,ii);


%             SigBnew(:,:,ii)=D*spineye.*Grd(:,:,ii); % TI spin
    preserving case
%             SiginBnew(:,:,ii)=D*spineye.*Gnd(:,:,ii);

            change1(ii)=sum(sum(abs(SigBnew(:,:,ii)-SigB(:,:,ii))));
            norm1(ii)=sum(sum(abs(SigBnew(:,:,ii)+SigB(:,:,ii))));
            change2(ii)=sum(sum(abs(SiginBnew(:,:,ii)-SiginB(:,:,ii))));
            norm2(ii)=sum(sum(abs(SiginBnew(:,:,ii)+SiginB(:,:,ii))));

            SigB(:,:,ii)=SigB(:,:,ii)+ctr*(SigBnew(:,:,ii)-SigB(:,:,ii))
                ;
            SiginB(:,:,ii)=SiginB(:,:,ii)+ctr*(SiginBnew(:,:,ii)-SiginB
                (:,:,ii));
        end
```

```
        fchange1=sum(change1)/sum(norm1);fchange2=sum(change2)/sum(norm1
            )
        iter=iter+1
    end % end of while loop

    TM(kk)=real(trace(gamR*(Gnd(:,:,Np))));
    TM(kk)
    %     E(kk)=EE;
    kk=kk+1;

end % length
toc
%% Electron density along the device
    for ii=1:Np
        eden(ii)=real(trace(Gnd(:,:,ii)))/real(trace(1i*(Grd(:,:,ii)-Grd
            (:,:,ii)')));
        edenyd(ii)=real(trace(kron(eye(NW),(eye(2)-sy))*Gnd(:,:,ii)))/
            real(trace(1i*(Grd(:,:,ii)-Grd(:,:,ii)')));
        edenyu(ii)=real(trace(kron(eye(NW),(eye(2)+sy))*Gnd(:,:,ii)))/
            real(trace(1i*(Grd(:,:,ii)-Grd(:,:,ii)')));
    end


%%
beta=TM/TMB;
aeden=(1-beta)*(1-linspace(0.5,Np-0.5,Np)'/Np)+beta/2;
% aeden=(1-beta)*(1-linspace(1,Np,Np)'/Np)+beta/2;
% aeden=(1-beta)*(1-linspace(0,Np-1,Np)'/Np)+beta/2;
figure(605);
hold on



qq=plot([1:1:Np]*a/1e-9,aeden,'k-');hold on
o=plot([1:1:Np]*a/1e-9,aeden+(1-aeden(1))*2/pi,'r-.');hold on
```

```
p=plot([1:1:Np]*a/1e-9,aeden-(1-aeden(1))*2/pi,'b--');hold on


NJ=3;
k=plot([1:NJ:Np]*a/1e-9,eden(1:NJ:Np),'ko');hold on
m=plot([1:NJ:Np]*a/1e-9,edenyd(1:NJ:Np),'ro');hold on
n=plot([1:NJ:Np]*a/1e-9,edenyu(1:NJ:Np),'bo');hold on

set(k,'linewidth',[3.0]);set(m,'linewidth',[3.0]);set(n,'linewidth',[3.0
    ]);
set(o,'linewidth',[3.0]);set(p,'linewidth',[3.0]);set(qq,'linewidth',[3
    .0]);
set(gca,'Fontsize',[24])
% title(['NEGF real,  N_w = ',num2str(NW),'   N_L = ',num2str(Np),''])
% ylabel('f_+_y, f, f_-_y');
% ylabel('F_{\vec{m}}');
% ylabel('$F_{\vec{m}}$','interpreter','latex');


% xlabel('Length [nm]','interpreter','latex');
% ylim([0 1])
box on
% grid on



function [G_old]=sancho_gs(alpha,beta) % beta is the matrix of same
    basis in a Raw

change=1;
N=size(alpha);
t_old=inv(alpha)*beta';
tt_old=inv(alpha)*beta;
T_old=t_old;
delta_old=tt_old;
```

```
while change>1e-10
    t_new=inv(eye(N)-t_old*tt_old-tt_old*t_old)*t_old*t_old;
    tt_new=inv(eye(N)-t_old*tt_old-tt_old*t_old)*tt_old*tt_old;
    delta_new=delta_old*tt_new;

    T_new=T_old+delta_old*t_new;
    change=sum(sum(abs(delta_new)))/sum(sum(abs(T_new)));
    t_old=t_new;
    tt_old=tt_new;
    delta_old=delta_new;
    T_old=T_new;
end
G_old=inv(alpha-beta*T_new);

function [Grd,Gnd,Gpd] = recursealgblock3d_new(Nc,Np,Ad,Au,Sigin)
% based on Dmitri Nikonov; Siyu Koswatta (2006), "recursive algorithm
   for NEGF in Matlab," https://nanohub.org/resources/1983.
% format long
edinC = eye(Nc,Nc);
grL = zeros(Nc,Nc,Np);                                  % initialize left-
   connected function
ginL = zeros(Nc,Nc,Np);                                 % initialize left-
   connected in-scattering function
% gipL = zeros(Nc,Nc,Np);                                 % initialize left-
   connected out-scattering function
Grl = zeros(Nc,Nc,Np-1);
Grd = zeros(Nc,Nc,Np);                                  % initialize the
   Green's function
Gru = zeros(Nc,Nc,Np-1);
% Gnl = zeros(Nc,Nc,Np-1);
Gnd = zeros(Nc,Nc,Np);                                  % initialize the
   electron coherence function
% Gnu = zeros(Nc,Nc,Np-1);
% Gpl = zeros(Nc,Nc,Np-1);
% initialize the hole coherence function
```

```
% Gpu = zeros(Nc,Nc,Np-1);
grL(:,:,1)=(Ad(:,:,1))\edinC;                                    % step 1
for q=2:Np                                                  % obtain the left-
    connected function
     obra = (Ad(:,:,q)-Au(:,:,q-1)'*grL(:,:,q-1)*Au(:,:,q-1));
     grL(:,:,q)=obra\edinC;
end

Grd(:,:,Np)=grL(:,:,Np);                                    % step 2
for q=(Np-1):-1:1
     Grl(:,:,q)=-Grd(:,:,q+1)*Au(:,:,q)'*grL(:,:,q);  % obtain the sub-
        diagonal of the Green's function
     Gru(:,:,q)=-grL(:,:,q)*Au(:,:,q)*Grd(:,:,q+1);  % obtain the super-
        diagonal of the Green's function
     prom = edinC-Au(:,:,q)*Grl(:,:,q);
     Grd(:,:,q)=grL(:,:,q)*prom;                            % obtain the
        diagonal of the Green's function
end




ginL(:,:,1)=grL(:,:,1)*Sigin(:,:,1)*grL(:,:,1)';      % step 3
for q=2:Np
     sla2 = Au(:,:,q-1)'*ginL(:,:,q-1)*Au(:,:,q-1);
     prom = Sigin(:,:,q) + sla2;
     ginL(:,:,q) = grL(:,:,q)*prom*grL(:,:,q)';      % left-connected in-
        scattering function
end
Gnd(:,:,Np)=(ginL(:,:,Np));                             % step 4
for q=(Np-1):-1:1
     %     Gnl(:,:,q) = - Grd(:,:,q+1)*Au(:,:,q)*ginL(:,:,q) - Gnd(:,:,q
        +1)*Al_cr(:,:,q)*grL'(:,:,q);
     nui = ginL(:,:,q) + grL(:,:,q)*Au(:,:,q)*Gnd(:,:,q+1)*Au(:,:,q)'*grL
        (:,:,q)' - ...
```

```
        ( ginL(:,:,q)*Au(:,:,q)*Gru(:,:,q)' + Gru(:,:,q)*Au(:,:,q)'*ginL
            (:,:,q) );
    Gnd(:,:,q) = nui;
end
clear grL ginL Grl Gru

Gpd = zeros(Nc,Nc,Np);
for k=1:Np

    Gpd(:,:,k) = i*(Grd(:,:,k)-Grd(:,:,k)')-Gnd(:,:,k);
                                % advanced Green's function
end
```

Codes for Fig. 3.3(b)

```
%% 2D real space
clear all

% Inputs
hbar=1.06e-34;q=1.6e-19;
% m=0.04*9.1e-31;
sx=[0 1;1 0];sy=[0 -i;i 0];sz=[1 0;0 -1];

a=10e-10; % 1/kF~1nm
% t0=(hbar^2)/(2*m*(a^2)*q);
qh=q/hbar;BB=0;
% eta=4.1;%[eV A]
eta=3.3;%[eV A]
t0=eta*1e-10/a;
NW=100;
% Np=10;
SX=kron(eye(NW),sx);SY=kron(eye(NW),sy);SZ=kron(eye(NW),sz);
spineye=kron(eye(NW,NW),ones(2,2));
vF=eta/hbar*1e-10*q;
% L=zeros(Np);R=L;L(1,1)=1;R(Np,Np)=1;
```

```
zplus=1i*1e-6;
Y=a*([0:1:NW-1]-0.5*NW);
D=1*1e-3; % coupling constant
    %%%%%%%%%%%%%%%%%%%%%%%%%%%%%%%%%%%%%%%%%%%%%%%%%%%%%%%%%%%%
ctr=0.5;
kk=1;
Elo=t0*1;
dE=1*1e-2; Ehi=Elo;
EE=Elo;
EE=0.3;
% t0=t0*10;
tic
leng_low=50;
leng_high=50;
if D==0
    leng_high=leng_low;
end
%%
HW=eye(NW);

% Ordinary spin degenerate
al=4*t0*eye(2);by=-t0*eye(2);bx=-t0*eye(2);

% Rashba
m=0.28*9.1e-31;rashba=(1)*0.79*1e-10; % mass change 0.28-> 0.05, alpha
    from PRL 107, 096802 (2011)
t0=(hbar^2)/(2*m*(a^2)*q);
by=-t0*eye(2)-1i*rashba/a/2*sx;
bx=-t0*eye(2)+1i*rashba/a/2*sy;
al=4*t0*eye(2);

% Topological insulator
%     al=-2*t0*sz;by=t0/2*(sz-1i*sx);bx=t0/2*(sz+1i*sy); % to=eta/a
if NW==1
    al=al/2;
```

```
end
% for EE=Elo:dE:Ehi


alpha=kron(HW,al);
alpha=alpha+kron(diag(ones(1,NW-1),+1),by)+kron(diag(ones(1,NW-1),-1),by
    ');

%         alpha=alpha+kron(diag(ones(1,1),1-NW),by')+kron(diag(ones(1,1)
    ,NW-1),by); %PBC
beta=kron(spdiags(exp(i*qh*BB*a*a*[1:1:NW]'),0,NW,NW),bx);


%% self energy of contact %%
galpha=(EE+zplus)*eye(2*NW)-alpha;
g1=sancho_gs(galpha,beta');
g2=sancho_gs(galpha,beta);
sigL=1*beta'*g1*beta;
sigR=1*beta*g2*beta';
gamL=1i*(sigL-sigL');
gamR=1i*(sigR-sigR');


for length=leng_low:5:leng_high
    leng(kk)=length;
    Np=length
    %% initialization for RGF
    % Al = zeros(2*NW,2*NW,Np-1);
    Ad = zeros(2*NW,2*NW,Np);
    Au = zeros(2*NW,2*NW,Np-1);
    Sigin=zeros(2*NW,2*NW,Np);
    % Sigout=zeros(2*NW,2*NW,Np);
    SigB=zeros(2*NW,2*NW,Np);SiginB=zeros(2*NW,2*NW,Np);

    TMRL(kk)=0;
```

```
%%        BLOCK SET-UP
fchange1=1;fchange2=1;iter=1;

while (fchange1+fchange2)>1e-4
    for ii=1:Np-1
        Ad(:,:,ii)=EE*eye(2*NW)-alpha-SigB(:,:,ii);
        Au(:,:,ii)=-beta;
        %         Al(:,:,ii)=-beta';
    end
    Ad(:,:,Np)=EE*eye(2*NW)-alpha-SigB(:,:,Np);

    Ad(:,:,1)=Ad(:,:,1)-sigL;
    Ad(:,:,Np)=Ad(:,:,Np)-sigR;

    Sigin=SiginB;
    Sigin(:,:,1)=Sigin(:,:,1)+gamL;    %

    [Grd,Gnd,Gpd] = recursealgblock3d_new2(2*NW,Np,Ad,Au,Sigin);
    if iter==1
        TMB=real(trace(gamR*(Gnd(:,:,Np))))
    end
    for ii=1:Np
        SigBnew(:,:,ii)=D*(SX*(spineye.*Grd(:,:,ii))*SX+SY*(spineye.
            *Grd(:,:,ii))*SY+SZ*(spineye.*Grd(:,:,ii))*SZ); % spin
            random
        SiginBnew(:,:,ii)=D*(SX*(spineye.*Gnd(:,:,ii))*SX+SY*(
            spineye.*Gnd(:,:,ii))*SY+SZ*(spineye.*Gnd(:,:,ii))*SZ);

%         SigBnew(:,:,ii)=D*eye(2*NW,2*NW).*Grd(:,:,ii);
%         SiginBnew(:,:,ii)=D*eye(2*NW,2*NW).*Gnd(:,:,ii);
```

```
%             SigBnew(:,:,ii)=D*spineye.*Grd(:,:,ii); % TI spin
    preserving case
%             SiginBnew(:,:,ii)=D*spineye.*Gnd(:,:,ii);

            change1(ii)=sum(sum(abs(SigBnew(:,:,ii)-SigB(:,:,ii))));
            norm1(ii)=sum(sum(abs(SigBnew(:,:,ii)+SigB(:,:,ii))));
            change2(ii)=sum(sum(abs(SiginBnew(:,:,ii)-SiginB(:,:,ii))));
            norm2(ii)=sum(sum(abs(SiginBnew(:,:,ii)+SiginB(:,:,ii))));

            SigB(:,:,ii)=SigB(:,:,ii)+ctr*(SigBnew(:,:,ii)-SigB(:,:,ii))
                ;
            SiginB(:,:,ii)=SiginB(:,:,ii)+ctr*(SiginBnew(:,:,ii)-SiginB
                (:,:,ii));
        end
        fchange1=sum(change1)/sum(norm1);fchange2=sum(change2)/sum(norm1
            )
        iter=iter+1
    end % end of while loop

    TM(kk)=real(trace(gamR*(Gnd(:,:,Np))));
    TM(kk)
    %     E(kk)=EE;
    kk=kk+1;

end % length
toc
%% Electron density along the device
    for ii=1:Np
        eden(ii)=real(trace(Gnd(:,:,ii)))/real(trace(1i*(Grd(:,:,ii)-Grd
            (:,:,ii)')));
        edenyd(ii)=real(trace(kron(eye(NW),(eye(2)-sy))*Gnd(:,:,ii)))/
            real(trace(1i*(Grd(:,:,ii)-Grd(:,:,ii)')));
        edenyu(ii)=real(trace(kron(eye(NW),(eye(2)+sy))*Gnd(:,:,ii)))/
            real(trace(1i*(Grd(:,:,ii)-Grd(:,:,ii)')));
    end
```

```
%%
beta=TM/TMB;
aeden=(1-beta)*(1-linspace(0.5,Np-0.5,Np)'/Np)+beta/2;
% aeden=(1-beta)*(1-linspace(1,Np,Np)'/Np)+beta/2;
% aeden=(1-beta)*(1-linspace(0,Np-1,Np)'/Np)+beta/2;
figure(605);
hold on


% kmax=abs(fzero(@(x) myfun(x,t0,rashba,a,EE), -1));
% kmin=abs(fzero(@(x) myfun(x,t0,rashba,a,EE), 1));

kmin=m/hbar^2*abs(-rashba+sqrt(rashba^2+2*EE*hbar^2/m/q));
kmax=m/hbar^2*abs(-rashba-sqrt(rashba^2+2*EE*hbar^2/m/q));

r=min(kmax,kmin)/max(kmax,kmin);
Pch=2/pi*(1-r)/(1+r); % Rashba
% Pch=2/pi;  % TI case

qq=plot([1:1:Np]*a/1e-9,aeden,'k-');hold on
oo=plot([1:1:Np]*a/1e-9,aeden-(1-aeden(1))*(Pch),'b--');hold on
pp=plot([1:1:Np]*a/1e-9,aeden+(1-aeden(1))*(Pch),'r-.');hold on

NJ=5;
kk=plot([1:NJ:Np]*a/1e-9,eden(1:NJ:Np),'ko');hold on
mm=plot([1:NJ:Np]*a/1e-9,edenyd(1:NJ:Np),'ro');hold on
nn=plot([1:NJ:Np]*a/1e-9,edenyu(1:NJ:Np),'bo');hold on


set(kk,'linewidth',[3.0]);set(mm,'linewidth',[3.0]);set(nn,'linewidth'
    ,[3.0]);
set(oo,'linewidth',[3.0]);set(pp,'linewidth',[3.0]);set(qq,'linewidth'
    ,[3.0]);
```

```
set(gca,'Fontsize',[16])
% title(['NEGF real,  N_w = ',num2str(NW),'   N_L = ',num2str(Np),''])
ylabel('f_+_y, f, f_-_y');
xlabel('Length [nm]');
ylim([0 1])
box on
% grid on
```

Codes for Fig. 3.3(c)

```
clear all
%% input parameters
hbar=1.06e-34;q=1.6e-19;a=1e-9;uB=5.78*1e-5;
A2=3.3; % [eV A]
t0=A2*1e-10/a; % [eV]
sx=[0 1;1 0];sy=[0 -i;i 0];sz=[1 0;0 -1];zplus=1i*1e-6;
Np=1;N1=ceil(Np/2);X=1*[0:1:Np-1];
L=diag([1 zeros(1,Np-1)]);
R=diag([zeros(1,Np-1) 1]);
ii=0;
tic

flag_ord=0; % 0 Rashba

kymin=1*(-1.1);dky=0.0005;kymax=-kymin;



ii=1;
Emin=-0.1;Emax=+0.2;dE=(Emax-Emin)/30; % Rashba
% Emin=-0.2;Emax=+0.2;dE=(Emax-Emin)/11; % TISS

for EE=Emin:dE:Emax
    E(ii)=EE;
    EE
    H0=diag(ones(1,Np));
```

```
HR=diag(ones(1,Np-1),1);HL=diag(ones(1,Np-1),-1);

jj=1; % ky mode sum
%% initialization
noeyd(ii)=0;noeyu(ii)=0;dos(ii)=0;
for ky=kymin:dky:kymax

    beta=t0*(1/2)*(1*sz+i*sy);
    alpha=-t0*sz+(EE*ky)*sx;


    if flag_ord==0
%           m=0.05*9.1e-31;rashba=(2)*8*1e-12;g=15;B=1;  % Koo's
                    m=0.28*9.1e-31;rashba=(1)*0.79*1e-10;
        t0=(hbar^2)/(2*m*(a^2)*q);
        %             kf=acos(1-(EE)/(2*t0))/a;
        kf=(rashba*q+sqrt((rashba*q)^2+2*hbar^2*EE*q/m))/(hbar^2/m);
        ky=kf*ky;
        Ey=2*t0*(1-cos(ky*a));
        beta=-t0*eye(2)+1i*rashba/a/2*sy;
        alpha=2*t0*eye(2)+Ey*eye(2)+rashba*sin(ky*a)/a*sx;

    end


    H=kron(H0,alpha)+kron(HL,beta')+kron(HR,beta);

    %% PBC condition along transport direction for Hamiltonian
    % H=H+kron(diag(ones(1,1),1-Np),beta)+kron(diag(ones(1,1),Np-1),
       beta'); %PBC
    %%

    g0=(EE+zplus)*eye(2)-alpha;

    %% Sancho
```

```
        gL=sancho_gs(g0,beta');
        sL=beta'*gL*beta;
        gR=sancho_gs(g0,beta);
        sR=beta*gR*beta';
        %%
        sigL=kron(L,sL);sigR=kron(R,sR);
        gamL=1i*(sigL-sigL');gamR=1i*(sigR-sigR');

        G=inv(((EE+zplus)*eye(2*Np))-H-sigL-sigR);
        Gn=G*(gamL)*G';

        noeyd(ii)=noeyd(ii)+real(trace((eye(2)-sy)*Gn));
        noeyu(ii)=noeyu(ii)+real(trace((eye(2)+sy)*Gn));
        dos(ii)=dos(ii)+real(trace(1i*(G-G')));



        %%
        jj=jj+1;
    end % end of ky sum

    Pch(ii)=(noeyu(ii)-noeyd(ii))/dos(ii);
    if dos(ii)<0
        Pch(ii)=0;
    end
    Pch(ii)

    %%

    ii=ii+1;
end %
toc


%%
```

```
figure(53)

hold on
if flag_ord==0 % Rashba
    h=plot(2/pi*ones(length(E),1),E,'b');hold on
    k=plot(Pch,E,'bo-');hold on
else

    h=plot(2/pi*ones(length(E),1),E,'b');hold on
    k=plot(-Pch,E,'rx');hold on
end



set(gca,'Fontsize',[16])
set(h,'linewidth',[3.0])
set(k,'linewidth',[3.0])
% set(l,'linewidth',[3.0])
% set(m,'linewidth',[3.0])

grid on
box on
xlim([-1 1])
% legend('NEGF','Resistor','Location','Northwest');
% legend('I_c','I_x','I_y','I_z','Location','Best');
xlabel('P_c_h');
% xlabel('c (in c\sigma_z)');
ylabel('E [eV]');


%%%%%%%%%%%%%%%%%%%%%%%%%%%%%%%%%%%%%%%%%%%%


%% 3D TI E(k) relation surface 2 by 2 band structure plot

clear all
```

```
%Constants (all MKS, except energy which is in eV)
hbar=1.06e-34;q=1.6e-19;qh=q/hbar;a=1e-11;

%inputs

TI_flag=0;

%% this is in unit of pi/a
% klo=1*0.67-0.06;khi=1*0.67+0.06;
% klo=0-0.01*1;khi=0.01*1;
klo=-.02;khi=-klo;

%Hamiltonian

sx=[0 1;1 0];sy=[0 -i;i 0];sz=[1 0;0 -1];temp1=[0,1;-1,0];
NW=1;
%% Rashba
% m=0.05*9.1e-31;rashba=(1)*0.36*1e-10;
m=0.28*9.1e-31;rashba=(1)*0.79*1e-10;
t0=(hbar^2)/(2*m*(a^2)*q);
by=-t0*eye(2)-1i*rashba/a/2*sx;
bx=-t0*eye(2)+1i*rashba/a/2*sy;
al=4*t0*eye(2);
al=al/2;
%%
if TI_flag==1

    % Topological insulator
    t0=3.3*1e-10/a;
    al=-2*t0*sz;by=t0/2*(sz-i*sx);bx=t0/2*(sz+i*sy); % to=eta/a
    al=al/2;
else
end
%%
```

```
HW=eye(NW);
alpha=kron(HW,al);
alpha=alpha+kron(diag(ones(1,NW-1),+1),by)+kron(diag(ones(1,NW-1),-1),by
    ');

%          alpha=alpha+kron(diag(ones(1,1),1-NW),by)+kron(diag(ones(1,1),
    NW-1),by'); %PBC

%     beta=kron(eye(NW),bx)+kron(-t0*diag(exp(i*q*B*a*Y/hbar)),1);
beta=kron(spdiags(exp(i*qh*0*a*a*[1:1:NW]'),0,NW,NW),bx);



%%
ii=1;
for kk=[klo:(khi-klo)/400:khi]
    H=alpha+beta*exp(i*kk)+beta'*exp(-i*kk);
    [V,D]=eig(H);E(:,ii)=sort(real(diag(D)));K(ii)=kk;ii=ii+1;
end
%%

figure(5)
hold on
% subplot(2,1,1)
% subplot(1,3,1)

h=plot(K/a/1e10,E,'b');hold on
set(h,'linewidth',[3.0])
set(gca,'Fontsize',[16]);
% h=plot(2/3,linspace(0,5,1000),'k.','linewidth',[2]);hold on
% h=plot(1/3,linspace(0,5,1000),'k.','linewidth',[2]);hold on
set(h,'linewidth',[3.0])
set(gca,'Fontsize',[16]);
% grid on
```

```
% xlim([-0.3 0.3])
ylim([-0.2 0.2])
% ylabel('E [eV]')
% xlabel('k')
% k [A^(-1)]
box on

% subplot(1,3,2)
%%
figure(6)
NE=400; % even number
yy=linspace(-0.2,0.2,NE);




% Rashba

temp1=((rashba*q)^2*m/2/hbar^2/q)/0.6*NE*3

xx=[zeros(floor(NE/2)-temp1,1); 2/pi*sqrt(1+2*yy(floor(NE/2)-temp1:floor
    (NE/2))*q*hbar^2/m/(rashba*q)^2)';...
     2/pi*1./sqrt(1+2*yy(floor(NE/2)+1:NE)*q*hbar^2/m/(rashba*q)^2)'];
%
if TI_flag==1
     xx=[2/pi*ones(floor(NE/2),1);2/pi*ones(floor(NE/2),1)];
else
end
%

hold on
g=plot(xx,yy,'b')
set(g,'linewidth',[3.0])
set(gca,'Fontsize',[16]);
```

```
ylabel('E [eV]')
xlabel('P_c_h')
box on
xlim([-1 1])
ylim([-0.2 0.2])

xlim([0 1])
```

Codes for Fig. 3.4(a)

```
%% 3D TI E(k) relation surface 2 by 2 band structure plot

clear all

%Constants (all MKS, except energy which is in eV)
hbar=1.06e-34;q=1.6e-19;qh=q/hbar;a=1e-11;
A2=3.3*1e-10; % [eV meter]
t0=A2/a; % [eV]
g=15;B=1;
%         m=0.05*9.1e-31;rashba=(2)*8*1e-12;  % Koo's
m=0.28*9.1e-31;rashba=(1)*0.79*1e-10;
%inputs

TI_flag=0;

%% this is in unit of pi/a
% klo=1*0.67-0.06;khi=1*0.67+0.06;
% klo=0-0.01*1;khi=0.01*1;
klo=-.02;khi=-klo;

%Hamiltonian

sx=[0 1;1 0];sy=[0 -i;i 0];sz=[1 0;0 -1];temp1=[0,1;-1,0];
NW=1;
```

```
ky=0;
kf=0
t0=1*A2/a; % [eV]
beta1=1*t0*(1/2)*(1*sz+i*sy);
alpha1=-t0*sz+(A2*kf*ky)*sx;


t1=(hbar^2)/(2*m*(a^2)*q);
%                       kf=acos(1-(EE)/(2*t0))/a;
%          kf=(rashba*q+sqrt((rashba*q)^2+2*hbar^2*EE*q/m))/(hbar^2/m);
kyr=0;
Ey=2*t1*(1-cos(kyr*a));
beta2=1*(-t1)*eye(2)+1i*rashba/a/2*sy;
alpha2=2*t1*eye(2)+Ey*eye(2)+rashba*sin(kyr*a)/a*sx;
alpha2=alpha2+0.4*eye(2); %shift

alpha=[alpha1 zeros(2); zeros(2) alpha2];
beta=[1*beta1 zeros(2); zeros(2) 1*beta2];


%%
ii=1;
for kk=[klo:(khi-klo)/400:khi]
    H=alpha+beta*exp(i*kk)+beta'*exp(-i*kk);
    [V,D]=eig(H);E(:,ii)=sort(real(diag(D)));K(ii)=kk;ii=ii+1;
end
%%

figure(5)
hold on
% subplot(2,1,1)
% subplot(1,3,1)

h=plot(K/a/1e10,E,'k');hold on
```

```
set(h,'linewidth',[3.0])
set(gca,'Fontsize',[16]);
% h=plot(2/3,linspace(0,5,1000),'k.','linewidth',[2]);hold on
% h=plot(1/3,linspace(0,5,1000),'k.','linewidth',[2]);hold on
set(h,'linewidth',[3.0])
set(gca,'Fontsize',[16]);
% grid on
% xlim([-0.3 0.3])
ylim([0 0.6])
% ylabel('E [eV]')
% xlabel('k')
% k [A^(-1)]
box on
```

Codes for Fig. 3.4(b)

```
clear all
%% input parameters
hbar=1.06e-34;q=1.6e-19;a=1e-11;uB=5.78*1e-7;
A2=3.3*1e-10; % [eV meter]
t0=A2/a; % [eV]
g=15;B=1;
%         m=0.05*9.1e-31;rashba=(2)*8*1e-12;  % Koo's
m=0.28*9.1e-31;rashba=(1)*0.79*1e-10;

sx=[0 1;1 0];sy=[0 -i;i 0];sz=[1 0;0 -1];zplus=1i*1e-5;
Np=1;N1=ceil(Np/2);X=1*[0:1:Np-1];
L=diag([1 zeros(1,Np-1)]);
R=diag([zeros(1,Np-1) 1]);
ii=0;
tic
% P2=[1 0 0];
flag_ord=0; % 0 Rashba
% P1=[0 1 0];
```

```
% kF=abs(EE)/(A2*1e-10);
% W=1e-6; % device width
% Mode=kF*W/pi;Mode=1;

% kymin=1*(-0.9);dky=0.05;kymax=-kymin;
% kymin=1*(-0.95);dky=0.01;kymax=-kymin;
kymin=1*(-1.2);dky=0.001;kymax=-kymin;
% kymin=1*(-0.99);dky=0.01;kymax=-kymin;

% kymin=0*(-1.2);dky=0.001;kymax=-kymin;

ii=1;
Emin=-0.011;Emax=+0.04;dE=(Emax-Emin)/11;
Emin=-0.0005;Emax=+0.001;dE=(Emax-Emin)/21;
Emin=0.38;Emax=+0.4;dE=(Emax-Emin)/11;
Emin=0.1;Emax=+0.6;dE=(Emax-Emin)/53;
for EE=Emin:dE:Emax
    E(ii)=EE;
    EE
    H0=diag(ones(1,Np));
    HR=diag(ones(1,Np-1),1);HL=diag(ones(1,Np-1),-1);

    jj=1; % ky mode sum
    %% initialization
    noeyd(ii)=0;noeyu(ii)=0;dos(ii)=0;
    for ky=kymin:dky:kymax

        kf=abs(EE)/(A2);
        t0=A2/a; % [eV]
        beta1=1*t0*(1/2)*(1*sz+i*sy);
        alpha1=-t0*sz+(A2*kf*ky)*sx;


        t1=(hbar^2)/(2*m*(a^2)*q);
        %                       kf=acos(1-(EE)/(2*t0))/a;
```

```
%         kf=(rashba*q+sqrt((rashba*q)^2+2*hbar^2*EE*q/m))/(hbar
    ^2/m);
kyr=kf*ky;
Ey=2*t1*(1-cos(kyr*a));
beta2=1*(-t1)*eye(2)+1i*rashba/a/2*sy;
alpha2=2*t1*eye(2)+Ey*eye(2)+rashba*sin(kyr*a)/a*sx+0*g/2*uB*B*
    sz;
alpha2=alpha2+0.4*eye(2); %shift

alpha=[alpha1 zeros(2); zeros(2) alpha2];
beta=[beta1 zeros(2); zeros(2) 1*beta2];

H=kron(H0,alpha)+kron(HL,beta')+kron(HR,beta);

%% PBC condition along transport direction for Hamiltonian
% H=H+kron(diag(ones(1,1),1-Np),beta)+kron(diag(ones(1,1),Np-1),
    beta'); %PBC
%%

ig0=(EE+zplus)*eye(4)-alpha;

%% Sancho
gL=sancho_gs(ig0,beta');
sL=beta'*gL*beta;
gR=sancho_gs(ig0,beta);
sR=beta*gR*beta';

%%
sigL=kron(L,sL);sigR=kron(R,sR);
gamL=1i*(sigL-sigL');gamR=1i*(sigR-sigR');

G=inv(((EE+zplus)*eye(4*Np))-H-sigL-sigR);
Gn=G*(gamL)*G';

noeyd(ii)=noeyd(ii)+real(trace(kron(eye(2),(eye(2)-sy))*Gn));
```

```
        noeyu(ii)=noeyu(ii)+real(trace(kron(eye(2),(eye(2)+sy))*Gn));
        dos(ii)=dos(ii)+real(trace(1i*(G-G')));


        %%
        jj=jj+1;
    end % end of ky sum

    Pch(ii)=(noeyu(ii)-noeyd(ii))/dos(ii);
    Pch(ii)
    kf;
    %%

    ii=ii+1;
end %
toc
% splitting=g*uB*B

%%
figure(53)

hold on
if flag_ord==0
    %     h=plot(2/pi*ones(length(E),1),E,'b');hold on
    k=plot(Pch,E,'bx-');hold on
else

    h=plot(2/pi*ones(length(E),1),E,'b');hold on
    k=plot(-Pch,E,'bx');hold on
end

% k=plot(pol,INX,'ro-');hold on
% l=plot(pol,INY,'bx-');hold on
% m=plot(pol,INZ,'c+--');hold on
% h=plot(pol,0.5-1/pi*pol,'r.-');hold on
```

```
% h=plot(parameter,VN_par,'bx-');hold on
% k=plot(pol,VR,'bo');hold on
set(gca,'Fontsize',[16])
% set(h,'linewidth',[3.0])
set(k,'linewidth',[3.0])
% set(l,'linewidth',[3.0])
% set(m,'linewidth',[3.0])

grid on
box on
xlim([-1 1])
% legend('NEGF','Resistor','Location','Northwest');
% legend('I_c','I_x','I_y','I_z','Location','Best');
xlabel('P_c_h');
% xlabel('c (in c\sigma_z)');
ylabel('E [eV]');
```

Codes for Fig. 4.3

```
clear all

% Inputs
hbar=1.06e-34;q=1.6e-19;m=0.04*9.1e-31;
sx=[0 1;1 0];sy=[0 -1i;1i 0];sz=[1 0;0 -1];

a=1e-9; % 1/kF~1nm
% t0=(hbar^2)/(2*m*(a^2)*q);
qh=q/hbar;BB=0;
% eta=4.1;%[eV A]
eta=3.3;%[eV A]
t0=eta*1e-10/a;
NW=1;
% Np=10;
SX=kron(eye(NW),sx);SY=kron(eye(NW),sy);SZ=kron(eye(NW),sz);
```

```
spineye=kron(eye(NW,NW),ones(2,2));
diaeye=kron(eye(NW,NW),eye(2,2));
vF=eta/hbar*1e-10*q;
% L=zeros(Np);R=L;L(1,1)=1;R(Np,Np)=1;
zplus=1i*1e-7;
Y=a*([0:1:NW-1]-0.5*NW);


ctr=0.5;
kk=1;
Elo=t0*1;
dE=1*1e-3; Ehi=Elo;
EE=Elo;
EE=0.2;

lambda_kF=2*pi*eta/EE*1e-10/1e-9;

% t0=t0*10;
tic

%%
HW=eye(NW);

% Ordinary spin degenerate
al=4*t0*eye(2);by=-t0*eye(2);bx=-t0*eye(2);

% Topological insulator

al=-2*t0*sz;by=t0/2*(sz-1i*sx);bx=t0/2*(sz+1i*sy); % to=eta/a


if NW==1
    al=al/2;
end
% for EE=Elo:dE:Ehi
```

```
alpha=kron(HW,al);
alpha=alpha+kron(diag(ones(1,NW-1),+1),by)+kron(diag(ones(1,NW-1),-1),by
    ');

%         alpha=alpha+kron(diag(ones(1,1),1-NW),by')+kron(diag(ones(1,1)
    ,NW-1),by); %PBC
beta=kron(spdiags(exp(i*qh*BB*a*a*[1:1:NW]'),0,NW,NW),bx);


%% self energy of contact %%
galpha=(EE+zplus)*eye(2*NW)-alpha;
g1=sancho_gs(galpha,beta');
g2=sancho_gs(galpha,beta);
sigL=1*beta'*g1*beta;
sigR=1*beta*g2*beta';
gamL=1i*(sigL-sigL');
gamR=1i*(sigR-sigR');


%%%%%%%%%%

fR=0;
N_kk=21;

Np=40;
D2=0*1e-3/2; % ordinary spin reversing scattering for intrinsic channel

%% initialization for RGF
Al = zeros(2*NW,2*NW,Np-1);
Ad = zeros(2*NW,2*NW,Np);
Au = zeros(2*NW,2*NW,Np-1);
Sigin=zeros(2*NW,2*NW,Np);
% Sigout=zeros(2*NW,2*NW,Np);
```

```
SigB=zeros(2*NW,2*NW,Np);SiginB=zeros(2*NW,2*NW,Np);SigoutB=zeros(2*NW
    ,2*NW,Np);
SigB1=zeros(2*NW,2*NW,Np);SiginB1=zeros(2*NW,2*NW,Np);SigoutB1=zeros(2*
    NW,2*NW,Np);
SigB2=zeros(2*NW,2*NW,Np);SiginB2=zeros(2*NW,2*NW,Np);SigoutB2=zeros(2*
    NW,2*NW,Np);

for kk=1:N_kk


    D1=2*1*1e-3*(kk-1)/3; % coupling constant %% spin eraser
    DD(kk)=D1;


    length(kk)=Np;




    TMRL(kk)=0;


    %%        BLOCK SET-UP
    fchange1=1;fchange2=1;iter=1;

    while (fchange1+fchange2)>1e-6
        for ii=1:Np-1
            Ad(:,:,ii)=EE*eye(2*NW)-alpha-SigB(:,:,ii);
            Au(:,:,ii)=-beta;
            Al(:,:,ii)=-beta';
        end
        Ad(:,:,Np)=EE*eye(2*NW)-alpha-SigB(:,:,Np);

        Ad(:,:,1)=Ad(:,:,1)-sigL;
```

```
Ad(:,:,Np)=Ad(:,:,Np)-sigR;

Sigin=SiginB;
Sigin(:,:,1)=Sigin(:,:,1)+gamL;     %
Sigin(:,:,Np)=Sigin(:,:,Np)+fR*gamR;     % in equilibrium

[Grd,Gnl,Gnd,Gnu,Gpd] = recursealgblock3d_m(2*NW,Np,Al,Ad,Au,
    Sigin);
if (kk==1)&&(iter==1)
     TMB=real(trace(gamR*(Gnd(:,:,Np))))

end
for ii=1:Np



     SigBnew1(:,:,ii)=D1*(SX*(spineye.*Grd(:,:,ii))*SX+1*SY*(
        spineye.*Grd(:,:,ii))*SY+SZ*(spineye.*Grd(:,:,ii))*SZ);
     SigBnew2(:,:,ii)=D2*(SX*(spineye.*Grd(:,:,ii))*SX+1*SY*(
        spineye.*Grd(:,:,ii))*SY+SZ*(spineye.*Grd(:,:,ii))*SZ);
     SigBnew(:,:,ii)=SigBnew1(:,:,ii)+SigBnew2(:,:,ii);



     SiginBnew1(:,:,ii)=D1*(SX*(spineye.*Gnd(:,:,ii))*SX+1*SY*(
        spineye.*Gnd(:,:,ii))*SY+SZ*(spineye.*Gnd(:,:,ii))*SZ);
     SiginBnew2(:,:,ii)=D2*(SX*(spineye.*Gnd(:,:,ii))*SX+1*SY*(
        spineye.*Gnd(:,:,ii))*SY+SZ*(spineye.*Gnd(:,:,ii))*SZ);
     SiginBnew(:,:,ii)=SiginBnew1(:,:,ii)+SiginBnew2(:,:,ii);



     change1(ii)=sum(sum(abs(SigBnew(:,:,ii)-SigB(:,:,ii))));
     norm1(ii)=sum(sum(abs(SigBnew(:,:,ii)+SigB(:,:,ii))));
     change2(ii)=sum(sum(abs(SiginBnew(:,:,ii)-SiginB(:,:,ii))));
```

```
        norm2(ii)=sum(sum(abs(SiginBnew(:,:,ii)+SiginB(:,:,ii))));


        SigB(:,:,ii)=SigB(:,:,ii)+ctr*(SigBnew(:,:,ii)-SigB(:,:,ii))
            ;
        SiginB(:,:,ii)=SiginB(:,:,ii)+ctr*(SiginBnew(:,:,ii)-SiginB
            (:,:,ii));


        SigB1(:,:,ii)=SigB1(:,:,ii)+ctr*(SigBnew1(:,:,ii)-SigB1(:,:,
            ii));
        SiginB1(:,:,ii)=SiginB1(:,:,ii)+ctr*(SiginBnew1(:,:,ii)-
            SiginB1(:,:,ii));

    end
    fchange1=sum(change1)/sum(norm1);fchange2=sum(change2)/sum(norm1
        );
    iter=iter+1;
end % end of while loop

TM(kk)=real(trace(-gamR*fR*(1i*(Grd(:,:,Np)-Grd(:,:,Np)'))+gamR*(Gnd
    (:,:,Np))));
TM2(kk)=real(trace(gamL*(1i*(Grd(:,:,1)-Grd(:,:,1)')-Gnd(:,:,1))));

TM(kk)
%     TM2(kk)

for ii=1:Np

    Ic(ii)=real(trace(kron(eye(NW),eye(2))*(SiginB1(:,:,ii)*Grd(:,:,
        ii)'-Grd(:,:,ii)*SiginB1(:,:,ii)+SigB1(:,:,ii)*Gnd(:,:,ii)-
        Gnd(:,:,ii)*SigB1(:,:,ii)')/(1i)));
    Ix(ii)=real(trace(SX*(SiginB1(:,:,ii)*Grd(:,:,ii)'-Grd(:,:,ii)*
        SiginB1(:,:,ii)+SigB1(:,:,ii)*Gnd(:,:,ii)-Gnd(:,:,ii)*SigB1
        (:,:,ii)')/(1i)));
```

```
    Iy(ii)=real(trace(SY*(SiginB1(:,:,ii)*Grd(:,:,ii)'-Grd(:,:,ii)*
        SiginB1(:,:,ii)+SigB1(:,:,ii)*Gnd(:,:,ii)-Gnd(:,:,ii)*SigB1
        (:,:,ii)')/(1i)));
    Iz(ii)=real(trace(SZ*(SiginB1(:,:,ii)*Grd(:,:,ii)'-Grd(:,:,ii)*
        SiginB1(:,:,ii)+SigB1(:,:,ii)*Gnd(:,:,ii)-Gnd(:,:,ii)*SigB1
        (:,:,ii)')/(1i)));


end
Ic_total(kk)=sum(Ic);
Ix_total(kk)=sum(Ix);
Iy_total(kk)=sum(Iy)
Iz_total(kk)=sum(Iz);

%% Electron density along the device
for ii=1:Np
    eden(ii)=real(trace(Gnd(:,:,ii)))/real(trace(1i*(Grd(:,:,ii)-Grd
        (:,:,ii)')));
    edenx(ii)=real(trace(kron(eye(NW),(0*eye(2)+sx))*Gnd(:,:,ii)))/
        real(trace(1i*(Grd(:,:,ii)-Grd(:,:,ii)')));
    edeny(ii)=real(trace(kron(eye(NW),(0*eye(2)+sy))*Gnd(:,:,ii)))/
        real(trace(1i*(Grd(:,:,ii)-Grd(:,:,ii)')));
    edenz(ii)=real(trace(kron(eye(NW),(0*eye(2)+sz))*Gnd(:,:,ii)))/
        real(trace(1i*(Grd(:,:,ii)-Grd(:,:,ii)')));

end


    Vx(kk)=edenx(floor(Np/5));
    Vy(kk)=edeny(floor(Np/5));
    Vz(kk)=edenz(floor(Np/5));
```

```
    kk=kk+1;


end %
toc

Tb=TM(1);

Iy_total=-Iy_total;
Vy=-Vy; % due to coordinate axis change, Old y axis = - New z axis
%%
beta=TM/TMB;



figure(810)
l=plot(Iy_total,Tb+Tb/2*Iy_total,'b-');hold on
k=plot(Iy_total,TM,'ro');hold on
set(k,'linewidth',[3.0]);
set(l,'linewidth',[3.0]);
set(gca,'Fontsize',[24])
xlabel('i^s/(G_BV)');
% xlabel('D [eV^2]');
ylabel('I/(G_BV)');
% ylim([0 1])
%  xlim([0 Np*a/1e-9])
box on

figure(910)
l=plot(TM,TM/2,'b-');hold on
k=plot(TM,Vy,'ro');hold on
set(k,'linewidth',[3.0]);
set(l,'linewidth',[3.0]);
set(gca,'Fontsize',[24])
ylabel('v^s/V');
```

```
% xlabel('D [eV^2]');
xlabel('I/(G_BV)');
% ylim([0 1])
%  xlim([0 Np*a/1e-9])
box on
```

```
function [Grd,Gnl,Gnd,Gnu,Gpd] = recursealgblock3d_m(Nc,Np,Al,Ad,Au,
    Sigin)

% format long
% based on Dmitri Nikonov; Siyu Koswatta (2006), "recursive algorithm
    for NEGF in Matlab," https://nanohub.org/resources/1983.


edinC = eye(Nc,Nc);
grL = zeros(Nc,Nc,Np);                                  % initialize left-
    connected function
ginL = zeros(Nc,Nc,Np);                                 % initialize left-
    connected in-scattering function
% gipL = zeros(Nc,Nc,Np);                                 % initialize left-
    connected out-scattering function
Grl = zeros(Nc,Nc,Np-1);
Grd = zeros(Nc,Nc,Np);                                  % initialize the
    Green's function
```

```
Gru = zeros(Nc,Nc,Np-1);
Gnl = zeros(Nc,Nc,Np-1);
Gnd = zeros(Nc,Nc,Np);                                  % initialize the
    electron coherence function
Gnu = zeros(Nc,Nc,Np-1);
% Gpl = zeros(Nc,Nc,Np-1);
% Gpd = zeros(Nc,Nc,Np);                                  % initialize the
    hole coherence function
% Gpu = zeros(Nc,Nc,Np-1);


grL(:,:,1)=(Ad(:,:,1))\edinC;                             % step 1
for q=2:Np                                              % obtain the left-
    connected function
    obra = (Ad(:,:,q)-Al(:,:,q-1)*grL(:,:,q-1)*Au(:,:,q-1));
    grL(:,:,q)=obra\edinC;
end
for k=1:Np
    gaL(:,:,k) = grL(:,:,k)';                             % advanced left-
        connected function
end
for k=1:(Np-1)
    Al_cr(:,:,k) = Au(:,:,k)';                            % Hermitean
        conjugate of the coefficient matrix
    Au_cr(:,:,k) = Al(:,:,k)';
end
Grd(:,:,Np)=grL(:,:,Np);                                % step 2
for q=(Np-1):-1:1
    Grl(:,:,q)=-Grd(:,:,q+1)*Al(:,:,q)*grL(:,:,q);  % obtain the sub-
        diagonal of the Green's function
    Gru(:,:,q)=-grL(:,:,q)*Au(:,:,q)*Grd(:,:,q+1);  % obtain the super-
        diagonal of the Green's function
    prom = edinC-Au(:,:,q)*Grl(:,:,q);
    Grd(:,:,q)=grL(:,:,q)*prom;                         % obtain the
        diagonal of the Green's function
```

```
end
for k=1:Np
    Gad(:,:,k) = Grd(:,:,k)';                          % advanced Green's
        function
end
for k=1:(Np-1)
    Gal(:,:,k) = Gru(:,:,k)';
    Gau(:,:,k) = Grl(:,:,k)';
end
ginL(:,:,1)=grL(:,:,1)*Sigin(:,:,1)*gaL(:,:,1);      % step 3
for q=2:Np
    sla2 = Al(:,:,q-1)*ginL(:,:,q-1)*Au_cr(:,:,q-1);
    prom = Sigin(:,:,q) + sla2;
    ginL(:,:,q) = grL(:,:,q)*prom*gaL(:,:,q);       % left-connected in-
        scattering function
end
Gnd(:,:,Np)=(ginL(:,:,Np));                          % step 4
for q=(Np-1):-1:1
    Gnl(:,:,q) = - Grd(:,:,q+1)*Al(:,:,q)*ginL(:,:,q) - Gnd(:,:,q+1)*
        Al_cr(:,:,q)*gaL(:,:,q);
    nui = ginL(:,:,q) + grL(:,:,q)*Au(:,:,q)*Gnd(:,:,q+1)*Al_cr(:,:,q)*
        gaL(:,:,q) - ...
         ( ginL(:,:,q)*Au_cr(:,:,q)*Gal(:,:,q) + Gru(:,:,q)*Al(:,:,q)*
            ginL(:,:,q) );
    Gnd(:,:,q) = nui;
end
for k=1:(Np-1)
    Gnu(:,:,k) = Gnl(:,:,k)';                          % upper diagonal
        of the electron function
end


        Gpl = i*(Grl-Gal) - Gnl;
        Gpd = i*(Grd-Gad) - Gnd;                              % hole Green
            's function
        Gpu = i*(Gru-Gau) - Gnu;
```

```
end
```

VITA

VITA

Seokmin Hong received the B.S. degree in electrical engineering from Seoul National University, Seoul, Korea, in 2003, and the M.S. degree in electrical engineering and computer science from the University of Florida, Gainesville, in 2007. He is currently working toward the Ph.D. degree in the Network for Computational Nanotechnology, School of Electrical and Computer Engineering, Purdue University, West Lafayette, IN. His research interests include the physics, modeling, and simulation of nanodevices and spintronics.